Thèse

UNIVERSITE
BRETAGNE
LOIRE

THESE INSA Rennes
sous le sceau de l'Université Bretagne Loire
pour obtenir le titre de
DOCTEUR DE L'INSA RENNES
Spécialité : Génie Mécanique

présentée par
Jiali XU

ECOLE DOCTORALE : *SDLM*
LABORATOIRE : *LGCGM, LS2N*

An improved design concept permitting the dynamic decoupling of serial manipulators taking into account the changing payload

Thèse soutenue le 21.04.2017
devant le jury composé de :

Philippe Wenger
Directeur de Recherche CNRS, LS2N Nantes / Président
Gabriel Abba
Professeur des Universités, Université de Lorraine / Rapporteur
Yannick Aoustin
Professeur des Universités, Université de Nantes / Rapporteur
Hervé Gueguen
Professeur, CentraleSupelec Rennes / Examinateur
Vigen Arakelyan
Professeur des Universités, INSA Rennes / Co-directeur de thèse
Jean-Paul Le Baron
Professeur des Universités, INSA Rennes / Directeur de thèse

An improved design concept permitting the dynamic decoupling of serial manipulators taking into account the changing payload

Jiali XU

En partenariat avec

Abstract

Simple structure, low cost, large workspace and mature technology, these advantages make the serial manipulators are widely used in many industrial fields. With the rapid development of industry and various applications of serial manipulators, new strict requirements are proposed, such as high stability, high positioning accuracy and high speed operation.

One of the efficient ways to improve the mentioned performances is the design of manipulators with dynamic decoupling. Therefore, the goal in this thesis is to find simple structure permitting to carry out complete dynamic decoupling of serial manipulators taking into account the changing payload.

The review, given in Chapter 1, summarizes the known solutions and discloses the drawbacks of different techniques permitting a simplification of the dynamics of manipulators. It allows an identification of objectives that are of interest and should be studied within the framework of this thesis.

Chapter 2 deals with the design of adjustable serial manipulators with linearized and decoupled dynamics. Without payload, the developed method accomplishes the dynamic decoupling via opposite rotation of links and optimal redistribution of masses. The payload which leads to the perturbation of the dynamic decoupling equations is compensated by the optimal control technique.

Chapter 3 deals with a new dynamic decoupling concept, which involves connecting to a serial manipulator a two-link group forming a Scott-Russell mechanism with the initial links of the manipulator. The opposite motion of links in the Scott-Russell mechanism combined with optimal redistribution of masses allows the cancellation of the coefficients of nonlinear terms in the manipulator's dynamic equations. Then, by using the control, the dynamic decoupling taking into account the changing payload is achieved.

In chapter 4, robustness properties (parametric uncertainties) of four various models of serial manipulators (one coupled manipulator, one decoupled manipulator by feedback linearization and the two decoupled manipulators that modeled in chapters 2

and 3) are considered. The given comparison performed via simulations is achieved with the same optimal control law and the same reference trajectory. Simulation results allow one to derive robustness assessments of manipulators described in chapters 2 and 3.

The suggested design methodology and control techniques are illustrated by simulations carried out using ADAMS and MATLAB software, which have confirmed the efficiency of the developed approaches.

Foreword

The journey of 42 months that to be a doctor will come to the end soon. Even now, I still remember the first that I arrive in Rennes. I am so lucky that I can study for my doctor's degree in France and to be the last student of my kind research supervisor, Prof. Jean-Paul Le Baron. I would like to thank him for the patient guidance, encouragement and advice that he has provided throughout all the past three years. He cares not only my work, but also my life in France.

I would also like to thank my co-supervisor, Prof. Vigen Arakelyan. He could always provide great source of ideas for the research. With his effective leadership, the work always goes well. He also cares my daily life in France. I have to say, both of them are very kind to me.

I would like to thank the Chinese Scholar Council, the Chinese government who provide the bourse to me.

Every doctor will experience a painful period, me too. I would like to thank everyone who helped me during this period.

Last, I would like to express all my gratitude and my love to my family, my father XU Changjun, my mather WANG Yonghua and my sister XU Xiaowen. Without yours patiences, comprehensions and loves, I can't make it. I also would like to thank my girlfriend JIAO Wenting, with yours great comprehension, I can totally focus on my thesis. I would like to express to them how important they are and how much I love them.

To everyone who I love

Contents

List of Figures

List of Tables

Nomenclature

This nomenclature references the principal variables and abbreviations used in this manuscript.

A	the state matrix of the system.
A_i	the state matrix of the *i*th subsystem.
B	the input matrix of the system.
B_i	the input matrix of the *i*th subsystem.
C	the output matrix of the system.
$C(\theta,\dot{\theta})$	the vector of Coriolis and centrifugal effects.
c_k	the centroid of link k.
d	the constant disturbance.
$\hat{d}$	the estimate of the constant disturbance.
d_{S2}	the distance between the center of mass S_2 of link 2 and joint center B.
$\dot{d}_{S2}$	the velocity of center of mass S_2 of link 2 relative to joint center B.
$\ddot{d}_{S2}$	the acceleration of center of mass S_2 of link 2 relative to joint center B.
E_i	the kinematic energy of the *i*th component of the manipulator.
E_{cw}	the kinematic energy of the counterweight.
f	the vector of performance function.
G_c	the controllability transient gramian.
G_i	the vector of feedback factor of the *i*th subsystem.
g	the gravitational acceleration.
$g(\theta)$	the torque vector due to gravity.
g_{ji}	the feedback factor of the *i*th output in the *j*th subsystem.
H_{ii}	the *i-j* element of the manipulator inertia matrix.
I	the unit matrix.
I_{Si}	the axial moment of inertia of link *i*.

i	an integer.
J	the index of performance.
j	an integer.
K_D	positive, diagonal matrices of derivative gains.
K_P	positive, diagonal matrices of proportional gains.
L	the Lagrangian factor.
L_i	the length of the *ith* link of the serial manipulator.
L_{AS1}	the distance between the centre of mass S_1 of link AB and joint center *A*.
L_{BS2}	the distance between the centre of mass S_2 of link BP and joint center *B*.
L_{BS2r}	the real center of mass and moment of inertia of the object which is constituted by link BP, Scott-Russell mechanism and counterweight
$M(\theta)$	the inertia matrix.
m_k	the mass tensor of link *k*.
m_{SR}	the mass of the Scott Russell mechanism.
m_{cw}	the mass of the counterweight.
P	the position of the end-effector.
P_i	the initial end-effector position.
P_f	the final end-effector position.
$r_{i,ck}$	the position vector from an arbitrary point on the *i*th joint axis to the centroid.
Ran	the random value matrix.
T	the total time for the rotation.
T_{cc}	the controllability matrix.
T_{pi}	the time when the peak value of the *ith* subsystem response is achieved.
W_c	the upper triangular Toeplitz matrix.
ω_n	natural frequency.
u	an input signal.
V	the Lyapunov function candidate.
x	the position of the end-effector along the X-axis of the base frame.
X	an axis.
y	the position of the end-effector along the Y-axis of the base frame.
Y	an axis.
τ_i	the inertia torque generated by the acceleration of the *i*th joint.
τ_{gi}	the torque terms in the dynamic equation of *i*th link due to gravity.
$\tau_{jwithout}$	the output torque value of the *j*th actuator when no payload is added on the

	end-effector of the serial manipulator.
τ_{jwith}	the output torque value of the *j*th actuator when taking into account the payload on the end-effector of the serial manipulator.
θ_i	the angular position of the *ith* link.
$\dot{\theta}_i$	the angular velocity of the *ith* link.
$\ddot{\theta}_i$	the angular acceleration of the *ith* link.
θ_d	a constant reference set-point.
θ_{iR}	the reference trajectory of the *ith* actuator.
θ_{iI}	the desired initial angle of the *ith* actuator.
θ_{iF}	the desired final angle of the *ith* actuator.
$\tilde{\theta}$	the angular difference between the renference angle and the real angle.
$\theta^i_{j(1)}$	the angular position of the *ith* joint when the initial position of the end-effector with “elbow down” solution.
$\theta^f_{j(1)}$	the angular position of the *ith* joint when the final position of the end-effector with “elbow down” solution.
$\theta^i_{j(2)}$	the angular position of the *ith* joint when the initial position of the end-effector with “elbow up” solution.
$\theta^f_{j(2)}$	the angular position of the *ith* joint when the final position of the end-effector with “elbow up” solution.
$\Delta\theta_i$	the angular distance between the initial and the final position of the *ith* joint.
$\Delta\tau_i$	the payload compensation of the dynamic for the *i*th actuator when taking into account the payload.
ξ	the state vector of the state equation.
ζ	the state vector of the controllable canonical form of the state equation
ρ	the element of the state vector of the second subsystem.
Σ_i	the symmetric matrix of the solution of Riccati equation in the *ith* subsystem
σ_i	the element of the symmetric matrix Σ.
$\varepsilon_{\theta i}$	the performance index of angular error of the *ith* joint.
ε_P	the performance index of position error of the *ith* joint.

Introduction

With the rapid development of industry and various applications of serial manipulators, new strict requirements are proposed, such as high stability, high positioning accuracy, high speed operation and etc. It is known that the serial manipulator dynamics are highly coupled and nonlinear. The complicated dynamics results from varying inertia, interactions between the different joints, and nonlinear forces such as Coriolis and centrifugal forces. Nonlinear forces cause errors in position response at high speed, and have been shown to be significant even at slow speed. Thus, the goal of this thesis is to deal with the problem of dynamic decoupling of the serial manipulators.

The critical review given in the first chapter showed that the known mechanical solutions for dynamic decoupling. They are the methods of actuator relocation, optimum inertia redistribution and addition of auxiliary links respectively. These methods can only be reached by a considerably more complicated design of the initial structure of the manipulator. One of the solutions is carried out by the connection of gears to the oscillating links. The gears added to the oscillating links of the manipulator are sources of shocks between teeth that lead to the perturbation of the operation of the manipulator, the noise and other negative effects. It is obvious that mechanical solutions for adjustment of nonlinear terms of dynamic equations can be reached by unreasonably complicated design. In addition, this problem is more complicated and unpredictable when it is necessary to take into account a variable payload. Because the variable payload introduce variable load which is nonlinear term on the dynamic models of the manipulators. Then the positioning accuracy will be influenced.

Considering the mentioned problems related to the dynamic decoupling of manipulators, in the thesis are proposed new solutions combining both mechanical and control solutions.

Chapter 2 deals with the problem of dynamic decoupling of adjustable serial manipulators via a new mechatronic design approach, which is based on the opposite motion of manipulator links and the optimal command design. It is carried out in two steps. At first, the dynamic decoupling of the serial manipulator with adjustable lengths of links is accomplished via an opposite rotation of links and optimal redistribution of

masses. Such a solution proposed for the first time allows one to carry out the dynamic decoupling without connection of gears to the oscillating links. The elimination of gears from design concept is a main advantage of the suggested solution. Thus, the proposed mechanical solution allows one to transform the original nonlinear system model into a fully linear system without using the feedback linearization technique. In addition, to ensure linearized and decoupled dynamics of the manipulator for any payload, an optimal control technique is applied. It is shown that the dynamic decoupling of the manipulator simplifies the control solution ensuring the dynamic decoupling taking into account the changing payload.

Chapter 3 deals with another dynamic decoupling principle, which involves connecting to a serial manipulator a two-link group forming a Scott-Russell mechanism with the initial links of the manipulator. It also be carried out in two steps. At first, the dynamic decoupling of the serial manipulator is accomplished via the Scott-Russell mechanism properties and optimal redistribution of masses. Thus, the modification of the mass redistribution allows one to transform the original nonlinear system model into a fully linear system without using the feedback linearization technique. However, as it mentioned above, the changing payload leads to the perturbation of the dynamic decoupling of the manipulator. To ensure decoupled dynamics of the manipulator for any payload, an optimal control technique has been applied.

All suggested design methodologies and control techniques are illustrated by simulations carried out using ADAMS and MATLAB software. According to the modeling process and the simulation results, the advantages of these two dynamic decoupling manipulators are:

- the dynamic equations are simplified and the controller can be treated as the superposition of serial SISO controller.
- the simplification of the controller based on the linearized input/output relationships, hence the computational burden caused by the huge amount of iterative calculation is vanished. Thus, the real-time performance can be improved.
- the positioning error can be reduced by the eliminations of the Coriolis and centrifugal forces. Therefor the robustness of the serial manipulators is improved.
- the changing payload can be taken into account based on the dynamic decoupling manipulator with simple linear control law.

In chapter 4, the tolerance capabilities of these two dynamic decoupling manipulators are investigated through the comparison with a coupled manipulator and one other manipulator which is decoupled by feedback linearization. In order to make the comparison analysis clearer, two kinds of indices are proposed to quantify the positioning accuracy of the manipulator. They are angular error of the actuators and the position error of the end-effector. And two kinds of simulations are implemented for complete analysis. Through the results, it is obvious that, during the whole process, the tracking trajectories of the decoupled manipulators are more precise and less sensitive to the variable errors. In the aspect of the final positioning accuracy, according to the quantitative analysis, it also shows that the tolerance capabilities of the two manipulators that dynamic decoupled by the mechatronic method are higher than the ones of the coupled model and the dynamic decoupled model by feedback linearization. In a result, the simulation results prove that the manipulators that decoupled by the mechatronic methods in this thesis are more robust.

Finally, in the last part of the discussion, the dynamic of serial manipulator with prismatic joints is a discussed. In this discussion, an attempt is made to carry out the dynamic decoupling of serial manipulators with prismatic joints by introducing the rhomboid pantograph mechanism which has the same properties as the Scott-Russell mechanism. As result, the added rhomboid pantograph mechanism allows one to carry out a partial decoupling. It ensures only the cancellation of the terms related to gravity.

Chapter 1

Manipulator design for simplified dynamics

To introduce the first chapter, we give a brief overview of the serial manipulators. Simple structure, low cost, large workspace and mature technology are principal and essential characteristics these advantages make the serial manipulators are widely used in many industrial fields.

With the rapid development of industry and various applications of serial manipulators, the increase in high stability and positioning accuracy were requested. It is known that the dynamics of the manipulator in series are strongly coupled and nonlinear. These non-linear forces cause high-speed position response errors and in certain cases to be significant even at slow speed. Thus, the dynamic decoupling of manipulators has been in permanent development in recent decades.

Through this review, which summarizes the known solutions, the drawbacks of different techniques permitting a simplification of the dynamics of manipulators are disclosed. It allows an identification of objectives that are of interest and should be studied within the framework of this dissertation.

1.1. The historical evolution of serial manipulators

The first industrial robots were created only one half century ago. George Devol applied for the first robotics patents in 1954 (granted in 1961) (George C 1961). The first company to produce a robot was Unimation. These robots were also called programmable transfer machines since their main use at first was to transfer objects from one point to another, less than a dozen feet or so apart. They used hydraulic actuators and were programmed in joint coordinates. The robotic production has been changed radically in the late 1970s when several big Japanese conglomerates began producing industrial robots. Nowadays, the robots play an indispensable role in the manufacturing. However, for the thinking and imagination of robot, the time necessary to develop these possibilities will be certainly very long.

1.1.1. From automatic machines to robot manipulators

"If every instrument would accomplish its own work, obeying or anticipating the will of others…if the shuttle could weave, and the pick touch the lyre, without a hand to guide them, chief workmen would not need servants" wrote by Aristote.

Actually, through the human history, the tools that be used by human have been continually improved and explored in order to accomplish works more convenient and more time-saving. In history, the tool which is considered one of the earliest mechanical devices is the clepsydra developed by the Babylonians 1400 BCE (Siciliano and Khatib 2016).

In 1495, Leonardo Da Vinci designed a clockwork knight. It is designed to sit up, wave its arms and move its head. And this design may constitute the first humanoid robot. Speaking of the word 'robot', it was first used to denote fictional humanoid in a 1921 play named Rossum's Universal Robots by the Czech writer, Karel Capek. This show described the extreme desire to create a kind of universal tools that can work hard for mankind. Since then, this word is known all over the world. According to the International Organization for Standardization (standard ISO 8373:2012), a robot is an "actuated mechanism programmable in two or more axes with a degree of autonomy, moving within its environment, to perform intended tasks."

In 1956, George Devol and Joseph Engelberger form the world's first robotics company, Unimation and then the first industrial robot called Unimate came out (Nof 1999). It was installed on the General Motors automotive assembly line to sequence and

stack hot pieces of die-casting metal in 1961. This successful example attracted the attention of other manufacturers such as Ford, Fiat and Chrysler. Soon, this first commercial industrial robot was widely used and it promoted the research on robot around the world.

After several years, in 1978, the Unimation took out a smaller manipulator arm, called PUMA (Programmable Universal Machine for Assembly) which is designed by Vic Schienman and financed by GM at MIT. It is specifically designed to handle smaller parts in the assembly of instruments and engines. According to different requirements, PUMA is represented in three categories: 200, 500 and 700 series (Gebizlioğlu 2003). The 500 Series is most commonly used in automated spot welding application. The model 560c has 6 degrees of freedom (Bejczy et al. 1985). This is a typical serial manipulator. Each link of the manipulator is connected to others by a rotation joint and driven by a permanent-magnet DC servomotor. And each motor contains an incremental encoder and a potentiometer driven through a 116 to 1 gear reduction. To achieve maximum strength with minimum weight, the upper arm and forearm are monocoque construction. And with the maximum payload of 4 kg, the max velocity that can be reached is 470 mm/sec straight line moves (Corke 1991).

For years, this type of manipulator is widely used in the automotive industry. Even now, PUMAs are probably the most common robot in the university laboratories and one of the most common assembly robots (Gupta and Guo 1991) (Elgazzar 1985) (Leahy 1989).

1.1.2. Industrial applications of serial manipulators

Advantages such as simple structure, low cost, large workspace and mature technology, make the serial manipulators are widely used in many industrial fields such as welding, painting, assembly, pick and place (such as packaging, palletizing and SMT), product inspection and testing.

This kind of manipulators also has some drawbacks such as, for example, accumulated position errors or low rigidity of links for machining. With the progress of these technologies, these drawbacks will become smaller and smaller. Actually, based on the PUMA model, lots of improved serial manipulators are designed to suit the requirements of different industrial fields that mentioned above (Cheng et al. 1997) (Kircanski and Boric 1992) (Armstrong et al. 1986).

- the SCARA (for Selective Compliance Assembly Robot Arm) was first introduced in Japan for fast pick-and-place operations (Fig. 1.1.a) (Angeles 2013). It has 4 degrees of freedom with three rotary (R) joints and a prismatic (P) joint. This kind of manipulator is characterized by high speed and accuracy.
- the IRB 460 (Fig. 1.1.b): this is a 4-axis robot with a reach of 2.4 meters and 110-kilogram capacity. As the smallest member in the palletizing family of ABB, it is considered as the world's fastest palletizing robot. With a payload of 60 kilograms, it can reach up to 2190 cycles per hour.
- FANUC 430i (Fig. 1.1.c) marked a significant change in arm design. It has 6 axes, three of them are driven by motors that are optimally located. This design can better balance the manipulator's weight and allows the robot to move with a great deal of flexibility. This arm design is similar to the KUKA design used on the IR360 and then on the KR series. The main difference is the sensible use of a mechanical spring to help axis 2 movements, rather than the gas spring used by KUKA. The standard version of this kind of manipulator can have a payload of 130 kg and a reach of 2643 mm. The VA1400 (Fig. 1.1.d): the first 7-axis robotic welder from YASKAWA. Innovative 7-axis design dramatically increases freedom of movement and maintains proper welding posture at all times. Located in lower arm, the seventh axis acts as elbow, providing tremendous additional flexibility. Normally, this kind of manipulator has low payload (from 3 kg to 10 kg). As the same, the maximum payload of this welder is 3 kg.
- LBR IIWA (Fig. 1.1.e): a 7-axis manipulator with sensory capabilities for safety, fast teaching and simple operator control (Waurzyniak 2015). Opens up new areas of application in the vicinity of humans that were previously off-limits for robots. For the first time, human and robot can work together on highly sensitive tasks in close cooperation.
- Canadarm 2 (Fig. 1.1.f): well-known as a part of the Mobile Servicing System which is the robotic system on board the International Space Station. It is 17.6 m long when fully extended and has 7 motorized joints. It plays a key role in station assembly and maintenance. This arm is capable of handling large payloads of up to 116,00 kg and is able to assist with docking the space shuttle.

(a) the SCARA from ABB

(b) the IRB 460 from ABB

(c) FANUC 430i

(d) the VA1400 II from YASKAWA

(e) LBR IIWA from KUKA

(f) Canadarm 2

Figure 1.1. – Serial manipulators applied in various fields.

Nowadays, industrial robots rapidly take their niche in the drilling (Zhu et al. 2013) (Olsson et al. 2010), milling (Matsuoka et al. 1999) (Vosniakos and Matsas 2010), friction stir welding (Guillo and Dubourg 2016) (Mendes et al. 2016) and other operations (Leali et al. 2013) (Guo et al. 2016) (Denkena and Lepper 2015).

Obviously, serial manipulators are widely used in the industrial domains even in the space exploration. Until now, they are still the main products of the four leading manufacturers of robotic systems worldwide (ABB, KUKA, FANUC and YASKAWA).

However, as mentioned above, serial manipulators still have some drawbacks, such as accumulated position errors. Accumulated position error is caused by the character of serial chain. The best way to solve this problem is to improve the processing and assembly accuracy. For some technological operations as friction stir welding the serial robots have low rigidity. However, it can be solved by using more rigid links. Compared with the others, the highly coupled dynamics which is the inherent character of the serial manipulator is considered one of the prominent problems that influence the trajectory tracking accuracy.

1.2. Dynamics and control of serial manipulators

An effective way to deal with the problem of high complex coupled dynamics is the decoupling. In fact, this concept was first proposed by Morgan in 1964 when he tried to introduce the design method of the typical control theory into the MIMO (Multi-Input and Multi-Output) linear system (Descusse et al. 1988). Morgan searches the necessary condition in order that the closed-loop transfer function matrix is a full rank diagonal rational matrix.

As known, the form of the dynamic equation of the serial manipulator can be written as:

$$\tau = M(\theta)\ddot{\theta} + C(\theta,\dot{\theta})\dot{\theta} + g(\theta) \tag{1.1}$$

where τ is a $n\times1$ torque vector applied to the joints of the manipulator; $\theta,\dot{\theta}$ and $\ddot{\theta}$ are $n\times1$ vectors representing the angular positions, velocities and accelerations, respectively; $M(\theta)$ is $n\times n$ inertia matrix; $C(\theta,\dot{\theta})$ is $n\times1$ vector of Coriolis and centrifugal effects; $g(\theta)$ is the torque vector due to gravity.

The first term on the right hand side represents the inertia torque. It can be divided into two parts: the main diagonal elements of the matrix and the off-diagonal elements of the matrix. The first part is generated by the acceleration of the corresponding joint.

The second part is the interactive inertia torque caused by the accelerations of the other joints. This interactive inertia torque is linearly proportional to acceleration. The second term represents the nonlinear velocity torques resulting from Coriolis and centrifugal effects. Generally, the dependence of the inertia matrix on the arm configuration produces these nonlinear velocity torques.

For an arbitrary arm configuration, the inertia matrix $M(\theta)$ is reduced to a diagonal matrix if the off-diagonal elements of the matrix $M(\theta)$ are all zero. Then it is defined as decoupled inertia matrix. Hence, the control system can be treated as a set of SISO (Single-Input and Single-Output) subsystems.

When the second term $C(\theta,\dot{\theta})\dot{\theta}$ disappears, the inertia matrix is constant for all arbitrary arm configurations (the matrix $M(\theta)=M$ is independent of joint displacements). In this case, the inertia matrix is referred to as configuration invariant inertia matrix. The significance of this form is that the linear control methods which are much simpler and easier to implement can be adopted.

However, the most desirable form for the manipulator dynamics is the one with decoupled and configuration-invariant inertia matrix where the effects of gravity are compensated by mechanical engineering, that is

$$\tau = M\ddot{\theta} \tag{1.2}$$

where M is $n\times n$ diagonal inertia matrix.

In this case, the system is completely decoupled and linearized. This system can be treated as SISO systems with constant parameters.

As the main inherent character of the serial manipulators, the dynamic coupled results from varying inertia, interactions between the different joints and nonlinear forces such as Coriolis and centrifugal forces have obvious influence on the positioning accuracy. This influence exists both at slow speed and high speed, especially for the latter. Hence, many researchers devote to achieve the dynamic decoupling and linear situation. When this situation is realized:

- dynamic equation can be simplified and the controller can be treated as the superposition of serial SISO controller;

- the controller design can be simplified, hence the real-time operational performance of the manipulator can be improved because of the reduction of the computational burden;
- positioning error can be reduced by the eliminations of the Coriolis and centrifugal forces. Therefor the robustness of the serial manipulators is improved.

In the part of control, lots methods proposed out to reduce or even to eliminate such dynamic complexity of the serial manipulators.

1.2.1. PD control of serial manipulators

The control of most industrial manipulators in use today is based on the application of conventional servo control techniques such as PD (proportional-derivative) or PID (proportional-integral-derivative) control (Rocco 1996) (Santibanez and Kelly 1998) (Senthil Kumar and Karthigai Amutha 2014) (Su et al. 2007) (Craig 2005) (Kiam Heong Ang et al. 2005) (Ouyang et al. 2015). In this kind of method, the tracking errors which describe the difference between the desired and real trajectories are multiplied by gains, and then contribute as part of input torque to reduce the difference. This traditional control method is widely used because of its simple structure, easy implementation and robust operation.

It has been shown that a simple PD control applied at each joint is adequate in most position control applications such as spot-welding or palletizing. An independent joint PD controller has been shown to be asymptotic stable for rigid manipulators (Asada and Slotine 1986b). Consider an equation, without the effects of friction, where the gravity is compensated by the control law:

$$M(\theta)\ddot{\theta} + C(\theta,\dot{\theta})\dot{\theta} = \tau - g(\theta) = u \tag{1.3}$$

where

$$u = K_P(\theta_d - \theta) - K_D\dot{\theta} \tag{1.4}$$

be an independent joint PD control, where θ_d represents a constant reference set-point; K_P and K_D are positive, diagonal matrices of proportional and derivative gains, respectively. Consider the Lyapunov function candidate

$$V = \frac{1}{2}\dot{\theta}^T M(\theta)\dot{\theta} + \frac{1}{2}(\theta_d - \theta)^T K_P(\theta_d - \theta) > 0 \tag{1.5}$$

Then a simple calculation using the skew symmetry property shows that:

$$\dot{V} = -\dot{\theta}^T K_D \dot{\theta} \leq 0 \tag{1.6}$$

The function $\dot{V}$ is not negative definite. In this case, the LaSalle's theorem (Lasalle 1961), known today as LaSalle's invariance principle, may be used to prove the asymptotic stability.

$$\dot{\theta} = 0 \Rightarrow \ddot{\theta} = 0 \Rightarrow M(\theta)\ddot{\theta} + C(\theta,\dot{\theta})\dot{\theta} = K_P(\theta_d - \theta) - K_D\dot{\theta} = 0 \Rightarrow \theta = \theta_d \tag{1.7}$$

However, as shown here, the gravity parameters must be known exactly. The other limitation is simply due to the inherent "mismatch" between the nonlinear dynamics character of the manipulators and the linear regulating behavior of the PID or PD controller (Ouyang et al. 2006). Hence, this control method is not satisfactory for applications which require high tracking accuracy and high speed performance.

1.2.2. Inverse dynamics control of serial manipulators

In inverse dynamics control method, the system outputs are assumed as anticipative values. Then the corresponding inputs are calculated through the reversed state function. So, the inputs are functions of time and state variables. This is an inverse system of the original system. Finally, the two systems combine together compose an artificial linear system. Based on time-scale separation principle, the system can be separated into an inner control loop subsystem and an outer control loop subsystem by time-scale (Atashzar et al. 2010). If the inner control loop has already realized decoupling and obtained control performance well, the outer control loop can be simplified with classical control method. So the crux of inverse dynamics control is the design of the inner loop (Fig. 1.2).

Consider the dynamic model of a manipulator that described by equation (1.1), then the nonlinear feedback control law is given as (Levine 1996):

$$\tau = M(\theta)a_\theta + C(\theta,\dot{\theta})\dot{\theta} + g(\theta) \tag{1.8}$$

where $a_\theta \in \mathbb{R}^n$ is, as yet, undetermined. Since the inertia matrix $M(\theta)$ is invertible for all θ, the closed-loop system reduces to the decoupled double integrator.

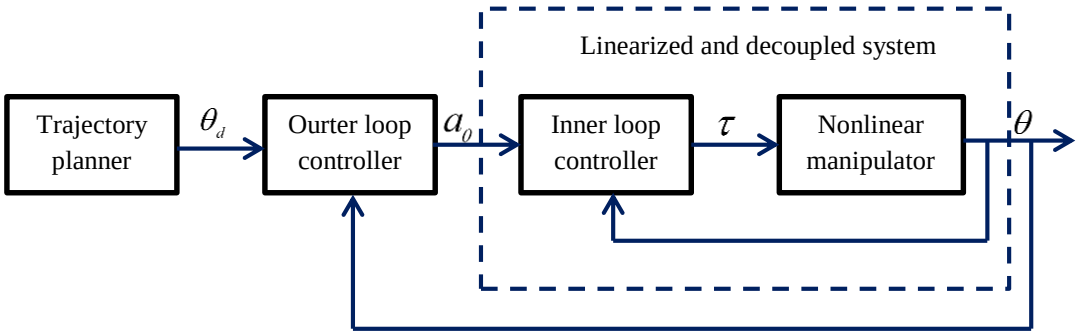

Figure 1.2. – The control scheme of inverse dynamics control.

$$\ddot{\theta} = a_\theta \tag{1.9}$$

Given a joint space trajectory, $\theta_d(t)$, an obvious choice for the outer loop term a_θ is as a PD plus feedforward acceleration control

$$a_\theta = \ddot{\theta}_d + K_P(\theta_d - \theta) - K_D(\dot{\theta}_d - \dot{\theta}) \tag{1.10}$$

Substituting equation (1.10) into equation (1.9) and defining

$$\tilde{\theta} = \theta - \theta_d \tag{1.11}$$

the linear and decoupled closed-loop system is obtained as

$$\ddot{\tilde{\theta}} + K_D\dot{\tilde{\theta}} + K_P\tilde{\theta} = 0 \tag{1.12}$$

In the robotics context, feedback linearization is also known as inverse dynamics. Although this method is possible in theory, it is difficult to achieve in practice, mainly because the coordinate transformation is a function of the system parameters and, hence, sensitive to uncertainty.

1.2.3. Control of the double integrator

The second-order linear and time-invariant dynamical system, called double integrator, is one of the most fundamental systems in control applications. It can be considered as single-degree-of-freedom translational and rotational motion. So, researchers are interested in double integrator since the early days of control theory when it was used extensively to illustrate minimum-time and minimum-fuel controllers

(Hocking 1991) (Yang and Slotine 1994) (Chen and Desrochers 1989). The equations of the double integrator are given by (Rao and Bernstein 2001).

$$\begin{aligned} \dot{x} &= Ax + Bu \\ y &= Cx \end{aligned} \tag{1.13}$$

where

$$x = \begin{bmatrix} \theta \\ \dot{\theta} \end{bmatrix}, A = \begin{bmatrix} 0 & 1 \\ 0 & 0 \end{bmatrix}, B = \begin{bmatrix} 0 \\ 1 \end{bmatrix}, C = \begin{bmatrix} 0 & 1 \end{bmatrix}.$$

Since the double integrator is unstable but completely controllable and observable, closed-loop control strategies can be used to drive the state to the origin in the finite time, some researches are carried out based on this kind of model (Bhat et al. 1998). In the other aspect, a simple linear double integrator relationship between the output and input is better for a tracking controller (Slotine et al. 1991).

In this thesis, the design of the controller is based on the state and the control law given by $u = -Gx$.

The function of the gain matrix $G = \begin{bmatrix} g_1 & g_2 \end{bmatrix}$ is to stabilize the system by moving the closed-loop poles in the left-half complex plane. We seek u that minimizes the cost

$$J = \int_0^\infty \left[\; Ly^2 + u^2 \; \right] dt = \int_0^\infty \left[\; x^T Q_C x + u^2 \; \right] dt \tag{1.14}$$

The matrix L is based on the controllability transient gramian defined by

$$G_C(0, T_P) = \int_0^{T_P} \left[\; e^{At} B B^T e^{A^T t} \; \right] dt \tag{1.15}$$

For the matrix $L = \left[\; T_P C G_C(0, T_P) C^T \; \right]^{-1}$, the matrix $Q_C = C^T L C$ is symmetric and semi-definite positive. The parameter T_p assume that poles of closed-loop system may be placed, in the S plane, at the left or near of the vertical straight with the abscissa $-\frac{1}{T_P}$. The output equation $u = -Gx$ of the controller is unique, optimal, full state feedback control law with $G = B^T \Sigma_C$ that minimizes the cost *J*.

The matrix Σ_C is the unique, symmetric, positive definite solution to the algebraic Riccati equation $A^T\Sigma_C + \Sigma_C A - \Sigma_C BB^T\Sigma_C + Q_C = 0$.

For the double integrator, the matrix G gives: $G = \left[\; g_1 = \frac{\sqrt{3}}{T_P^2} \quad g_2 = \frac{\sqrt{2\sqrt{3}}}{T_P} \; \right]$.

Then the closed-loop characteristic polynomial is: $P_C(s) = s^2 + \frac{\sqrt{2\sqrt{3}}}{T_P} s + \frac{\sqrt{3}}{T_P^2}$.

If $P_C(s) = s^2 + 2\zeta\omega_n s + \omega_n^2$, we have: $\omega_n = \frac{\sqrt{\sqrt{3}}}{T_P}$ and $\zeta = \frac{\sqrt{2}}{2}$.

The closed-loop control law, presented by Fig. 1.3, can be written as

$$u = \ddot{\theta}_R - g_1[\theta - \theta_R] - g_2[\dot{\theta} - \dot{\theta}_R] \tag{1.16}$$

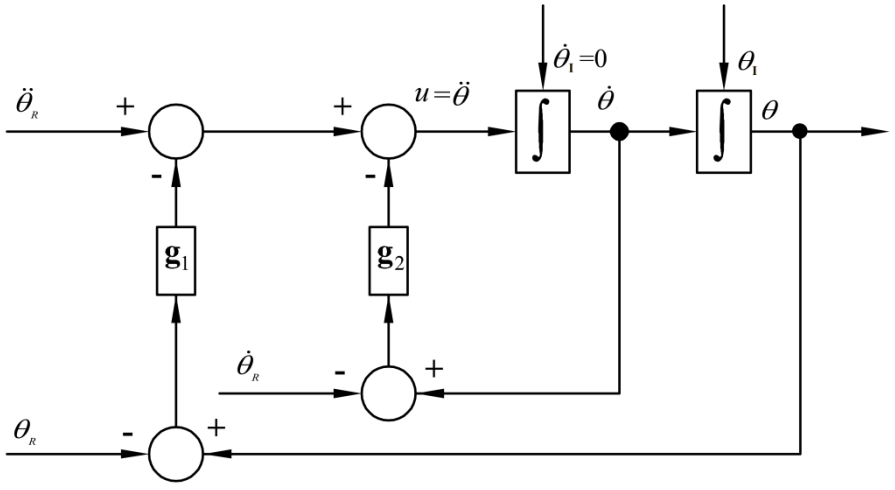

Figure 1.3. – The closed-loop control law of double integrator system.

In the case of some characterization of the model uncertainties, we propose a robust controller based from estimate state and implicit integral action (Arakelian et al. 2016b).

The zero-steady-state error optimal control law is given by $u(t) = -G\hat{x} - \hat{d}$.

The gain matrix G is given by same manner as previously because feedback and observer can be design separately without destroying stability properties for each other.

The estimate of the state-vector x is $\hat{x}$ and $\hat{d}$ is an estimate of the constant disturbance d placed in the state equation of the double integrator.

For obtain the observer, we model the constant disturbance as $\dot{d} = 0$.

The steady-state optimal observer which allows estimating x and d is

$$\underbrace{\begin{bmatrix} \dot{\hat{\theta}} \\ \ddot{\hat{\theta}} \end{bmatrix}}_{\dot{\hat{x}}} = \underbrace{\begin{bmatrix} 0 & 1 \\ 0 & 0 \end{bmatrix}}_{A} \underbrace{\begin{bmatrix} \hat{\theta} \\ \dot{\hat{\theta}} \end{bmatrix}}_{\hat{x}} + \underbrace{\begin{bmatrix} 0 \\ 1 \end{bmatrix}}_{B} u(t) + \underbrace{\begin{bmatrix} 0 \\ 1 \end{bmatrix}}_{B} \hat{d} + \begin{bmatrix} k_1 \\ k_2 \end{bmatrix} \left(y - \underbrace{\begin{bmatrix} 1 & 0 \end{bmatrix}}_{C} \underbrace{\begin{bmatrix} \theta \\ \dot{\theta} \end{bmatrix}}_{x} \right) \tag{1.17}$$

$$\dot{\hat{d}}(t) = k_3 \left(y - \underbrace{\begin{bmatrix} 1 & 0 \end{bmatrix}}_{C} \underbrace{\begin{bmatrix} \hat{\theta} \\ \dot{\hat{\theta}} \end{bmatrix}}_{\hat{x}} \right) \tag{1.18}$$

The state-equations of the observer are:

$$\underbrace{\begin{bmatrix} \dot{\hat{\theta}} \\ \ddot{\hat{\theta}} \\ \dot{\hat{d}} \end{bmatrix}}_{\dot{x}_E} = \underbrace{\begin{bmatrix} -k_1 & 1 & 0 \\ -k_2 & 0 & 1 \\ -k_3 & 0 & 0 \end{bmatrix}}_{A_E} \underbrace{\begin{bmatrix} \theta \\ \dot{\theta} \\ \hat{d} \end{bmatrix}}_{x_E} + \underbrace{\begin{bmatrix} 0 \\ 1 \\ 0 \end{bmatrix}}_{B_E} u + \underbrace{\begin{bmatrix} k_1 \\ k_2 \\ k_3 \end{bmatrix}}_{K} y \tag{1.19}$$

where, $y = \underbrace{\begin{bmatrix} 1 & 0 & 0 \end{bmatrix}}_{C_E} x_E$.

The function of the gain matrix $K = \begin{bmatrix} k_1 & k_2 & k_3 \end{bmatrix}^T$ is to stabilize asymptotically the observer. The duality between the optimal regulator and the optimal observer (Kalman filter) enables us to transfer from the regulator to the observer all important results. The Riccati equation can be rephrased as $A_E \Sigma_O + \Sigma_O A_E^T - \Sigma_O C_E^T C_E \Sigma_O + Q_O = 0$.

The matrix $Q_O = \left[\ T_R G_O(0,T_R)\ \right]^{-1}$ is based on the observability transient gramian defined by $G_O(0,T_R) = \int_0^{T_R} \left[\ e^{A_E^T t} C_E^T C_E e^{A_E t}\ \right] dt$. The parameter T_R assume that poles of the observer may be placed, in the s plane, at the left or near of the vertical straight with the abscissa $-\frac{1}{T_R}$. The solution of the Riccati equation is given by:

$$K = \Sigma_O C_E^T = \left[k_1 = \frac{c_1}{T_R} \quad k_2 = \frac{c_2}{T_R^{\,2}} \quad k_3 = \frac{c_3}{T_R^{\,3}} \right]^T \tag{1.20}$$

For $c_1^2 - 2c_2 = 9$ and $c_3 = 12\sqrt{5}$, the values are: $c_1 = 7.198; c_2 = 21.408; c_3 = 26.83$.

Then the characteristic polynomial is: $P_O(s) = \left(s + \frac{3.0735}{T_R} \right)\left(s^2 + \frac{4.1248}{T_R} s + \frac{8.7303}{T_R^2} \right)$.

If $P_O(s) = \left(s + \omega_1\right)\left(s^2 + 2\zeta\omega_0 s + \omega_0^2\right)$, we have $\omega_0 = \frac{2.9547}{T_R}$ and $\zeta = 0.698$.

The Fig. 1.4 shows the closed-loop control system which accumulates information about the double integrator during operation and allows a zero steady-state tracking error in spite of constant disturbance d defined by $\dot{d} = 0$.

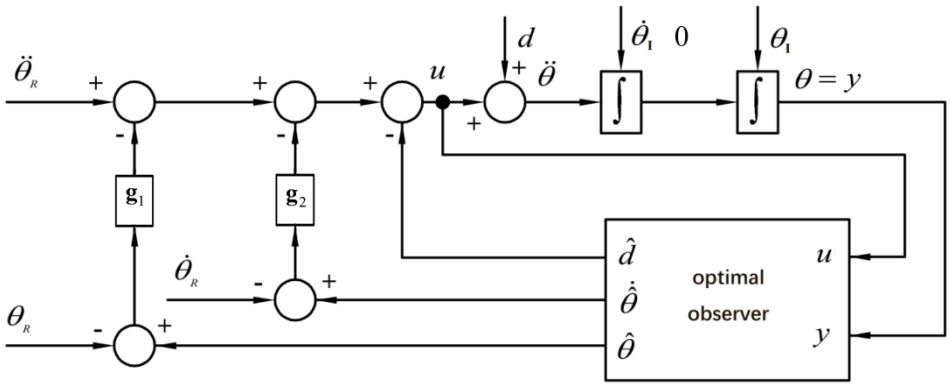

Figure 1.4. – The closed-loop control system of the double integrator with optimal observer block.

The closed-loop control law can be written as

$$u = \ddot{\theta}_R - g_1\left[\theta - \theta_R\right] - g_2\left[\dot{\theta} - \dot{\theta}_R\right] - \hat{d} \tag{1.21}$$

1.2.4. The other control methods

Adaptive control in where the coupled term is treated as measurable disturbance, then a self-tuning feed-forward control method is used to response to the changes in the dynamics of the manipulator (Kolhe et al. 2013) (Slotine and Li 1987). Thus, the exact real-time decoupling can be achieved. This method can deal with the parameter uncertainties (Tran et al. 2015) (Tran et al. 2016), however, it requires real-time online model identification which causes extensive computational burdens. In addition, since the adaptive control generally does not guarantee that the estimated parameters of the manipulators converge to their real values, tracking errors will be repeated as the manipulators repeat their tasks (Sun and Mills 1999).

A certain number of control methods are identified as intelligent control, such as artificial neural networks (Nawrocka et al. 2016) (Sun et al. 2016), fuzzy logic (Chen Ken et al. 1988) (Xu et al. 1991) (Piltan et al. 2011) and expert systems (De Silva and MacFarlane 1989). The common character of these control methods is that they usually involve learning in some form or another. Like adaptive control method, these intelligent controls also can deal well with the non-structural uncertainties. A major advantage of using these intelligent controls as compared to conventional adaptive system is the lack of necessity to be familiar with the mathematical description of the dynamics of the process. However, in common, these methods have no standard system-theoretic approach to algorithms.

Besides, there are optimal control (Lin and Brandt 1998) (Bobrow et al. 1985), robust control (Kolhe et al. 2013), feedback control, iterative learning control (Kuc et al. 1991) (Sugie and Ono 1991) and etc. Moreover, the hybrid control which concluding at least two or three control methods, such fuzzy PID control (Petrov et al. 2002) (Li et al. 2001), adaptive fuzzy control (Yoo and Ham 2000) (Jin 1998).

As known, these control methods really works for improving the performance of the serial manipulator. However, if only taking into account the design of controller, its algorithm which becomes huger and more complex will be a big computational burden, the burden of iterative calculations consumes a lot of memory and also they are relatively slow in comparison with nonlinear controllers. The overall high cost of practically implementing such controllers made them unattractive to customers' opinion.

1.3. Design of manipulators with linear and decoupled dynamics

As mentioned above, the dynamics of a manipulator arm depends upon the mass properties of individual arm links and the kinematic structure of the arm linkages. Hence, usually, the redistribution of mass and modification of the arm structure are used to reducing the dynamic complexity of the manipulators.

Let us consider three main approaches developed for dynamic decoupling of manipulators.

1.3.1. Decoupling of dynamic equations via mass redistribution

The necessary conditions for the decoupled and configuration-invariant inertia of the general manipulator are given in (Youcef-Toumi and Asada 1986a). Let us disclose the necessary properties of mass distribution to reach this goal.

Let θ_i and τ_i, be the joint displacement and torque of the *i*th joint, respectively, then the equation of motion of the manipulator is given by

$$\tau_i = H_{ii}\ddot{\theta}_i + \sum_{j\neq i} H_{ij}\ddot{\theta}_j + \sum_j \sum_k \left(\frac{\partial H_{ij}}{\partial \theta_k} - \frac{1}{2}\frac{\partial H_{jk}}{\partial \theta_i} \right) \dot{\theta}_j \dot{\theta}_k + \tau_{gi} \qquad (1.22)$$

where H_{ij} is the *i*-*j* element of the manipulator inertia matrix, and τ_{gi} is the torque due to gravity. The first term of this equation represents the inertia torque generated by the acceleration of the *i*th joint, while the second term is the interactive inertia torque caused by the accelerations of the other joints. The interactive inertia torque is linearly proportional to acceleration. The third term represents the nonlinear velocity torques resulting from Coriolis and centrifugal effects. In general, the dependence of the inertia matrix on the arm configuration produces these nonlinear velocity torques.

Consider the inertia matrix that reduces to a diagonal matrix for an arbitrary arm configuration, then the second term in equation mentioned above vanishes and no interactive torques appear. The manipulator inertia matrix in this case is referred to as a decoupled inertia matrix. The significance of the decoupled inertia matrix is that the control system can be treated as a set of single-input, single-output subsystems associated with individual joint motions.

The equation of motion under these conditions reduces to

$$\tau_i = H_{ii}\ddot{\theta}_i + \sum_k \left(\frac{\partial H_{ii}}{\partial \theta_k} \dot{\theta}_j \dot{\theta}_k - \frac{1}{2} \frac{\partial H_{kk}}{\partial \theta_k} \dot{\theta}_k^2 \right) + \tau_{gi} \tag{1.23}$$

where the second term represents the nonlinear velocity torques resulting from the spatial dependency of the diagonal elements of the inertia matrix. Note that the number of terms involved in this equation is much smaller than the number of original nonlinear velocity torques, because all the off diagonal elements are zero for $\theta_1,...,\theta_n$. This reduces the computational complexity of the nonlinear torques.

Another significant form of the inertia matrix that reduces the dynamic complexity is a configuration-invariant form. The inertia matrix in this case does not vary from an arbitrary arm configuration. In other words, the matrix is independent of joint displacements, hence the third term in first equation vanishes and the equation of motion reduces to

$$\tau_i = H_{ii}\ddot{\theta}_i + \sum_j H_{ij}\ddot{\theta}_j + \tau_{gi} \tag{1.24}$$

Note that the coefficients H_{ii} and H_{ij} are constant for all arm configurations. Thus, the equation is linear except the last term, that is, the gravity torque. The inertia matrix in this form is referred to as an invariant inertia matrix. The significance of this form is that linear control schemes can be adopted, which are much simpler and easier to implement.

When the inertia matrix is both decoupled and configuration invariant, the equation of motion reduces to

$$\tau_i = H_{ii}\ddot{\theta}_i + \tau_{gi} \tag{1.25}$$

The system is completely decoupled and linearized, except the gravity term. Thus, we can treat the system as single-input, single-output systems with constant parameters.

Now let us consider the optimum mass redistribution to ensure a dynamic decoupling.

As shown in Fig. 1.5, the manipulator is assumed to be an open kinematic chain consisting of only revolute joints. The joints are numbered 1 through *n* from the proximal joint to the distal joint. The link between joints *i* and *i*+1 is called link *i*. The

direction of the axis of joint *i* is represented by a unit vector b_i, and the displacement of link *i* is denoted by θ_i which is the angle of rotation about the unit vector.

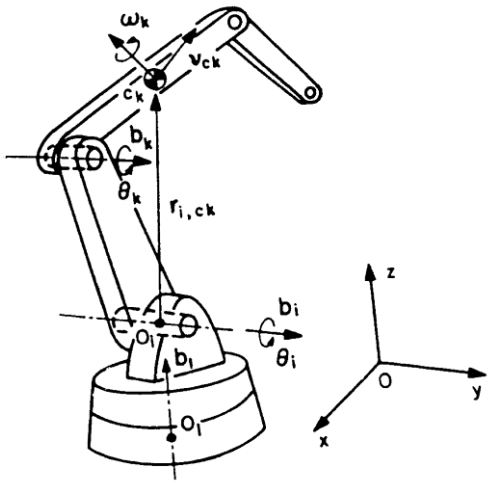

Figure 1.5. – An open kinematic chain manipulator with revolute joints.

The center of mass of link *k* is shown by point c_k in the figure, the velocity vector of the center of mass is denoted by V_k and the angular velocity vector by ω_k. Let m_k and I_k be the mass and the inertia tensor of link *k* with respect to the *O-xyz* inertial reference frame, then the total kinetic energy stored in the arm links from 1 to *n* is given by

$$T = \sum_{k=1}^{n} \frac{1}{2} \left(m_k V_{ck}^T V_{ck} + \omega_k^T I_k \omega_k \right) \tag{1.26}$$

The motion of link *k* is generated by the preceding joint motions. The angular velocity ω_k, for example, is given by

$$\omega_k = \sum_{i=1}^{k} b_i \dot{\theta}_i \tag{1.27}$$

To represent the linear velocity of the center of mass c_k, we denote the position vector from an arbitrary point on the *i*th joint axis to the center of mass c_k by vector $r_{i,ck}$. Then,

$$V_{ck} = \sum_{i=1}^{k} b_i \dot{\theta}_i \times r_{i,ck} \tag{1.28}$$

Substituting two last equations into equation $T = \sum_{k=1}^{n} \frac{1}{2}\left(m_k V_{ck}^T V_{ck} + \omega_k^T I_k \omega_k \right)$, we obtain

$$T = \frac{1}{2} \sum_{i=1}^{n} \sum_{j=1}^{n} H_{ij} \dot{\theta}_i \dot{\theta}_j \tag{1.29}$$

where H_{ij} is the *i*–*j* element of the $n \times n$ manipulator inertia matrix given by

$$H_{ij} = \sum_{k=\max[i,j]}^{n} \left[m_k \left(b_i^T b_j \cdot r_{i,ck}^T r_{j,ck} - b_j^T r_{i,ck} \cdot b_i^T r_{j,ck} \right) + b_i^T I_k b_j \right] \tag{1.30}$$

Note that the inertia matrix is symmetric, hence $H_{ij} = H_{ji}$.

In order to eliminate the coupling and nonlinear torques, the inertia matrix must be diagonalized and made invariant for all the arm configurations.

Figure 1.6 shows two kinds of structure designs for serial manipulators with decoupled and configuration invariant torques.

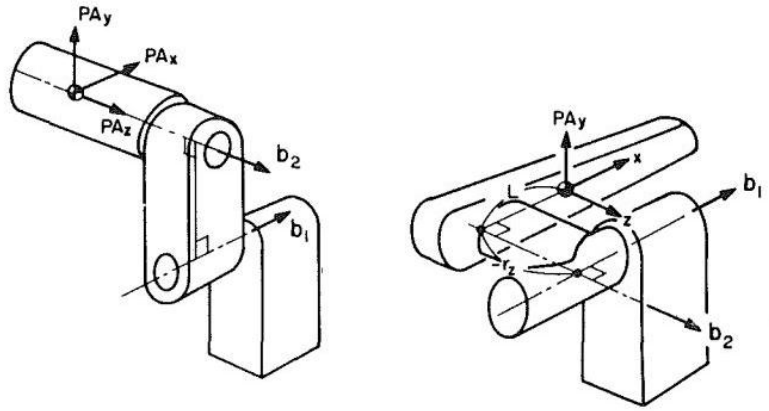

(a) (b)

Figure 1.6. – Two kinds of structure designs for serial manipulators with decoupled and configuration invariant torques (Youcef-Toumi and Asada 1987).

The linearization of the dynamic equations and their decoupling via optimum inertia redistribution (Abdel-Rahman and Elbestawi 1991; Arakelian and Dahan 1995;

Asada and Slotine 1986a; Asada and Youcef-Toumi 1984a; Filaretov and Vukobratović 1993; Minotti and Pracht 1992; Yang and Tzeng 1985, 1986, Youcef-Toumi and Asada 1985, 1986), which can be achieved when the inertia tensors are diagonal and independent of manipulator configuration.

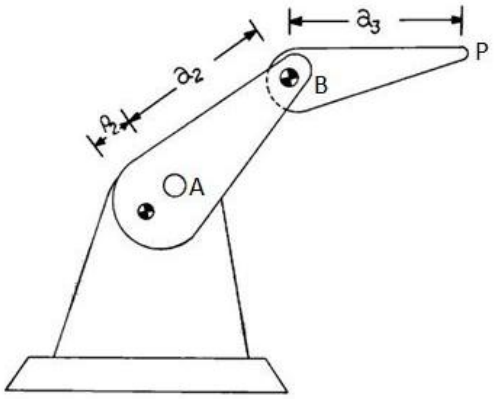

Figure 1.7. – Design for a 3 DOF manipulator with linear dynamics.

Figure 1.8. – KUKA robot with mass redistribution simplifying its dynamics.

In the research (Yang and Tzeng 1986), a three-link model is considered (Fig. 1.7). As shown, the form of the links is modified to achieve the linearization condition. The mass centers should be located in the extensions of links AB and BP. Meanwhile, the inertia of links is required to be nearly symmetrical in both axial and transverse directions. Based on this kind of structure, the complexity of its dynamics is significantly reduced.

Figure 1.8 shows a KUKA robot in which the motor arrangements and the mass redistribution are based on the mentioned above design concept simplifying the complexity of its dynamics.

The linearization and dynamic decoupling of 3 DOF manipulators have also been considered (Youcef-Toumi and Asada 1987). As shown in Fig. 1.9, axis b_1 and b_2 are perpendicular to each other, that is, these two rotations along axis b_1 and b_2 are decoupled. The axis b_2 and b_3 are parallel, however, the center mass of link 3 coincide with its rotational axis b_3, and the total mass center of link 2 and link 3 is right on the rotational axis b_2. These conditions derive the invariant inertia. In this research, all of the arm constructions that yielded the decoupled inertia matrices were determined. The approach in this research is applied to serial manipulators in which the axis of joints are

not parallel. In the case of parallel axes such an approach allows linearization of the dynamic equations but not their dynamic decoupling (Gompertz and Yang 1989). Thus, in the case of planar serial manipulators, it cannot be used.

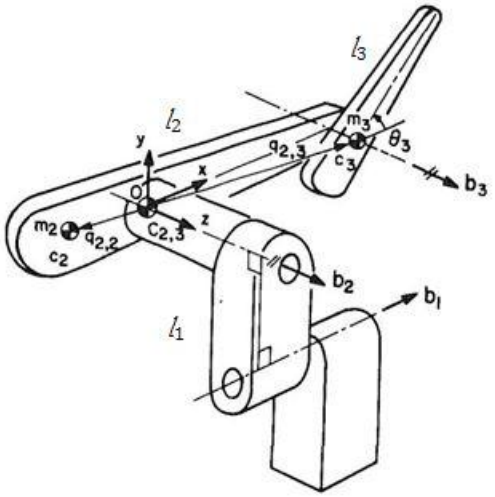

Figure 1.9. – Designs for 3 DOF manipulators with configuration invariant inertia.

Finally, it should be noted that for serial manipulator arms with an open kinematic chain structure, the inertia matrix cannot be decoupled unless the joint axes are orthogonal to each other (Fig. 1.6).

1.3.2. Decoupling of dynamic equations via actuator relocation

A popular configuration for the actuation of robot manipulators with actuated joints is to have motors directly attached to the joints. This design does not involve any transmission elements between the actuators and the joints. However, in certain cases this configuration may not be appropriate and manipulators with remotely-actuated joints may be desirable from point of view of the simplified dynamics.

In this case the dynamic decoupling follows from the kinematic decoupling of motion when the rotation of any link is due to only one actuator. It is obvious that it must be accompanied by an optimal choose the mass properties of certain links.

The five-bar-link mechanism shown in Fig. 1.10 (Asada and Youcef-Toumi 1984b) is the first structure that achieves the dynamic decoupling. The distance between the two motors is zero and fixed on the base. Because of this special motor location, the weight of one motor is not a load on the other. Also the reaction torque of one motor does not

act directly upon the other. An arm mechanism in which motors are mounted on a fixture and the weight and reaction torque of one motor do not affect the other motors directly is referred to as a parallel drive mechanism. In this mechanism, the overall inertias about the two motor axes are invariant respectively. Furthermore, the interactive inertia torques are eliminated by modification of the mass ratio of link 3 and link 4 and the ratio of mass center distances of the two links. Thus, the inertia tensor is invariant and completely decoupled.

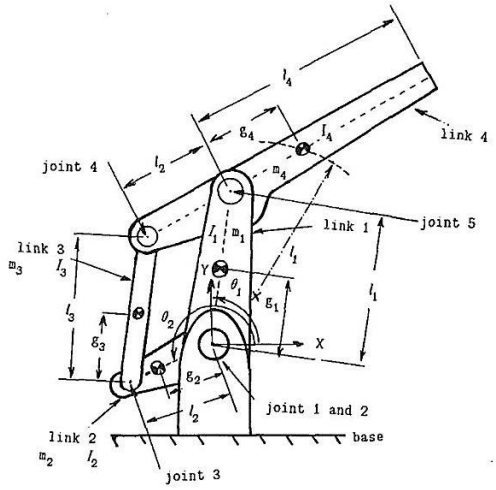

Figure 1.10. - The first structure with dynamic decoupling.

The review have shown that the design concept with remote actuation is not optimal from the point of view of the precise reproduction of the end-effector tasks because it accumulates all errors due to the clearances and elasticity of the belt transmission mainly used (Fig. 1.11).

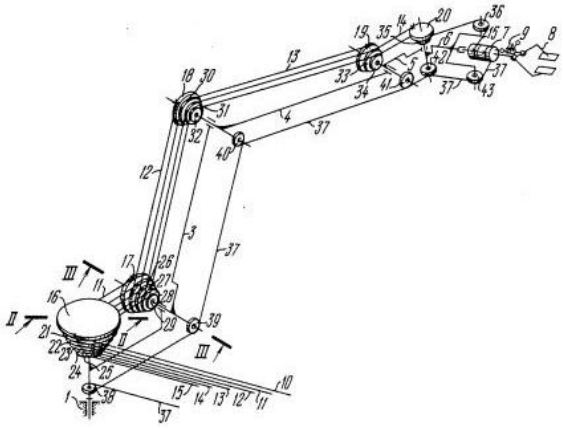

Figure 1.11. – A linearization and dynamic decoupling model via actuator relocation (Belyanin et al. 1981).

Obviously, it is lot better to connect actuators directly with links than to use transmission mechanisms. The manufacturing and assembly errors of the added transmission mechanisms also have a negative impact to the robot precision.

1.3.3. Decoupling of dynamic equations via addition of auxiliary links

The linearization of the dynamic equations and their decoupling via redesign of the manipulator by adding auxiliary links has also been developed (Arakelian et al. 2011) (Arakelian and Sargsyan 2012) (Coelho et al. 2004) (Moradi et al. 2010). The dynamic decoupling via redesign of the manipulator by adding auxiliary links is a promising new approach in the robotics.

Figure 1.12 shows a modified 2-DOF serial manipulator with two added gears (Coelho et al. 2004).

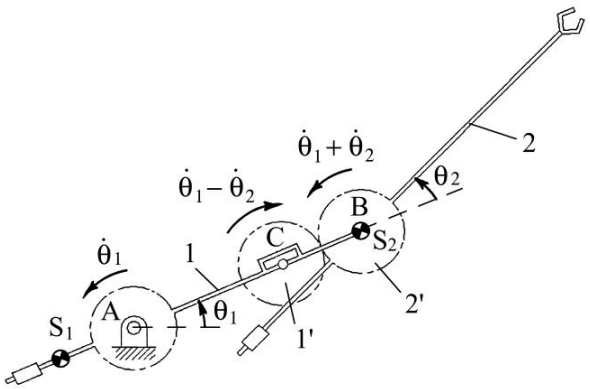

Figure 1.12. – A 2 DOF manipulator with addition of two gears.

Ensuring condition

$$I_{S2}+I_{S2'}=I_{S1'} \tag{1.31}$$

the dynamic equations of the manipulator are decoupled:

$$\tau_1=\left[m_1 l_{AS1}^2+\left(m_2+m_{2'}\right)l_1^2+m_{1'}l_{AC}^2+I_{S1}+I_{S1'}+I_{S2}+I_{S2'}\right]\ddot{\theta}_1 \tag{1.32}$$

$$\tau_2=\left(I_{S2}+I_{S2'}+I_{S1'}\right)\ddot{\theta}_2 \tag{1.33}$$

where, l_1, l_2 are the lengths of links 1 and 2; l_{AS1} is the distance between the centre of mass S_1 of link 1 and joint centre *A*; l_{AC} is the distance between the centre of joint *A* and joint centre *C*; m_1, m_2 are the masses of links 1 and 2; I_{S1} is the axial moment of inertia of link 1 relative to the centre of mass S_1 of link 1; I_{S2} is the axial moment of inertia of link 2 relative to the centre of mass S_2 of link 2; $I_{S1'}$ is the axial moment of inertia of gear *1'*; $I_{S2'}$ is the axial moment of inertia of gear *2'*; $\ddot{\theta}_1$ is the angular acceleration of link 1 relative to the base; $\ddot{\theta}_2$ is the angular acceleration of link 2 relative to link 1.

However, the design methodology proposed in (Coelho et al. 2004), which claims that it is the first time the added links have been used for dynamic decoupling, leads to the unavoidable increase of the total mass of the manipulator. This is due to the disposition of the added elements in the end of each link.

In (Arakelian and Sargsyan 2012) a solution has been proposed permitting the dynamic decoupling of the serial manipulators with a relatively small increase in the total mass of the moving links (Fig. 1.13).

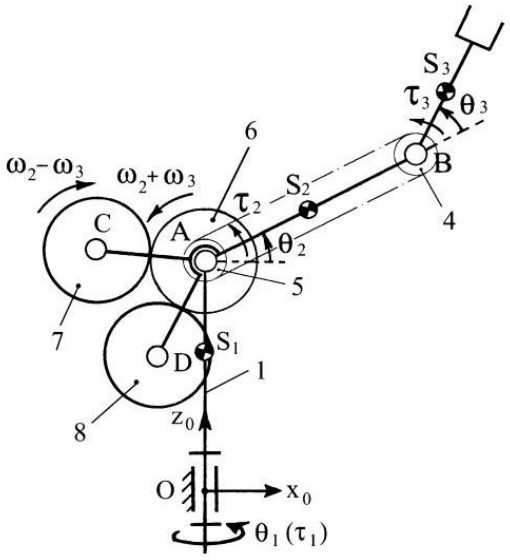

Figure 1.13. – A 3 DOF manipulator with addition of gear group.

In (Arakelian et al. 2016a), epicyclic gear train has been used to carry out the dynamic decoupling of the exoskeleton arm.

Nevertheless, it should be noted that such a technique has a major disadvantage: the need for the connection of gears to the oscillating links. The gears added to the oscillating links of the manipulator are sources of shocks between teeth that will lead to the perturbation of the operation of the manipulator, and to noise and other negative effects.

1.4. Summary

In this chapter, a brief review of serial manipulators with simplified dynamics has been presented. Simple structure, low cost, large workspace and mature technology, these advantages make the serial manipulators are widely used in many industrial fields. With the rapid development of industry, some new strict requirements are proposed, such as high stability, high positioning accuracy, high speed operation and etc.

One of the ways to improve the mentioned requirements is the design of manipulators with dynamic decoupling. As was mentioned above it can be reached by control or design solutions.

The dynamic decoupling via mass redistribution is simple and it found practical applications. However, as was mentioned above this solution can be used for dynamic decoupling of serial manipulators with orthogonal dispositions of joint axes. In the case of serial manipulators with parallel axes actuator relocation or auxiliary mechanisms are used.

However, from the above review can be concluded that all known mechanical solutions can only be reached by a considerably more complicated design of the initial structure via adding gears to the oscillating links leading to the unavoidable drawbacks. The gears added to the oscillating links of the manipulator are sources of shocks between teeth that will lead to the perturbation of the operation of the manipulator, and to noise and other negative effects.

Thus, it becomes evident that it is more optimal to carry out the dynamic decoupling via adding simple linkages ensuring an opposite motion of links without using gears. Therefore, one of the goals is to find simple linkages permitting to carry out complete dynamic decoupling of serial manipulators.

The review has shown that the influence of the payload on the dynamic coupling remains lightly studied. It is obvious that mechanical solutions for adjustment of nonlinear terms of dynamic equations due to the changing payload can be reached by very complicated design solutions. It is not attractive for practical applications. Therefore, it becomes evident that it is necessary to find new more simple solutions permitting to take into account the changing payload in the problems of dynamic decoupling.

On the other hand, dynamic decoupling via optimal control of a manipulator with a nonlinear system model and a changing payload is also rather complex task. That is why, this work will propose new approaches of dynamic decoupling, which are a symbiosis of mechanical and control solutions. To reach this purpose, the dynamic decoupling may be carried out in two steps.

In the first step, the dynamic decoupling of serial manipulator will achieved via the opposite rotation of links and their optimal redistribution of masses. Such a solution will eliminate the need for the connection of gears to the oscillating links. This is the first main advantage of the suggested mechatronic approach. Thus, the proposed mechanical solution will allow one to transform the original nonlinear system model into a fully linear system without using the feedback linearization technique.

It is obvious that the changing payload leads to the perturbation of the dynamic decoupling of the manipulator and it must be eliminated.

Therefore, in second step, the dynamic decoupling of the equation of motion due to the changing payload will be carried out using control techniques.

Such an approach is promising because it combines the advantages of two different principles: mechanical and control. As mentioned above the mechanical solutions, which can be used for dynamic decoupling of motion equations taking into account the changing payload, can only be reached with any undue complication of the design. Divers actuated counterweights should be applied. Such an approach is not viable. However, the linearized dynamic of the manipulator via opposite rotation of manipulator’s links leads to the relatively simple equations, which are easier to analyze for further dynamic decoupling taking into account the changing payload. In other terms, the mechanical solution to be developed will lead to the linearized equations of the manipulator, which then facilitate the optimal control design for decoupling of dynamic equations taking into account the changing payload. This is the second main advantage of the mechatronic design to be developed.

These mechatronic solutions will certainly improve the known design concepts permitting the dynamic decoupling of serial manipulators with a relatively small increase in to total mass of the moving links and it takes into account the changing payload.

Chapter 2

Design of adjustable serial manipulators with decoupled dynamics

In this chapter, a new approach for dynamic decoupling of serial planar manipulators, which is a symbiosis of mechanical and control solutions is proposed. It is based on the opposite motion of manipulator links and the optimal command design. The opposite motion of links with optimal redistribution of masses allows the cancellation of the coefficients of nonlinear terms in the manipulator's kinetic and potential energy equations.

Then, based on this completely linearized and decoupled manipulator, the simple linear control method is used. Furthermore, the changing payload is taken into account as a forward compensation in the controller. Finally, in order to stabilize the manipulator linearized and decoupled, a full state feedback is set up.

The suggested design methodology is illustrated by simulations carried out using ADAMS and MATLAB software, which have confirmed the efficiency of the developed approach.

2.1. Design concept of manipulators with adjustable links

As mentioned in the previous chapter, the inherent character of coupled dynamics is the prominent factor that impacts the operation accuracy and velocity performances of the serial manipulators. In this chapter, a mechatronic method is proposed to achieve the dynamic decoupling. The advantages of the suggested solution are：

- a simple linkage is added for achieving the dynamic decoupling of the serial planar manipulators. It allows a dynamic decoupling of manipulators without connection of gears to the oscillating links of the manipulator having leading to imperfections reviewed in chapter 1.
- the simplification of the controller based on the linearized input/output relationships, hence the computational burden caused by the huge amount of iterative calculation is vanished. The real-time performance can be improved.
- the feasibility of the linear control method that used in this kind of manipulator.
- the changing payload can be taken into account based on the dynamic decoupling manipulator.

Figure 2.1 shows the proposed adjustable serial manipulator for ensuring the dynamic decoupling of motion equations.

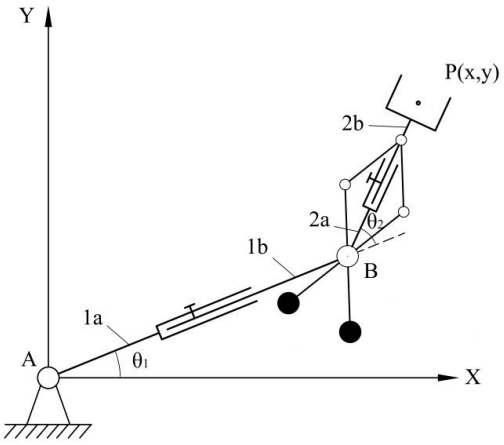

Figure 2.1. – Design concept of dynamically decoupled planar serial manipulator with adjustable links.

It is composed of link 1 with elements 1a, 1b and link 2 with elements 2a, 2b. The adjustable links of the manipulator allow an optimal selection of the lengths $L_1 = L_{AB}$ and $L_2 = L_{BP}$ of links 1 and 2, which ensures an identical and opposite rotation of links.

It can also be seen that the proposed manipulator is provided with a double Scott–Russell mechanism, which ensures the static balancing of link 2 for any position of element 2b.

To disclose the operation of the proposed adjustable manipulators, let's first consider the dynamic decoupling of an arbitrary serial manipulator.

2.1.1. Dynamic decoupling modeling of an arbitrary serial manipulator

So let’s start by the dynamic decoupling of a serial planar manipulator with two degrees of freedom shown in Fig. 2.2.

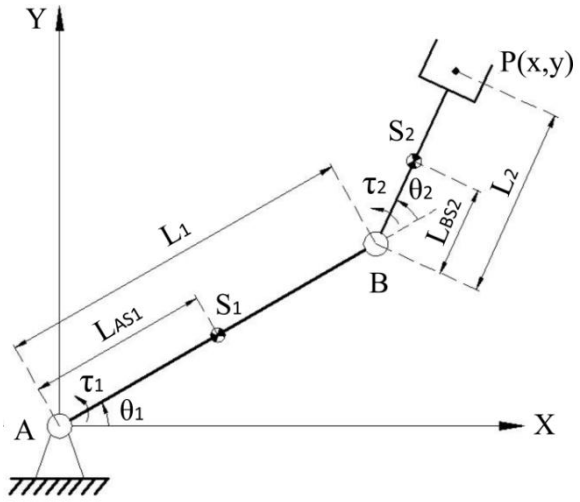

Figure 2.2. – An arbitrary planar serial manipulator.

According to Lagrangian dynamics, the equations of motion can be written as

$$\begin{bmatrix}\tau_1\\ \tau_2\end{bmatrix}=\begin{bmatrix}D_{11} & D_{12}\\ D_{21} & D_{22}\end{bmatrix}\begin{bmatrix}\ddot{\theta}_1\\ \ddot{\theta}_2\end{bmatrix}+\begin{bmatrix}D_{111} & D_{122}\\ D_{211} & D_{222}\end{bmatrix}\begin{bmatrix}\dot{\theta}_1^2\\ \dot{\theta}_2^2\end{bmatrix}+\begin{bmatrix}D_{112} & D_{121}\\ D_{212} & D_{221}\end{bmatrix}\begin{bmatrix}\dot{\theta}_1\dot{\theta}_2\\ \dot{\theta}_1\dot{\theta}_2\end{bmatrix}+\begin{bmatrix}D_1\\ D_2\end{bmatrix} \quad (2.1)$$

with

$$D_{11} = m_1 L_{AS1}^2 + m_2 L_1^2 + m_2 L_{BS2}^2 + 2m_2 L_1 L_{BS2}\cos\theta_2 + I_{S1} + I_{S2} \quad (2.2)$$

$$D_{12} = D_{21} = m_2 L_{BS2}^2 + m_2 L_1 L_{BS2} \cos\theta_2 + I_{S2} \tag{2.3}$$

$$D_{22} = m_2 L_{BS2}^2 + I_{S2} \tag{2.4}$$

$$D_{111} = 0 \tag{2.5}$$

$$D_{122} = -m_2 L_1 L_{BS2} \sin\theta_2 \tag{2.6}$$

$$D_{211} = m_2 L_1 L_{BS2} \sin\theta_2 \tag{2.7}$$

$$D_{222} = 0 \tag{2.8}$$

$$D_{112} = D_{121} = -m_2 L_1 L_{BS2} \sin\theta_2 \tag{2.9}$$

$$D_{212} = D_{221} = 0 \tag{2.10}$$

$$D_1 = \left(m_1 L_{AS1} + m_2 L_1\right) g \cos\theta_1 + m_2 g L_{BS2} \cos\left(\theta_1 + \theta_2\right) \tag{2.11}$$

$$D_2 = m_2 g L_{BS2} \cos\left(\theta_1 + \theta_2\right) \tag{2.12}$$

where τ_1 and τ_2 are respectively the actuator torques in A and B; L_1, L_2 are the lengths of links AB and BP; θ_1 is the angular displacement of link AB relative to the base; θ_2 is the angular displacement of link BP relative to link AB; $\dot{\theta}_1$ is the angular velocity of link AB relative to the base; $\dot{\theta}_2$ is the angular velocity of link BP relative to link AB; m_1, m_2 are the masses of links AB and BP; $\ddot{\theta}_1$ is the angular acceleration of link AB relative to the base; $\ddot{\theta}_2$ is the angular acceleration of link BP relative to link AB; m_1, m_2 are the masses of links AB and BP; L_{AS1} is the distance between the center of mass S_1 of link AB and joint center A; L_{BS2} is the distance between the center of mass S_2 of link BP and joint center B; I_{S1} is the axial moment of inertia of link AB relative to the center of mass S_1 of link AB; I_{S2} is the axial moment of inertia of link BP relative to the center of mass S_2 of link BP; g is the gravitational acceleration.

As known, this is a typical dynamic coupled and nonlinear model. In order to reduce or even eliminate the influence that cased by the coupling, the dynamic model must be improved further.

Now, let us consider that the second link is statically balanced, i.e. $L_{BS2} = 0$ and the gravitational forces are perpendicular to the motion plane xOy, i.e. $D_1 = D_2 = 0$.

With the conditions above, the equation (2.1) can be rewritten as

$$\begin{bmatrix} \tau_1 \\ \tau_2 \end{bmatrix} = \begin{bmatrix} a+b & a \\ a & a \end{bmatrix} \begin{bmatrix} \ddot{\theta}_1 \\ \ddot{\theta}_2 \end{bmatrix} \tag{2.13}$$

where, $a = I_{S2}$; $b = I_{S1} + m_1 L_{AS1}^2 + m_2 L_1^2$.

Obviously, this is linearized dynamic model but still uncoupled.

To ensure the dynamic decoupling, it is necessary to ensure the condition $\ddot{\theta}_1 = -\ddot{\theta}_2$.

Then the equation (2.13) can be simplified as

$$\begin{cases} \tau_1 = b\ddot{\theta}_1 \\ \tau_2 = 0 \end{cases} \tag{2.14}$$

Thus, we obtain a completely decoupled and linearized model.

Next step is the geometric synthesis of the mechanical structure which should ensure two identical motions of links in opposite directions for any given initial and final positions of the end-effector.

2.1.2. Adjustment lengths of links for ensuring opposite rotations

According to the inverse kinematics of the planar serial manipulator shown in Fig. 2.1, the joint angles can be expressed as

$$\theta_1 = \tan^{-1}\left[\frac{y\left(L_1 + L_2\cos\theta_2\right) - xL_2\sin\theta_2}{x\left(L_1 + L_2\cos\theta_2\right) + yL_2\sin\theta_2}\right] \tag{2.15}$$

$$\theta_2 = \pm\cos^{-1}\left[\frac{x^2 + y^2 - L_1^2 - L_2^2}{2L_1L_2}\right] \tag{2.16}$$

where *x* and *y* are the coordinates of the end-effector in Fig.2.2.

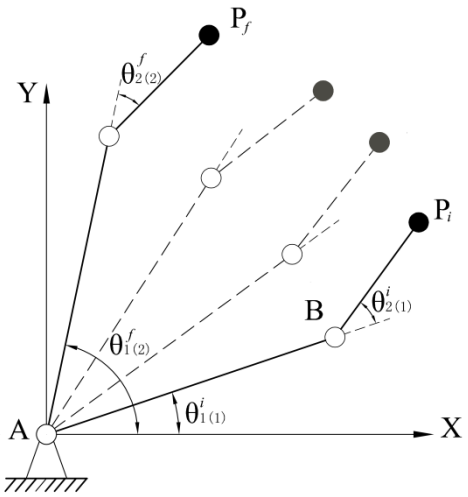

Figure 2.3. – Two configurations of the serial manipulator corresponding to the initial and final end-effector positions.

The given expressions show that for the same end-effector position there are two possible configurations of the manipulator called “elbow down” (configuration noted (1)) and “elbow up” (configuration noted (2)). The fact that a manipulator has multiple solutions would be used for ensuring the dynamic decoupling. Two configurations of the manipulator corresponding to the initial end-effector position P_i and the final end-effector position P_f are shown in Fig. 2.3. As it has been mentioned above, the initial position of the end-effector can be found by the following solutions: $\theta^i_{1(1)}, \theta^i_{2(1)}$ “elbow down” solution, $\theta^i_{1(2)}, \theta^i_{2(2)}$ “elbow up” solution (not shown) and the final position of the end-effector by $\theta^f_{1(1)}, \theta^f_{2(1)}$ “elbow down” solution (not shown), $\theta^f_{1(2)}, \theta^f_{2(2)}$ “elbow up” solution. Thus, the links of the manipulator move in such a manner that in the initial end-effector position (P_i), where the configuration of the manipulator will correspond to the “elbow down” solution; and, in the final end-effector position (P_f), where the configuration of the manipulator will correspond to the “elbow up” solution.

This choice of initial and final end-effector configurations of the manipulator with an optimal selection of lengths L_1 and L_2 allows equal ($\Delta\theta_1 = \Delta\theta_2$) and opposite ($\dot{\theta}_1 = -\dot{\theta}_2$) rotations of links AB and BP, i.e. $\left| \theta^f_{1(2)} - \theta^i_{1(1)} \right| = - \left| \theta^f_{2(2)} - \theta^i_{2(1)} \right|$. These conditions lead to $\ddot{\theta}_1 = -\ddot{\theta}_2$ and consequently to equations (2.14).

Now consider the selection of lengths L_1 and L_2 of links 1 and 2 for any given trajectory. To limit the variables in the specified conditions, suppose that the following parameters are given:

- the initial position P_i of the end-effector: x_i, y_i;
- the final position P_f of the end-effector: x_f, y_f;
- the initial angular position of the second link: $\theta^i_{2(1)}$;
- the rotating angle of the first link: $\Delta\theta_1 = \theta^f_{1(2)} - \theta^i_{1(1)}$.

The geometrical equations of the manipulator with the mentioned conditions lead to the following expressions:

$$L_1 = \frac{x_f^2 + y_f^2 - x_i^2 - y_i^2}{2L_2(\cos\theta^f_{2(2)} - \cos\theta^i_{2(1)})} \tag{2.17}$$

$$L_2 = \left[\frac{-\xi - (\xi^2 - 4\chi)^{1/2}}{2}\right]^{1/2} \tag{2.18}$$

where

$$\chi = \left[\frac{x_f^2 + y_f^2 - x_i^2 - y_i^2}{2(\cos\theta^f_{2(2)} - \cos\theta^i_{2(1)})}\right]^2 \tag{2.19}$$

$$\xi = 2(\chi)^{1/2}\cos\theta^i_{21} - x_i^2 - y_i^2 \tag{2.20}$$

$$\theta^f_{2(2)} = -(\Delta\theta_1 - \theta^i_{2(1)}) \tag{2.21}$$

Thus, for any initial and final positions of the end-effector, the lengths L_1 and L_2 determined from equations (2.17) and (2.18) will ensure an equal ($\Delta\theta_1 = \Delta\theta_2$) and opposite ($\dot\theta_1 = -\dot\theta_2$) rotations of links AB and BP.

Let us now consider the Scott-Russell mechanism.

The Scott-Russell mechanism is usually used as a straight line generator, so it is also called exact straight line mechanism (Fig. 2.4). In this mechanism, the point C on the connecting rod copies the line traced by the slider B in a perpendicular direction OC, if OA=AB=AC. It should be noticed that the straight-line or linear path exhibits great potential for high-speed pick and place operations in many manufacturing sectors(Liao 2011).

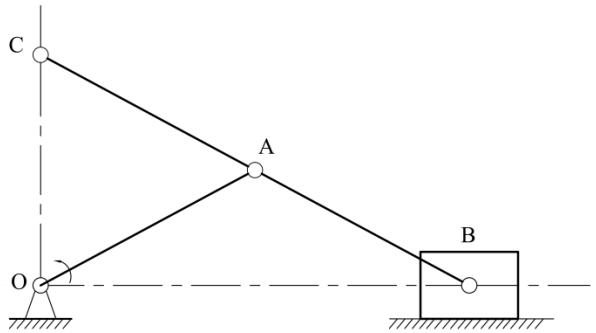

Figure 2.4. – Scott-Russell mechanism (Dukkipati 2007).

As shown in Fig. 2.5, a pair of Scott-Russell mechanism is added. Thus, the proposed structure ensures the complete static balancing for any arbitrary configuration of the adjustable link BP.

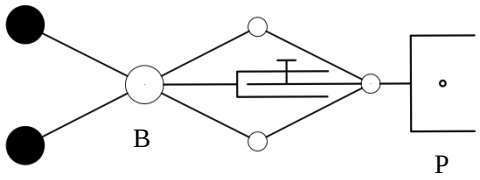

Figure 2.5. – Adjustable link BP with added Scott-Russell mechanisms.

2.2. Motion generation and dynamic decoupling of the adjustable manipulators

In previous sections, we studied the kinematics and dynamics of the adjustable manipulator. This means that using the obtained equations of motion of the manipulator, we can determine the manipulator's positions.

The present section relates to the way the adjustable manipulator is moved from initial position to the final position, as well as the conditions of dynamic decoupling during the generated motions.

2.2.1. Motion generation via fifth-order polynomial trajectory planning

For motion generation between initial and final positions, a fifth-degree and secondary derivative polynomial is used

$$\theta = \sum_{i=0}^{5} c_i t^i \quad (i = 1,...,5) \tag{2.22}$$

Thus,we have

$$\theta(t) = c_0 + c_1 t + c_2 t^2 + c_3 t^3 + c_4 t^4 + c_5 t^5 \tag{2.23}$$

$$\dot{\theta}(t) = c_1 + 2c_2 t + 3c_3 t^2 + 4c_4 t^3 + 5c_5 t^4 \tag{2.24}$$

$$\ddot{\theta}(t) = 2c_2 + 6c_3 t + 12c_4 t^2 + 20c_5 t^3 \tag{2.25}$$

The initial and final conditions are given by $\begin{bmatrix} \theta(0) \\ \dot{\theta}(0) \\ \ddot{\theta}(0) \end{bmatrix} = \begin{bmatrix} \theta_I \\ 0 \\ 0 \end{bmatrix}$ and $\begin{bmatrix} \theta(T) \\ \dot{\theta}(T) \\ \ddot{\theta}(T) \end{bmatrix} = \begin{bmatrix} \theta_F \\ 0 \\ 0 \end{bmatrix}$, where T is the total time for the rotation. θ_I and θ_F are the initial and final positions in the joint space, respectively.

Substituting these conditions into equations (2.23)-(2.25). Then, we obtain that

$$\theta(t) = \theta_I + [\theta_F - \theta_I]\left(\frac{t}{T}\right)^3 \left[10 - 15\left(\frac{t}{T}\right) + 6\left(\frac{t}{T}\right)^2\right] \tag{2.26}$$

$$\dot{\theta}(t) = [\theta_F - \theta_I]\frac{30}{T}\left(\frac{t}{T}\right)^2 \left[1 - 2\left(\frac{t}{T}\right) + \left(\frac{t}{T}\right)^2\right] \tag{2.27}$$

$$\ddot{\theta}(t) = [\theta_F - \theta_I]\frac{60}{T^2}\left(\frac{t}{T}\right) \left[1 - 3\left(\frac{t}{T}\right) + 2\left(\frac{t}{T}\right)^2\right] \tag{2.28}$$

To ensure the opposite rotation of links, the actuators generate the same motions. Hence, for joint A, we get

$$\begin{cases} \theta_1(t) = \theta_{1I} + [\theta_{1F} - \theta_{1I}]\left(\frac{t}{T}\right)^3\left[10 - 15\left(\frac{t}{T}\right) + 6\left(\frac{t}{T}\right)^2\right] \\ \dot{\theta}_1(t) = [\theta_{1F} - \theta_{1I}]\frac{30}{T}\left(\frac{t}{T}\right)^2\left[1 - 2\left(\frac{t}{T}\right) + \left(\frac{t}{T}\right)^2\right] \\ \ddot{\theta}_1(t) = [\theta_{1F} - \theta_{1I}]\frac{60}{T^2}\left(\frac{t}{T}\right)\left[1 - 3\left(\frac{t}{T}\right) + 2\left(\frac{t}{T}\right)^2\right] \end{cases} \quad (2.29)$$

for joint B, we get

$$\begin{cases} \theta_2(t) = \theta_{2I} + [\theta_{2F} - \theta_{2I}]\left(\frac{t}{T}\right)^3\left[10 - 15\left(\frac{t}{T}\right) + 6\left(\frac{t}{T}\right)^2\right] \\ \dot{\theta}_2(t) = [\theta_{2F} - \theta_{2I}]\frac{30}{T}\left(\frac{t}{T}\right)^2\left[1 - 2\left(\frac{t}{T}\right) + \left(\frac{t}{T}\right)^2\right] \\ \ddot{\theta}_2(t) = [\theta_{2F} - \theta_{2I}]\frac{60}{T^2}\left(\frac{t}{T}\right)\left[1 - 3\left(\frac{t}{T}\right) + 2\left(\frac{t}{T}\right)^2\right] \end{cases} \quad (2.30)$$

2.2.2. Dynamic decoupling without payload

For the dynamic decoupling of the model, the Scott-Russell mechanism should be added. In consequence, the second link will be characterized by the link BP with the Scott-Russell mechanism and the counterweight.

The kinematic energies of all parts of the manipulator are:

$$E_1 = \frac{1}{2} m_1 L_{AS1}^2 \dot{\theta}_1^2 + \frac{1}{2} I_{S1} \dot{\theta}_1^2 \quad (2.31)$$

$$\begin{aligned} E_2 &= \frac{1}{2} m_{2+SR+cw}[L_1^2\dot{\theta}_1^2 + L_{BS2r}^2(\dot{\theta}_1+\dot{\theta}_2)^2 + 2L_1L_{BS2r}\cos(\theta_2)\dot{\theta}_1(\dot{\theta}_1+\dot{\theta}_2)] \\ &\quad + \frac{1}{2} I_{S2+SR+cw}(\dot{\theta}_1+\dot{\theta}_2)^2 \end{aligned} \tag{2.32}$$

with,

$$\begin{aligned} m_{2+SR+cw} &= m_2 + m_{SR} + m_{cw} \\ L_{BS2r} &= \frac{m_2 L_{BS2} + m_{SR} L_{BS2} - m_{cw} L_{cw}}{m_{2+SR+cw}} \\ I_{S2+SR+cw} &= I_{S2} + I_{SR} + m_2(L_{BS2} - L_{BS2r})^2 + m_{SR}(L_{BS2} - L_{BS2r})^2 + m_{cw}(L_{cw} + L_{BS2r})^2 \end{aligned} \tag{2.33}$$

where, m_2, m_{SR}, m_{cw} are the masses of link BP, Scott-Russell mechanism and counterweight, respectively; L_{BS2r} is referred to as the real distance between joint center B and center of mass of the object which is constituted by link BP, Scott-Russell mechanism and counterweight; $I_{S2+SR+cw}$ is referred to as the moment of inertia of this new combined object. In addition, the friction effect and gravity force are ignored here.

Thus, according to the Lagrangian equations, the torques of the manipulator without payload are:

$$\begin{aligned} \tau_{1without} &= \frac{d}{dt}\left(\frac{\partial L}{\partial \dot{\theta}_1}\right) - \frac{\partial L}{\partial \theta_1} \\ &= m_1 L_{AS1}^2 \ddot{\theta}_1 + I_{S1}\ddot{\theta}_1 + m_{2+SR+cw} L_1^2 \ddot{\theta}_1 \\ &\quad + m_{2+SR+cw} L_{BS2r}^2(\ddot{\theta}_1+\ddot{\theta}_2) + m_{2+SR+cw} L_1 L_{BS2r}\cos(\theta_2)(2\ddot{\theta}_1+\ddot{\theta}_2) \\ &\quad - m_{2+SR+cw} L_1 L_{BS2r}\sin(\theta_2)(2\dot{\theta}_1\dot{\theta}_2 + \dot{\theta}_2^2) + I_{S2+SR+cw}(\ddot{\theta}_1+\ddot{\theta}_2) \end{aligned} \tag{2.34}$$

$$\begin{aligned} \tau_{2without} &= \frac{d}{dt}\left(\frac{\partial L}{\partial \dot{\theta}_2}\right) - \frac{\partial L}{\partial \theta_2} \\ &= m_{2+SR+cw} L_{BS2r}^2(\ddot{\theta}_1+\ddot{\theta}_2) + m_{2+SR+cw} L_1 L_{BS2r}\cos(\theta_2)\ddot{\theta}_1 \\ &\quad + m_{2+SR+cw} L_1 L_{BS2r}\sin(\theta_2)\dot{\theta}_1^2 + I_{S2+SR+cw}(\ddot{\theta}_1+\ddot{\theta}_2) \end{aligned} \tag{2.35}$$

where, $\tau_{1without}$ and $\tau_{2without}$ are torques of the manipulator without any payload.

Introducing the static equilibrium equations considered above, the dynamic equations can be simplified as

$$\begin{bmatrix} \tau_{1without} \\ \tau_{2without} \end{bmatrix} = \begin{bmatrix} a'+b' & a' \\ a' & a' \end{bmatrix} \begin{bmatrix} \ddot{\theta}_1 \\ \ddot{\theta}_2 \end{bmatrix} \tag{2.36}$$

where, $a' = I_{S2} + I_{SR} + m_2 L_{BS2}^2 + m_{SR} L_{BS2}^2 + m_{cw} L_{cw}^2$; $b' = m_1 L_{AS1}^2 + I_{S1} + m_{2+SR+cw} L_1^2$.

With the condition of opposite rotations ($\ddot{\theta}_2 = -\ddot{\theta}_1$), the equation (2.36) can be simplified as

$$\begin{cases} \tau_{1without} = b'\ddot{\theta}_1 \\ \tau_{2without} = 0 \end{cases} \tag{2.37}$$

2.3. Closed-loop control

As known, an open-loop system cannot correct any errors that it could make. And it will also not compensate for disturbances during the process. A closed-loop control system, also known as a feedback control system is a control system which uses the concept of an open-loop system as its forward path but has one or more feedback loops between its output and its input. A closed-loop control system is necessary when the open-loop system is unstable (double integrator).

Closed-loop systems are designed to automatically achieve and maintain the desired output trajectory by compensating an error signal which is the difference between the actual output and the reference input. Meanwhile, it can be used for compensating the disturbance during the while process.

According to the inverse calculation of the equation (2.36), the state equation of the MIMO model can be obtained with the state vector $\xi = [\theta_1 \quad \dot{\theta}_1 \quad \theta_2 \quad \dot{\theta}_2]^T$

$$\underbrace{\begin{bmatrix} \dot{\xi}_1 \\ \dot{\xi}_2 \\ \dot{\xi}_3 \\ \dot{\xi}_4 \end{bmatrix}}_{\dot{\xi}} = \underbrace{\begin{bmatrix} 0 & 1 & 0 & 0 \\ 0 & 0 & 0 & 0 \\ 0 & 0 & 0 & 1 \\ 0 & 0 & 0 & 0 \end{bmatrix}}_{A} \underbrace{\begin{bmatrix} \xi_1 \\ \xi_2 \\ \xi_3 \\ \xi_4 \end{bmatrix}}_{\xi} + \underbrace{\begin{bmatrix} 0 & 0 \\ \frac{1}{b'} & -\frac{1}{b'} \\ 0 & 0 \\ -\frac{1}{b'} & \frac{1}{a'}+\frac{1}{b'} \end{bmatrix}}_{B} \underbrace{\begin{bmatrix} \tau_{1without} \\ \tau_{2without} \end{bmatrix}}_{\tau} \tag{2.38}$$

Before the further research, the controllable canonical form of the state equation should be built by the following transformation:

$$\xi = \left[T_{cc} W_c\right]\zeta \tag{2.39}$$

where, T_{cc} is the controllability matrix, and it is formed as

$$T_{cc} = [B \mid AB] = \begin{bmatrix} 0 & 0 & \frac{1}{b'} & -\frac{1}{b'} \\ \frac{1}{b'} & -\frac{1}{b'} & 0 & 0 \\ 0 & 0 & -\frac{1}{b'} & \frac{1}{a'}+\frac{1}{b'} \\ -\frac{1}{b'} & \frac{1}{a'}+\frac{1}{b'} & 0 & 0 \end{bmatrix}$$

W_c, is the upper triangular Toeplitz matrix, and it is formed by characteristic equation of matrix A: $|sI-A|=s^4 + a_3 s^3 + a_2 s^2 + a_1 s + a_0 = s^4$. So,

$$W_c = \begin{bmatrix} 1 & a_3 & a_2 & a_1 \\ 0 & 1 & a_3 & a_2 \\ 0 & 0 & 1 & a_3 \\ 0 & 0 & 0 & 1 \end{bmatrix} = \begin{bmatrix} 1 & 0 & 0 & 0 \\ 0 & 1 & 0 & 0 \\ 0 & 0 & 1 & 0 \\ 0 & 0 & 0 & 1 \end{bmatrix} = I$$

As known,

$$\dot{\xi} = A\xi + B\tau_{without} \tag{2.40}$$

Substituting the equation (2.39) into equation (2.40), we obtain

$$\dot{\zeta} = \left[T_{cc}\right]^{-1} A \left[T_{cc}\right]\zeta + \left[T_{cc}\right]^{-1} B\tau_{without} \tag{2.41}$$

Hence, the controllable canonical form is given by

$$\begin{bmatrix} \dot{\zeta}_1 \\ \dot{\zeta}_2 \\ \dot{\zeta}_3 \\ \dot{\zeta}_4 \end{bmatrix} = \begin{bmatrix} 0 & 0 & 0 & 0 \\ 0 & 0 & 0 & 0 \\ 1 & 0 & 0 & 0 \\ 0 & 1 & 0 & 0 \end{bmatrix} \begin{bmatrix} \zeta_1 \\ \zeta_2 \\ \zeta_3 \\ \zeta_4 \end{bmatrix} + \begin{bmatrix} 1 & 0 \\ 0 & 1 \\ 0 & 0 \\ 0 & 0 \end{bmatrix} \begin{bmatrix} \tau_{1without} \\ \tau_{2without} \end{bmatrix} \tag{2.42}$$

and the sate vector

$$\begin{bmatrix}\zeta_1\\ \zeta_2\\ \zeta_3\\ \zeta_4\end{bmatrix}=[T_{cc}]^{-1}\xi=\begin{bmatrix}(a'+b')\dot{\theta}_1+a'\dot{\theta}_2\\ a'\dot{\theta}_1+a'\dot{\theta}_2\\ (a'+b')\theta_1+a'\theta_2\\ a'\theta_1+a'\theta_2\end{bmatrix} \tag{2.43}$$

It is obviously that, the system that described by state equation (2.42) can be divided into two independent subsystems:

$$\begin{cases}\begin{bmatrix}\dot{\zeta}_1\\ \dot{\zeta}_3\end{bmatrix}=\begin{bmatrix}0 & 0\\ 1 & 0\end{bmatrix}\begin{bmatrix}\zeta_1\\ \zeta_3\end{bmatrix}+\begin{bmatrix}1\\ 0\end{bmatrix}\tau_{1without}\\ \begin{bmatrix}\dot{\zeta}_2\\ \dot{\zeta}_4\end{bmatrix}=\begin{bmatrix}0 & 0\\ 1 & 0\end{bmatrix}\begin{bmatrix}\zeta_2\\ \zeta_4\end{bmatrix}+\begin{bmatrix}1\\ 0\end{bmatrix}\tau_{2without}\end{cases} \tag{2.44}$$

Hence, when taking into account the feedback control, the closed-loop can be added firstly on each simple subsystem, then combine them together for the whole system. Obviously, both of these two subsystems are simple double integrator structures. Hence, the linear control method can be employed.

2.3.1. Command of the first double integrator

According to the first double integrator, we can deduce:

$$\begin{cases}\dot{\zeta}_1=\tau_{1without}\\ \dot{\zeta}_3=\zeta_1\end{cases} \tag{2.45}$$

Assuming that $\begin{cases}\rho=\zeta_3\\ \dot{\rho}=\zeta_1\end{cases}$

Then the state equation of the double integrator is given by

$$\begin{bmatrix}\dot{\rho}\\ \ddot{\rho}\end{bmatrix}=\underbrace{\begin{bmatrix}0 & 1\\ 0 & 0\end{bmatrix}}_{A_1}\begin{bmatrix}\rho\\ \dot{\rho}\end{bmatrix}+\underbrace{\begin{bmatrix}0\\ 1\end{bmatrix}}_{B_1}\tau_{1without} \tag{2.46}$$

Obviously, this is a simple double integrator structure. For the closed-loop control, the control law can be written as

$$\tau_{1without} = \mu_1 - g_{11}\dot{\rho} - g_{12}\rho \tag{2.47}$$

Substituting this control law in the equation (2.46), then the state equation of the double integrator can be rewritten as

$$\begin{bmatrix} \dot{\rho} \\ \ddot{\rho} \end{bmatrix} = \begin{bmatrix} 0 & 1 \\ -g_{12} & -g_{11} \end{bmatrix} \begin{bmatrix} \rho \\ \dot{\rho} \end{bmatrix} + \begin{bmatrix} 0 \\ 1 \end{bmatrix} \mu_1 \tag{2.48}$$

Assuming that

$$\mu_1 = \omega_1 + g_{11}\dot{\rho} + g_{12}\rho \tag{2.49}$$

then

$$\begin{bmatrix} \dot{\rho} \\ \ddot{\rho} \end{bmatrix} = \begin{bmatrix} 0 & 1 \\ 0 & 0 \end{bmatrix} \begin{bmatrix} \rho \\ \dot{\rho} \end{bmatrix} + \begin{bmatrix} 0 \\ 1 \end{bmatrix} \omega_1 \tag{2.50}$$

hence, $\omega_1 = \ddot{\rho}$. It can be found that

$$\mu_1 = \ddot{\rho} + g_{11}\dot{\rho} + g_{12}\rho \tag{2.51}$$

It is concluded that a balance position of the double integrator is given by the conditions about ρ and its continual derivatives. Hence, if a trajectory ρ_R which is secondary derivable over a range [0, T] is given, we can deduce:

$$\mu_{1R} = \ddot{\rho}_R + g_{11}\dot{\rho}_R + g_{12}\rho_R \tag{2.52}$$

Finally, the control law of the closed-loop double integrator is

$$\tau_{1without} = \ddot{\rho}_R - g_{11}[\dot{\rho} - \dot{\rho}_R] - g_{12}[\rho - \rho_R] \tag{2.53}$$

As known, $\rho = (a' + b')\theta_1 + a'\theta_2$, the control law can be rewritten as

$$\begin{aligned} \tau_{1without} = {} & (a' + b')\ddot{\theta}_{1R} + a'\ddot{\theta}_{2R} \\ & - g_{11}[(a' + b')[\dot{\theta}_1 - \dot{\theta}_{1R}] + a'[\dot{\theta}_2 - \dot{\theta}_{2R}]] \\ & - g_{12}[(a' + b')[\theta_1 - \theta_{1R}] + a'[\theta_2 - \theta_{2R}]] \end{aligned} \tag{2.54}$$

2.3.2. Feedback parameters of the first double integrator

According to the last section, the double integration state equation of the first double integrator is obtained.

For realize the control law: $\tau_{1without} = -G_1 \left[\rho \ \dot{\rho}\right]^T$, the matrix of state feedback parameter $G_1 = [g_{12} \ \ g_{11}]$ should be obtained. It is calculated by minimizing the index of performance J below:

$$J = \int_0^\infty \left[\left[\rho \ \ \dot{\rho}\right] Q_1 \begin{bmatrix} \rho \\ \dot{\rho} \end{bmatrix} + \tau_{1without}^T R_1 \tau_{1without} \right] dt \tag{2.55}$$

where

$R_1 = 1 > 0$

$$Q_1 = \left[T_{p1} \left(\int_0^{T_{p1}} e^{A_1 \tau} B_1 B_1^T e^{A_1^T \tau} d\tau \right) \right]^{-1} = \begin{bmatrix} \dfrac{12}{T_{p1}^4} & -\dfrac{6}{T_{p1}^3} \\ -\dfrac{6}{T_{p1}^3} & \dfrac{4}{T_{p1}^2} \end{bmatrix} > 0$$

Assuming that the symmetric matrix Σ_1 is the solution of Riccati equation

$$A_1^T \Sigma_1 + \Sigma_1 A_1 - \Sigma_1 B_1 R_1^{-1} B_1^T \Sigma_1 + Q_1 = 0 \tag{2.56}$$

where $\mathbf{\Sigma}_1 = \begin{bmatrix} \sigma_1 & \sigma_2 \\ \sigma_2 & \sigma_3 \end{bmatrix}$.

It is known that, the matrix will be positive if : $\begin{cases} \sigma_1 > 0 \\ \sigma_1 \sigma_3 - \sigma_2^2 > 0 \end{cases}$

thus

$$\sigma_1 = \sigma_2 \sigma_3 + \frac{6}{T_{p1}^3} > 0;$$

$$\sigma_2^2 = \frac{12}{T_{p1}^4} \Rightarrow \sigma_2 = \pm \frac{2\sqrt{3}}{T_{p1}^2};$$

$$\sigma_3^2 = 2\sigma_2 + \frac{4}{T_{p1}^2} > 0.$$

we obtain

$$\begin{cases} 2\sigma_2 + \dfrac{4}{T_{p1}^2} > 0 \Rightarrow \sigma_2 = \dfrac{2\sqrt{3}}{T_{p1}^2} \Rightarrow \sigma_3^2 = \dfrac{4(1+\sqrt{3})}{T_{p1}^2} \\ \sigma_2\sigma_3 + \dfrac{6}{T_{p1}^3} > 0 \Rightarrow \sigma_3 = \dfrac{2\sqrt{1+\sqrt{3}}}{T_{p1}} \\ \sigma_1 = \sigma_2\sigma_3 + \dfrac{6}{T_{p1}^3} = \dfrac{6+4\sqrt{3}\sqrt{1+\sqrt{3}}}{T_{p1}^3} \end{cases} \tag{2.57}$$

Hence, the expression of matrix Σ_1 is obtained

$$\Sigma_1 = \begin{bmatrix} \dfrac{6+4\sqrt{3}\sqrt{1+\sqrt{3}}}{T_{p1}^3} & \dfrac{2\sqrt{3}}{T_{p1}^2} \\ \dfrac{2\sqrt{3}}{T_{p1}^2} & \dfrac{2\sqrt{1+\sqrt{3}}}{T_{p1}} \end{bmatrix} \tag{2.58}$$

As known, the matrix G_1 is noted as

$$G_1 = R_1^{-1} B_1^T \Sigma_1 \tag{2.59}$$

Then,

$$G_1 = \begin{bmatrix} \dfrac{2\sqrt{3}}{T_{p1}^2} & \dfrac{2\sqrt{1+\sqrt{3}}}{T_{p1}} \end{bmatrix} \tag{2.60}$$

As result, we obtain

$g_{12} = \dfrac{2\sqrt{3}}{T_{p1}^2}$ and $g_{11} = \dfrac{2\sqrt{1+\sqrt{3}}}{T_{p1}}$.

The state model of the closed-loop system is written as follows

$$\begin{bmatrix} \dot{\rho} \\ \ddot{\rho} \end{bmatrix} = [A_1 - B_1 G_1] \begin{bmatrix} \rho \\ \dot{\rho} \end{bmatrix} = \begin{bmatrix} 0 & 1 \\ -\dfrac{2\sqrt{3}}{T_{p1}^2} & -\dfrac{2\sqrt{1+\sqrt{3}}}{T_{p1}} \end{bmatrix} \begin{bmatrix} \rho \\ \dot{\rho} \end{bmatrix} \tag{2.61}$$

The characteristic polynomial P(s) is given by

$$P(s) = | sI - A_1 + B_1 G_1 | = s^2 + \frac{2\sqrt{1+\sqrt{3}}}{T_{p1}} s + \frac{2\sqrt{3}}{T_{p1}^2} \tag{2.62}$$

If $P(s) = s^2 + 2\zeta\omega_n s + \omega_n^2$, we obtain $\omega_n = \frac{\sqrt{2\sqrt{3}}}{T_{p1}}$ and $\zeta = \frac{\sqrt{1+\sqrt{3}}}{\sqrt{2\sqrt{3}}} \approx 0.89$.

As shown in equation (2.44), the two subsystems have the same state equations. Hence, the control law and feedback parameters of the first double integrator that obtained above are also suitable for the second double integrator:

$$\begin{aligned} \tau_{2without} &= a'\ddot{\theta}_{1R} + a'\ddot{\theta}_{2R} \\ &\quad - g_{21}[a'[\dot{\theta}_1 - \dot{\theta}_{1R}] + a'[\dot{\theta}_2 - \dot{\theta}_{2R}]] \\ &\quad - g_{22}[a'[\theta_1 - \theta_{1R}] + a'[\theta_2 - \theta_{2R}]] \end{aligned} \tag{2.63}$$

where,

$$g_{22} = \frac{2\sqrt{3}}{T_{p2}^2} \text{ and } g_{21} = \frac{2\sqrt{1+\sqrt{3}}}{T_{p2}}.$$

2.4. Dynamic decoupling taking into account the payload

The introduction of the payload leads to new loads on the actuators which are also nonlinear. Here, consider the payload also as one part of link BP. The energies of both of the two links are described as

$$\begin{aligned} E_1 &= \frac{1}{2} m_1 L_{AS1}^2 \dot{\theta}_1^2 + \frac{1}{2} I_{S1} \dot{\theta}_1^2 \\ E_2 &= \frac{1}{2} M_2 [L_1^2 \dot{\theta}_1^2 + L_{BS2r}^2 (\dot{\theta}_1 + \dot{\theta}_2)^2 \\ &\quad + 2L_1 L_{BS2r} \cos(\theta_2) \dot{\theta}_1 (\dot{\theta}_1 + \dot{\theta}_2)] + \frac{1}{2} I_{S2+SR+cw+p} (\dot{\theta}_1 + \dot{\theta}_2)^2 \end{aligned} \tag{2.64}$$

where,

$$M_2 = m_{2+SR+cw} + m_p; \quad L_{BS2r} = \frac{m_2 L_{BS2} + m_{SR} L_{BS2} - m_{cw} L_{cw} + m_p L_2}{M_2};$$

$$I_{S2+SR+cw+P} = I_{S2} + I_{SR} + m_2 (L_{BS2} - L_{BS2r})^2 + m_{SR} (L_{BS2} - L_{BS2r})^2 + m_{cw} (L_{cw} + L_{BS2r})^2 + m_p (L_2 - L_{BS2r})^2.$$

According to the Lagrangian, the dynamic equations are

$$\begin{aligned} \tau_{1with} &= \frac{d}{dt}\left(\frac{\partial L}{\partial \dot{\theta}_1}\right) - \frac{\partial L}{\partial \theta_1} \\ &= m_1 L_{AS1}^2 \ddot{\theta}_1 + I_{S1} \ddot{\theta}_1 + M_2 L_1^2 \ddot{\theta}_1 + M_2 L_{BS2r}^2 (\ddot{\theta}_1 + \ddot{\theta}_2) \\ &+ M_2 L_1 L_{BS2r} \cos(\theta_2)(2\ddot{\theta}_1 + \ddot{\theta}_2) - M_2 L_1 L_{BS2r} \sin(\theta_2)(2\dot{\theta}_1 \dot{\theta}_2 + \dot{\theta}_2^2) \\ &+ I_{S2+SR+cw+p} (\ddot{\theta}_1 + \ddot{\theta}_2) \end{aligned} \tag{2.65}$$

$$\begin{aligned} \tau_{2with} &= \frac{d}{dt}\left(\frac{\partial L}{\partial \dot{\theta}_2}\right) - \frac{\partial L}{\partial \theta_2} \\ &= M_2 L_{BS2r}^2 (\ddot{\theta}_1 + \ddot{\theta}_2) + M_2 L_1 L_{BS2r} \cos(\theta_2) \ddot{\theta}_1 \\ &+ M_2 L_1 L_{BS2r} \sin(\theta_2) \dot{\theta}_1^2 + I_{S2+SR+cw+p} (\ddot{\theta}_1 + \ddot{\theta}_2) \end{aligned} \tag{2.66}$$

where, τ_{1with} and τ_{2with} are the output torque values of the first actuator and the second actuator respectively when taking into account the payload on the end-effector of the serial manipulator.

Substituting the equation (2.33) into these dynamic equations, then they can be simplified as

$$\begin{aligned} \begin{bmatrix} \tau_{1with} \\ \tau_{2with} \end{bmatrix} &= \begin{bmatrix} m_1 L_{AS1}^2 + I_{S1} + M_2 L_1^2 + I_{S2} + I_{SR} & I_{S2} + I_{SR} \\ I_{S2} + I_{SR} & I_{S2} + I_{SR} \end{bmatrix} \begin{bmatrix} \ddot{\theta}_1 \\ \ddot{\theta}_2 \end{bmatrix} \\ &+ \begin{bmatrix} (m_2 + m_{SR}) L_{BS2}^2 + m_{cw} L_{cw}^2 & (m_2 + m_{SR}) L_{BS2}^2 + m_{cw} L_{cw}^2 \\ (m_2 + m_{SR}) L_{BS2}^2 + m_{cw} L_{cw}^2 & (m_2 + m_{SR}) L_{BS2}^2 + m_{cw} L_{cw}^2 \end{bmatrix} \begin{bmatrix} \ddot{\theta}_1 \\ \ddot{\theta}_2 \end{bmatrix} \\ &+ \begin{bmatrix} m_p L_2^2 + 2 m_p L_1 L_2 \cos(\theta_2) & m_p L_2^2 + m_p L_1 L_2 \cos(\theta_2) \\ m_p L_2^2 + m_p L_1 L_2 \cos(\theta_2) & m_p L_2^2 \end{bmatrix} \begin{bmatrix} \ddot{\theta}_1 \\ \ddot{\theta}_2 \end{bmatrix} \\ &+ \begin{bmatrix} -2 m_p L_1 L_2 \sin(\theta_2) \dot{\theta}_2 & -m_p L_1 L_2 \sin(\theta_2) \dot{\theta}_2 \\ m_p L_1 L_2 \sin(\theta_2) \dot{\theta}_1 & 0 \end{bmatrix} \begin{bmatrix} \dot{\theta}_1 \\ \dot{\theta}_2 \end{bmatrix} \end{aligned} \tag{2.67}$$

Introducing the condition of opposite rotations ($\ddot{\theta}_2 = -\ddot{\theta}_1$), then

$$\begin{aligned}\begin{bmatrix}\tau_{1with}\\ \tau_{2with}\end{bmatrix} &= \begin{bmatrix} m_1 L_{AS1}^2 + I_{S1} + m_{2+SR+cw} L_1^2 & 0 \\ 0 & 0\end{bmatrix}\begin{bmatrix}\ddot{\theta}_1\\ \ddot{\theta}_2\end{bmatrix} \\ &+ \begin{bmatrix} m_p L_1^2 + m_P L_1 L_2 \cos(\theta_2) & 0 \\ m_p L_1 L_2 \cos(\theta_2) & 0\end{bmatrix}\begin{bmatrix}\ddot{\theta}_1\\ \ddot{\theta}_2\end{bmatrix} \\ &+ \begin{bmatrix} -m_p L_1 L_2 \sin(\theta_2)\dot{\theta}_2 & 0 \\ m_p L_1 L_2 \sin(\theta_2)\dot{\theta}_1 & 0\end{bmatrix}\begin{bmatrix}\dot{\theta}_1\\ \dot{\theta}_2\end{bmatrix}\end{aligned} \tag{2.68}$$

Compare equation (2.68) with equation (2.37), the torques that caused by the introduction of the payload can be found

$$\begin{aligned}\begin{bmatrix}\Delta\tau_1\\ \Delta\tau_2\end{bmatrix} &= \begin{bmatrix} m_p L_1^2 + m_p L_1 L_2 \cos(\theta_2) & 0 \\ m_p L_1 L_2 \cos(\theta_2) & 0\end{bmatrix}\begin{bmatrix}\ddot{\theta}_1\\ \ddot{\theta}_2\end{bmatrix} \\ &+ \begin{bmatrix} -m_p L_1 L_2 \sin(\theta_2)\dot{\theta}_2 & 0 \\ m_p L_1 L_2 \sin(\theta_2)\dot{\theta}_1 & 0\end{bmatrix}\begin{bmatrix}\dot{\theta}_1\\ \dot{\theta}_2\end{bmatrix}\end{aligned} \tag{2.69}$$

Hence, the dynamic equation with payload can be rewritten as

$$\begin{cases}\tau_{1with} = \tau_{1without} + \Delta\tau_1 \\ \tau_{2with} = \tau_{2without} + \Delta\tau_2\end{cases} \tag{2.70}$$

This part is referred to as payload compensation. Extracting the payload compensation from the dynamic equation of the model taking into account the payload, then the model can be treated still as a dynamic decoupling model. This is another advantage that building a dynamic decoupling model taking into account the changing payload.

Under this mechatronic method, the dynamic model can be greatly simplified and meanwhile achieve the dynamic decoupling. In addition, the changing payload is also considered. As a result, no matter there is payload or not, the simple linear control law can always be used.

2.5. Illustrative example with the SIMULINK block of MATLAB

In this section, a simulation model will be built in the SIMULINK block of the MATLAB. The performance of the proposed technique is examined. First, the inverse transformation of the dynamic model with payload must be found. Rewritten the equation (2.64) as fellows

$$\begin{cases} \tau_1 = \psi(\theta_2)\ddot{\theta}_1 + \left[\gamma_2 + \beta(\theta_2)\right]\ddot{\theta}_2 - 2\alpha(\theta_2)\dot{\theta}_1\dot{\theta}_2 - \alpha(\theta_2)\dot{\theta}_2^2 \\ \tau_2 = \left[\gamma_2 + \beta(\theta_2)\right]\ddot{\theta}_1 + \gamma_2\ddot{\theta}_2 + \alpha(\theta_2)\dot{\theta}_1^2 \end{cases} \tag{2.71}$$

where

$\alpha(\theta_2) = M_2 L_1 L_{BS2r} \sin(\theta_2)$;
$\beta(\theta_2) = M_2 L_1 L_{BS2r} \cos(\theta_2)$;
$\gamma_1 = I_{S1} + m_1 L_{AS1}^2$;
$\gamma_2 = I_{S2+SR+cw+p} + M_2 L_{BS2r}^2$;
$\psi(\theta_2) = \gamma_1 + \gamma_2 + M_2 L_1^2 + 2\beta(\theta_2)$.

The inverse dynamic equations of the system are:

$$\begin{aligned} \ddot{\theta}_1 = {} & \frac{\gamma_2}{\Delta(\theta_2)}\tau_1 - \frac{\left[\gamma_2 + \beta(\theta_2)\right]}{\Delta(\theta_2)}\tau_2 + \frac{\gamma_2\alpha(\theta_2)}{\Delta(\theta_2)}\dot{\theta}_1\dot{\theta}_2 \\ & + \frac{\alpha(\theta_2)\left[\gamma_2 + \beta(\theta_2)\right]}{\Delta(\theta_2)}\dot{\theta}_1^2 + \frac{\gamma_2\alpha(\theta_2)}{\Delta(\theta_2)}(\dot{\theta}_1 + \dot{\theta}_2)\dot{\theta}_2 \end{aligned} \tag{2.72}$$

$$\begin{aligned} \ddot{\theta}_2 = {} & -\frac{\left[\gamma_2 + \beta(\theta_2)\right]}{\Delta(\theta_2)}\tau_1 + \frac{\psi(\theta_2)}{\Delta(\theta_2)}\tau_2 - \frac{\alpha(\theta_2)\left[\gamma_2 + \beta(\theta_2)\right]}{\Delta(\theta_2)}\dot{\theta}_1\dot{\theta}_2 \\ & - \frac{\alpha(\theta_2)\psi(\theta_2)}{\Delta(\theta_2)}\dot{\theta}_1^2 - \frac{\alpha(\theta_2)\left[\gamma_2 + \beta(\theta_2)\right]}{\Delta(\theta_2)}(\dot{\theta}_1 + \dot{\theta}_2)\dot{\theta}_2 \end{aligned} \tag{2.73}$$

where $\Delta(\theta_2) = \gamma_1\gamma_2 + M_2 L_1^2 I_{S2} + \left[\alpha(\theta_2)\right]^2 > 0$.

2.5.1. Simulation model of open-loop control system

In order to demonstrate the influence of the payload compensation, an open-loop control system is built. In the simulation model, it mainly contains two blocks, a controller block and a manipulator block, shown as Fig. 2.6. The controller block is used to provide the desired trajectories and the payload compensation. The manipulator block is used to simulate the real planar serial manipulator:

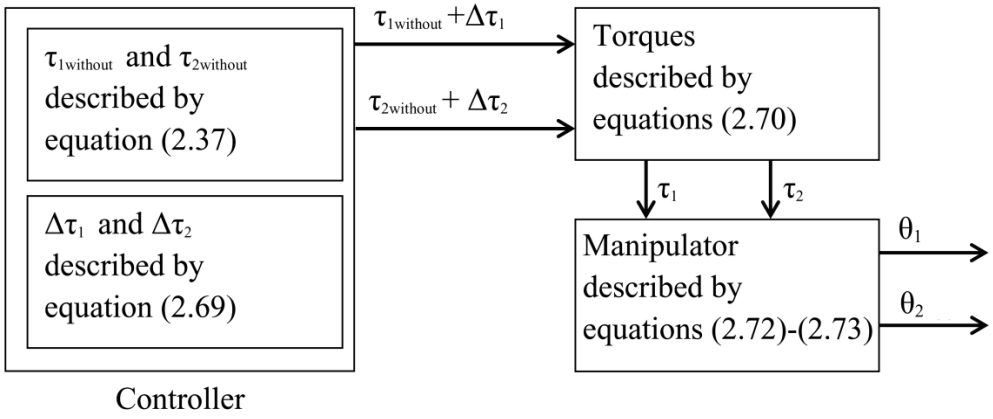

Figure 2.6. – The schema of the open-loop control system.

The simulation parametric values are obtained by using the ADAMS software. It should note that, this software is good at dynamic simulation and the model that built in this software is the same with the model in real word. Thus, these parametric values in (Tab. 2.1) can be considered as the real parametric values of a real manipulator.

As shown, they can be divided into three mainly categories: mass parameter, length parameter and moment of inertia parameter.

Table 2.1. – The parametric values of the open-loop control system.

mass (kg)		length (m)		moment of inertia ($kg \cdot m^2$)	
m_1	13.193	L_1/L_{AS1}	0.8/0.4	I_{S1}	0.77754
m_2	8.477	L_2/L_{BS2}	0.5/0.25	I_{S2}	0.20744
m_{SR}	0.811	L_{BSR}	0.25	I_{SR}	0.01717
m_{cw}	9.288	L_{cw}	0.25		
m_p	5				

It should be noted that, for simplify the calculation, the parametric values of counterweight are given by

$$\begin{aligned} m_{cw} &= m_2 + m_{SR} \\ L_{cw} &= L_{BS2} \end{aligned} \tag{2.74}$$

Until now, a whole simulation model of the open-loop control system can be built. For the operation of the model, the desired trajectories that described by the equations (2.29) and (2.30) are used, and the initial and final positions of the manipulator are given as (Tab. 2.2). Here, the total operation time $T = 1s$.

Table 2.2. – The initial and final values of the desired trajectories.

Angle ($^\circ$)		Velocity (m/s)		Acceleration (m/s^2)	
θ_{1I}	33	$\dot{\theta}_{1I}$	0	$\ddot{\theta}_{1I}$	0
θ_{1F}	110	$\dot{\theta}_{1F}$	0	$\ddot{\theta}_{1F}$	0
θ_{2I}	0	$\dot{\theta}_{2I}$	0	$\ddot{\theta}_{2I}$	0
θ_{2F}	-77	$\dot{\theta}_{2F}$	0	$\ddot{\theta}_{2F}$	0

According to the equations (2.29) and (2.30), the desired trajectories, velocities and accelerations of the two actuators are shown in Fig. 2.7. Fig. 2.7(a1)-(a3) are the curves of the angular trajectory, angular velocity and angular acceleration of the first actuator respectively. As the same, Fig. 2.7(b1)-(b3) are the curves of the angular trajectory, angular velocity and angular acceleration of the second actuator respectively. It is obvious that these two trajectories are totally opposite.

As proposed, this is a dynamic decoupling manipulator. The torque of each motor is only influence by one kind of parameter. Especially for the second actuator, its output torque is completely cancelled (Fig. 2.8).

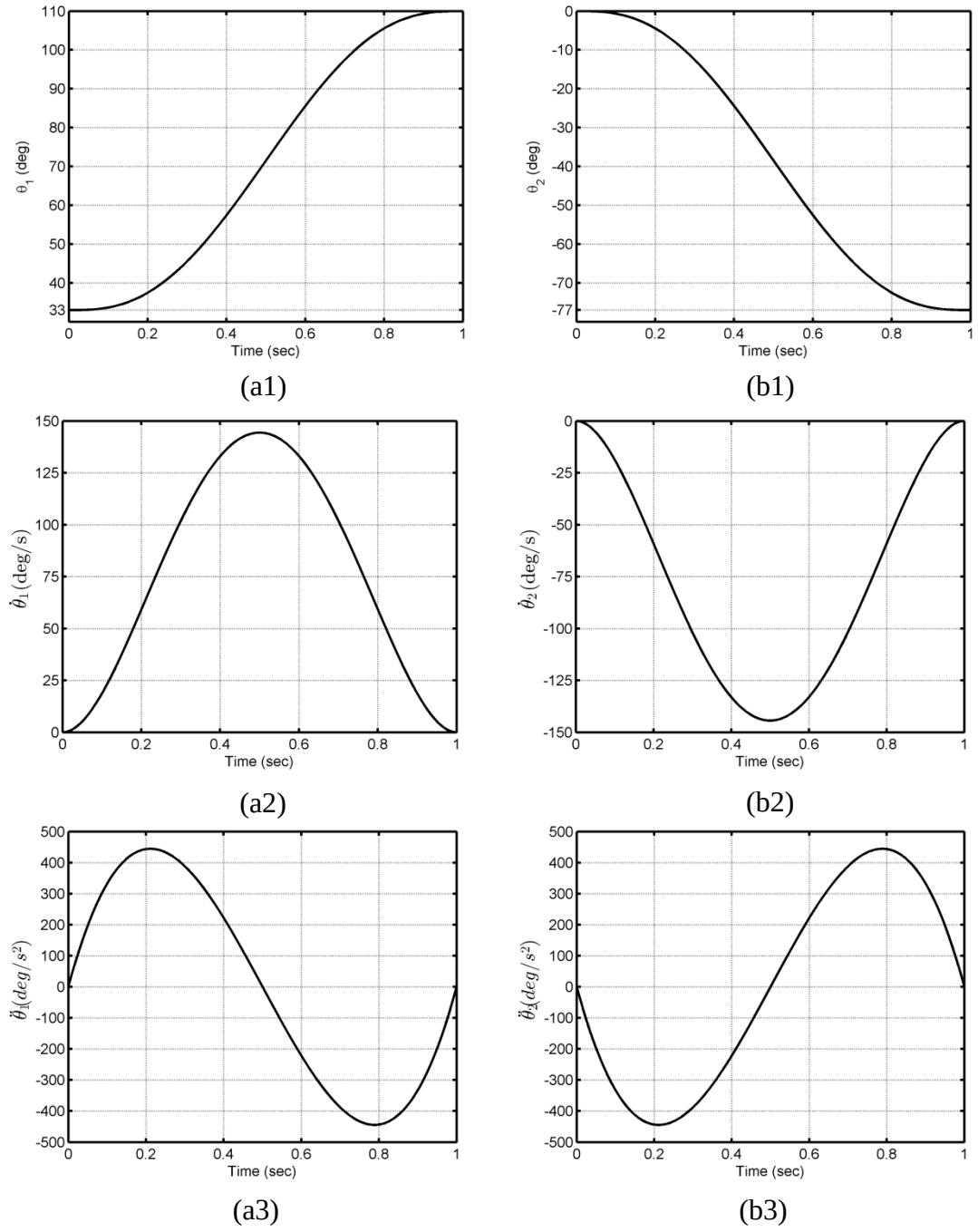

Figure 2.7. – Desired trajectories, velocities and accelerations of the two actuators.

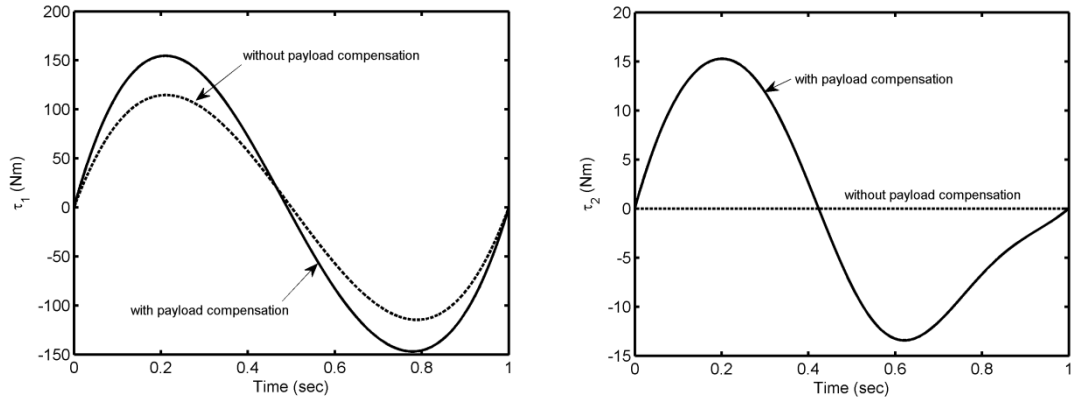

Figure 2.8. – Torques with payload compensation (solid line) and without it (dashed line) for the open-loop system.

In the controller of this system, the payload is considered as a forward compensation based on the linear and dynamic decoupling model. With payload compensation, both links of the manipulator can rotate exactly to the target angles, shown as the solid line in Fig. 2.9, because that the controller model reflects precisely the structure of the manipulator.

However, there are always some disturbances that can influence the precision. One of the extremely examples is cancellation of the payload compensation, shown as the dashed line in Fig. 2.9. Under this situation, the errors of angular displacements of link AB and BP are, respectively, 12.34% and 40.87%.

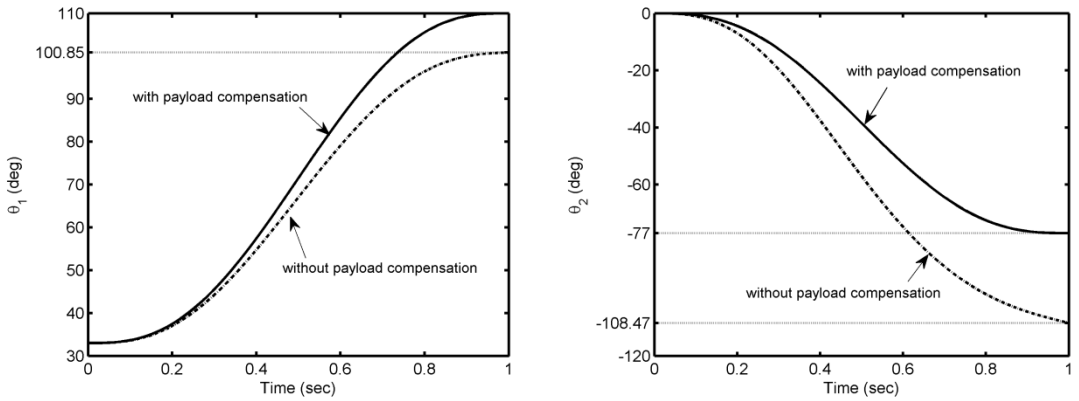

Figure 2.9. – Angular displacements of links with load compensation (solid line) and without it (dashed line) for the open-loop system.

2.5.2. Simulation model of closed-loop control system

In order to reduce the impact of disturbance on tracking accuracy, the closed-loop is added. The closed-loop control law can be written as

$$\begin{aligned}\tau_1 &= \tau_{1without} + \Delta\tau_1 \\ &\quad - g_{11}[(a'+b')[\dot{\theta}_1 - \dot{\theta}_{1R}] + a'[\dot{\theta}_2 - \dot{\theta}_{2R}]] \\ &\quad - g_{12}[(a'+b')[\theta_1 - \theta_{1R}] + a'[\theta_2 - \theta_{2R}]] \\ \tau_2 &= \tau_{2without} + \Delta\tau_2 \\ &\quad - g_{21}[a'[\dot{\theta}_1 - \dot{\theta}_{1R}] + a'[\dot{\theta}_2 - \dot{\theta}_{2R}]] \\ &\quad - g_{22}[a'[\theta_1 - \theta_{1R}] + a'[\theta_2 - \theta_{2R}]]\end{aligned} \tag{2.75}$$

where, $\tau_{1without}$, $\tau_{2without}$, $\Delta\tau_1$ and $\Delta\tau_2$ are given by equations (2.37) and (2.69). The simulation diagram in SIMULINK of MATLAB is shown in Fig. 2.10, and the detailed information is shown in Appendix A.

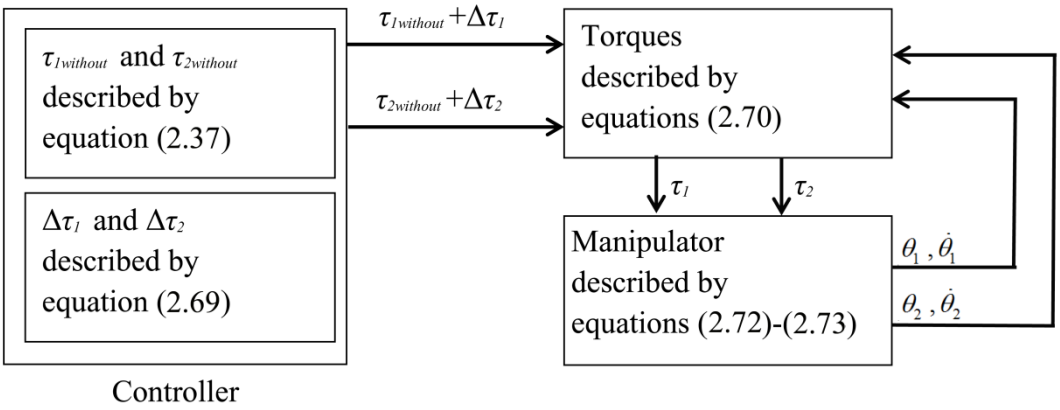

Figure 2.10. - The schema of the open-loop control system.

As in the case of open-loop system, the dashed curves show the torques and the angular displacements of the manipulator without payload compensation and the solid curves show the simulation results of the model with payload compensation in Fig.2.11 and Fig. 2.12, respectively.

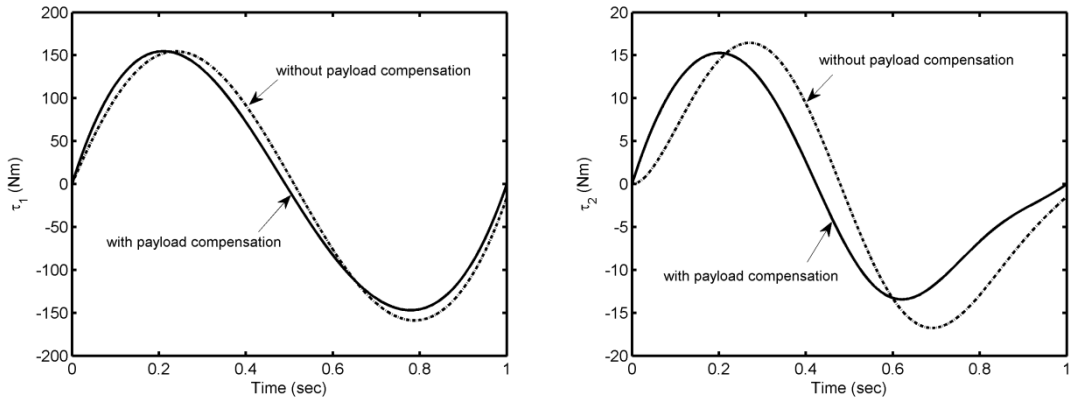

Figure 2.11. – Torques with payload compensation (solid line) and without it (dashed line) for the closed-loop system.

Comparing the torque curves of closed-loop control system with the ones of open-loop control system, it is obviously that, the two torque curves of the simulation with and without payload compensation are closer in the closed-loop control system, especially for the second actuator (Fig. 2.11). In aspect of tracking accuracy, in this closed-loop control system, the payload compensation allows an exact reproduction of manipulator motions. However, it should note that, the closed-loop can reduce the influence of absence of payload compensation, shown in Fig. 2.12. The errors of angular displacements of link AB and link BP are 1.43% and 1.18%.

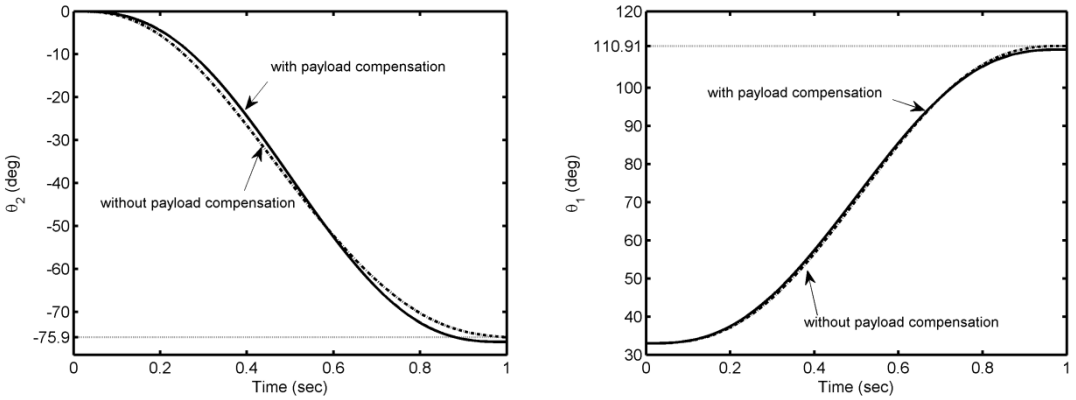

Figure 2.12. – Angular displacements of links with payload compensation (solid line) and without it (dashed line) for the closed-loop system.

2.6. Summary

This chapter deals with the design concept of adjustable serial manipulators with linearized and decoupled dynamics taking into account the changing payload. It is achieved by using links with adjustable lengths connected to the double Scott-Russell mechanism and by means of an optimal control technique. Such a dynamic decoupling is a symbiosis of mechanical and control solutions. It is carried out in two steps. At first, the dynamic decoupling of the serial manipulator with adjustable lengths of links is accomplished via an opposite rotation of links and optimal redistribution of masses. Such a solution proposed for the first time allows one to carry out the dynamic decoupling without connection of gears to the oscillating links. The elimination of gears from design concept is a main advantage of the suggested solution. Thus, the proposed mechanical solution allows one to transform the original nonlinear system model into a fully linear system without using the feedback linearization technique.

However, it is obvious that the changing payload leads to the perturbation of the dynamic decoupling of the manipulator. To ensure linearized and decoupled dynamics of the manipulator for any payload, an optimal control technique is applied. It is shown that the dynamic decoupling of the manipulator simplifies the control solution ensuring the dynamic decoupling taking into account the changing payload. The perturbation of required motions of the manipulator with payload compensation and without it is shown via ADAMS and MATLAB simulations. Two kinds of simulations are carried out with open-loop control system which is a non-feedback system and closed-loop control system. The obtained results showed the efficiency of the proposed solution.

Chapter 3

Dynamic decoupling of planar serial manipulators with revolute joints

This chapter deals with a new dynamic decoupling principle, which involves connecting to a serial manipulator with revolute joints a two-link group forming a Scott-Russell mechanism with the initial links of the manipulator. The opposite motion of links in the Scott-Russell mechanism combined with optimal redistribution of masses allows the cancellation of the coefficients of nonlinear terms in the manipulator's kinetic and potential energy equations. Then, by using the optimal control design, the dynamic decoupling due to the changing payload is achieved. The suggested design methodology is illustrated by simulations carried out using ADAMS and MATLAB software, which have confirmed the efficiency of the developed approach.

3.1. Dynamic decoupling modeling via adding a two-link group

Fig.3.1 shows a serial planar manipulator with two degrees of freedom, which consists of two principal links 1, 2 and a sub-group with links 3 and slider 4. The movements of this manipulator are planar motions which are perpendicular to the vertical plane, and therefore, not subjected to gravitational forces. The slider 4 can slide freely along the link 1, and it's connected with link 3 by revolute joint D.

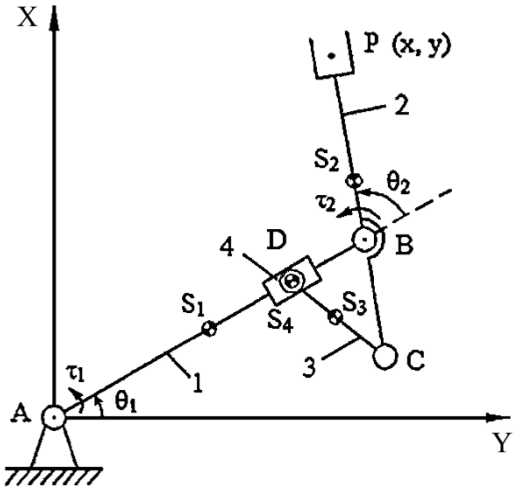

Figure 3.1. - The 2-dof planar serial manipulator with added two-link group.

Thus, the added sub-group with links 2 forms a Scott-Russell mechanism. As said above, the Scott-Russell mechanism has been developed to generate a rectilinear motion. Here, another property of this mechanism is used. The Scott-Russell linkage generates also rotations of links by identic angular accelerations, i.e. the angular accelerations of links 2 and 3 are similar.

Let us consider the equations of motion of the unbalanced mechanism. In this case, the Lagrangian of the system is equal to the total kinetic energy. The kinetic energy expressions of all parts of the structure are:

$$E_1 = \frac{1}{2} m_1 L_{AS1}^2 \dot{\theta}_1^2 + \frac{1}{2} I_{S1} \dot{\theta}_1^2 \tag{3.1}$$

$$E_2 = \frac{1}{2} m_2 [L_1^2 \dot{\theta}_1^2 + L_{BS2}^2 (\dot{\theta}_1 + \dot{\theta}_2)^2 + 2 L_1 L_{BS2} \cos(\theta_2) \dot{\theta}_1 (\dot{\theta}_1 + \dot{\theta}_2)] + \frac{1}{2} I_{S2} (\dot{\theta}_1 + \dot{\theta}_2)^2 \tag{3.2}$$

$$\begin{aligned} E_3 = \frac{1}{2} m_3[L_1^2\dot{\theta}_1^2 + L_3^2(\dot{\theta}_1+\dot{\theta}_2)^2 + L_{CS3}^2(\dot{\theta}_1-\dot{\theta}_2)^2 - 2L_1L_3\cos(\theta_2)\dot{\theta}_1(\dot{\theta}_1+\dot{\theta}_2) \\ - 2L_1L_{CS3}\cos(\theta_2)\dot{\theta}_1(\dot{\theta}_1-\dot{\theta}_2) + 2L_3L_{CS3}\cos(2\theta_2)(\dot{\theta}_1^2-\dot{\theta}_2^2)] + \frac{1}{2} I_{S3}(\dot{\theta}_1-\dot{\theta}_2)^2 \end{aligned} \tag{3.3}$$

$$E_4 = \frac{1}{2} m_4[(2L_3\cos(\theta_2)-L_1)^2\dot{\theta}_1^2 + 4L_3^2\sin^2(\theta_2)\dot{\theta}_2^2] + \frac{1}{2} I_{S4}\dot{\theta}_1^2 \tag{3.4}$$

Here, E_1, E_2, E_3 and E_4 are the kinetic energy of link 1, link 2, link 3 and slider 4 respectively. Then the dynamic equation of the serial planar manipulator can be obtained

$$\begin{bmatrix} \tau_1 \\ \tau_2 \end{bmatrix} = \begin{bmatrix} D_{11} & D_{12} \\ D_{21} & D_{22} \end{bmatrix} \begin{bmatrix} \ddot{\theta}_1 \\ \ddot{\theta}_2 \end{bmatrix} + \begin{bmatrix} D_{111} & D_{122} \\ D_{211} & D_{222} \end{bmatrix} \begin{bmatrix} \dot{\theta}_1^2 \\ \dot{\theta}_2^2 \end{bmatrix} + \begin{bmatrix} D_{112} & D_{121} \\ D_{212} & D_{221} \end{bmatrix} \begin{bmatrix} \dot{\theta}_1\dot{\theta}_2 \\ \dot{\theta}_1\dot{\theta}_2 \end{bmatrix} \tag{3.5}$$

with

$$\begin{aligned} D_{11} = {} & m_1L_{AS1}^2 + I_{S1} + m_2L_1^2 + m_2L_{BS2}^2 + 2m_2L_1L_{BS2}\cos\theta_2 + I_{S2} + m_3L_1^2 \\ & + m_3L_3^2 + m_3L_{CS3}^2 - 2m_3L_1L_3\cos\theta_2) - 2m_3L_1L_{CS3}\cos\theta_2 \\ & + 2m_3L_3L_{CS3}\cos(2\theta_2) + I_{S3} + m_4(2L_3\cos\theta_2 - L_1)^2 + I_{S4} \end{aligned} \tag{3.6}$$

$$\begin{aligned} D_{12} = D_{21} = {} & m_2L_{BS2}^2 + m_2L_1L_{BS2}\cos\theta_2 + I_{S2} + m_3L_3^2 - m_3L_{CS3}^2 - m_3L_1L_3\cos\theta_2 \\ & + m_3L_1L_{CS3}\cos\theta_2 - I_{S3} \end{aligned} \tag{3.7}$$

$$D_{22} = m_2L_{BS2}^2 + I_{S2} + m_3L_3^2 + m_3L_{CS3}^2 - 2m_3L_3L_{CS3}\cos(2\theta_2) + I_{S3} + 4m_4L_3^2\sin^2\theta_2 \tag{3.8}$$

$$D_{111} = 0 \tag{3.9}$$

$$D_{122} = -m_2L_1L_{BS2}\sin\theta_2 + m_3L_1L_3\sin\theta_2 - m_3L_1L_{CS3}\sin\theta_2 \tag{3.10}$$

$$\begin{aligned} D_{211} = {} & m_2L_1L_{BS2}\sin\theta_2 - m_3L_1L_3\sin\theta_2 - m_3L_1L_{CS3}\sin\theta_2 + 2m_3L_3L_{CS3}\sin(2\theta_2) \\ & + 2m_4L_3(2L_3\cos\theta_2 - L_1)\sin\theta_2 \end{aligned} \tag{3.11}$$

$$D_{222} = 2m_3L_3L_{CS3}\sin(2\theta_2) + 2m_4L_3^2\sin(2\theta_2) \tag{3.12}$$

$$\begin{aligned} D_{112} = {} & -2m_2L_1L_{BS2}\sin\theta_2 + 2m_3L_1L_3\sin\theta_2 + 2m_3L_1L_{CS3}\sin\theta_2 \\ & - 4m_3L_3L_{CS3}\sin(2\theta_2) - 4m_4L_3^2\sin(2\theta_2) + 4m_4L_1L_3\sin(\theta_2) \end{aligned} \tag{3.13}$$

$$D_{121} = D_{212} = D_{221} = 0 \tag{3.14}$$

where, m_1, m_2, m_3, and m_4 are the masses of link 1, link 2, link 3 and slider 4 respectively; I_{S1}, I_{S2}, I_{S3} and I_{S4} are the moments of inertia of link 1, link 2, link 3 and slider respectively; L_1, L_2, L_3 are the lengths of link 1, link 2 , link 3 respectively, and L_3 also the distance between centers of revolute joints B and C; L_{AS1} is the distance between the center of mass S_1 of link 1 and joint center A; L_{BS2} is the distance between the center of mass S_2 of link 2 and joint center B; L_{CS3} is the distance between the center of joint C and center of mass of link 3; θ_1 is angular displacement of link 1 relative to the base; θ_2 is angular displacement of link 2 relative to link 1; $\dot{\theta}_1$ is angular velocity of link 1 relative to the base; $\dot{\theta}_2$ is angular velocity of link 2 relative to link 1; $\ddot{\theta}_1$ is the angular acceleration of link 1relative to the base; $\ddot{\theta}_2$ is the angular acceleration of link 2 relative to link 1.

In order to further simplify this dynamic equation, two balancing conditions are applied

$$m_3 L_{CS3} + m_4 L_3 = 0 \tag{3.15}$$

$$(m_3 + m_4) L_3 - m_2 L_{BS2} = 0 \tag{3.16}$$

Substituting these two equations into the dynamic equation (3.5), then it can be simplified as

$$\begin{cases} \tau_1 = d\ddot{\theta}_1 + b\ddot{\theta}_2 \\ \tau_2 = b\ddot{\theta}_1 + c\ddot{\theta}_2 \end{cases} \tag{3.17}$$

where

$$d = I_{S1} + I_{S2} + I_{S3} + I_{S4} + m_1 L_{AS1}^2 + (m_2 + m_3 + m_4) L_1^2 + \left[\frac{(m_3 + m_4)^2}{m_2} + \frac{(m_3 + m_4)^2}{m_3} \right] L_3^2$$

$$b = I_{S2} - I_{S3} + \left[\frac{(m_3 + m_4)^2}{m_2} + \frac{m_3^2 - m_4^2}{m_3} \right] L_3^2$$

$$c = I_{S2} + I_{S3} + \left[\frac{(m_3 + m_4)^2}{m_2} + \frac{(m_3 + m_4)^2}{m_3} \right] L_3^2$$

Obviously, we obtain linear dynamic equations.

Furthermore, if

$$I_{S3} = I_{S2} + \left[\frac{(m_3 + m_4)^2}{m_2} + \frac{m_3^2 - m_4^2}{m_3} \right] L_3^2 \tag{3.18}$$

then we get b=0.

Thus, the complete dynamic decoupling of the serial planar manipulator without payload is achieved:

$$\begin{cases} \tau_{1without} = d'\ddot{\theta}_1 \\ \tau_{2without} = c'\ddot{\theta}_2 \end{cases} \tag{3.19}$$

where,

$$\begin{aligned} d' &= I_{S1} + 2I_{S2} + I_{S4} + m_1 L_{AS1}^2 + (m_2 + m_3 + m_4) L_1^2 \\ &\quad + 2\frac{(m_3 + m_4)(m_2 + m_3 + m_4)}{m_2} L_3^2 \\ c' &= 2[I_{S2} + \frac{(m_3 + m_4)(m_2 + m_3 + m_4)}{m_2} L_3^2] \end{aligned}$$

3.2. Closed-loop control

The main goal of the closed-loop control is actually to stabilize this serial planar manipulator which is instable. The feedback design allows good tracking properties.

Define the state vector as $\xi = [\theta_1 \quad \dot{\theta}_1 \quad \theta_2 \quad \dot{\theta}_2]^T$.

According to the inverse calculation of the equation (3.19), the state equation of the MIMO model can be obtained

$$\begin{bmatrix} \dot{\xi}_1 \\ \dot{\xi}_2 \\ \dot{\xi}_3 \\ \dot{\xi}_4 \end{bmatrix} = \underbrace{\begin{bmatrix} 0 & 1 & 0 & 0 \\ 0 & 0 & 0 & 0 \\ 0 & 0 & 0 & 1 \\ 0 & 0 & 0 & 0 \end{bmatrix}}_{A} \begin{bmatrix} \xi_1 \\ \xi_2 \\ \xi_3 \\ \xi_4 \end{bmatrix} + \underbrace{\begin{bmatrix} 0 & 0 \\ \frac{1}{d'} & 0 \\ 0 & 0 \\ 0 & \frac{1}{c'} \end{bmatrix}}_{B} \underbrace{\begin{bmatrix} \tau_{1without} \\ \tau_{2without} \end{bmatrix}}_{\tau} \tag{3.20}$$

The controllable canonical form of the state equation should be built for the further research. It needs to use the following transformation:

$$\xi = \left[T_{cc} W_c\right]\zeta \tag{3.21}$$

where, T_{cc} is the controllability matrix, and it is formed as

$$T_{cc} = [B \mid AB] = \begin{bmatrix} 0 & 0 & \frac{1}{d'} & 0 \\ \frac{1}{d'} & 0 & 0 & 0 \\ 0 & 0 & 0 & \frac{1}{c'} \\ 0 & \frac{1}{c'} & 0 & 0 \end{bmatrix}$$

W_c, is the upper triangular Toeplitz matrix, and it is formed by characteristic equation of matrix A: $|sI\text{-}A|=s^4 + a_3 s^3 + a_2 s^2 + a_1 s + a_0 = s^4$. So,

$$W_c = \begin{bmatrix} 1 & a_3 & a_2 & a_1 \\ 0 & 1 & a_3 & a_2 \\ 0 & 0 & 1 & a_3 \\ 0 & 0 & 0 & 1 \end{bmatrix} = \begin{bmatrix} 1 & 0 & 0 & 0 \\ 0 & 1 & 0 & 0 \\ 0 & 0 & 1 & 0 \\ 0 & 0 & 0 & 1 \end{bmatrix} = I$$

As known,

$$\dot{\xi} = A\xi + B\tau \tag{3.22}$$

Substituting the equation (3.39) into equation (3.40), we obtain

$$\dot{\zeta} = \left[T_{cc}\right]^{-1} A \left[T_{cc}\right]\zeta + \left[T_{cc}\right]^{-1} B\tau \tag{3.23}$$

Hence, the controllable canonical form is given by

$$\begin{bmatrix} \dot{\zeta}_1 \\ \dot{\zeta}_2 \\ \dot{\zeta}_3 \\ \dot{\zeta}_4 \end{bmatrix} = \begin{bmatrix} 0 & 0 & 0 & 0 \\ 0 & 0 & 0 & 0 \\ 1 & 0 & 0 & 0 \\ 0 & 1 & 0 & 0 \end{bmatrix} \begin{bmatrix} \zeta_1 \\ \zeta_2 \\ \zeta_3 \\ \zeta_4 \end{bmatrix} + \begin{bmatrix} 1 & 0 \\ 0 & 1 \\ 0 & 0 \\ 0 & 0 \end{bmatrix} \begin{bmatrix} \tau_{1without} \\ \tau_{2without} \end{bmatrix} \tag{3.24}$$

and the state vector

$$\begin{bmatrix}\zeta_1\\ \zeta_2\\ \zeta_3\\ \zeta_4\end{bmatrix}=[T_{cc}]^{-1}\xi(t)=\begin{bmatrix}d'\dot{\theta}_1\\ c'\dot{\theta}_2\\ d'\theta_1\\ c'\theta_2\end{bmatrix} \tag{3.25}$$

It is obviously that, the system that described by state equation (3.42) can be divided into two independent subsystems:

$$\begin{cases}\begin{bmatrix}\dot{\zeta}_1\\ \dot{\zeta}_3\end{bmatrix}=\begin{bmatrix}0 & 0\\ 1 & 0\end{bmatrix}\begin{bmatrix}\zeta_1\\ \zeta_3\end{bmatrix}+\begin{bmatrix}1\\ 0\end{bmatrix}\tau_{1without}\\ \begin{bmatrix}\dot{\zeta}_2\\ \dot{\zeta}_4\end{bmatrix}=\begin{bmatrix}0 & 0\\ 1 & 0\end{bmatrix}\begin{bmatrix}\zeta_2\\ \zeta_4\end{bmatrix}+\begin{bmatrix}1\\ 0\end{bmatrix}\tau_{2without}\end{cases} \tag{3.26}$$

Hence, when taking into account the feedback control, the closed-loop can be added firstly on each simple subsystem, then combine them together for the whole system. Obviously, both of these two subsystems are simple double integrator structures. Hence, the linear control method can be employed.

3.2.1. Command of the first double integrator

According to the first double integrator, we can deduce:

$$\begin{cases}\dot{\zeta}_1=\tau_{1without}\\ \dot{\zeta}_3=\zeta_1\end{cases} \tag{3.27}$$

Assuming that $\begin{cases}\rho=\zeta_3\\ \dot{\rho}=\zeta_1\end{cases}$

Then the state equation of the double integrator is given by

$$\begin{bmatrix}\dot{\rho}\\ \ddot{\rho}\end{bmatrix}=\underbrace{\begin{bmatrix}0 & 1\\ 0 & 0\end{bmatrix}}_{A_1}\begin{bmatrix}\rho\\ \dot{\rho}\end{bmatrix}+\underbrace{\begin{bmatrix}0\\ 1\end{bmatrix}}_{B_1}\tau_{1without} \tag{3.28}$$

Obviously, this is a simple double integrator structure. For the closed-loop control, the control law can be written as

$$\tau_{1without}=\mu_1-g_{11}\dot{\rho}-g_{12}\rho \tag{3.29}$$

Sustituting this control law in the equation (3.28), then the state equation of the double integrator can be rewritten as

$$\begin{bmatrix} \dot{\rho} \\ \ddot{\rho} \end{bmatrix} = \begin{bmatrix} 0 & 1 \\ -g_{12} & -g_{11} \end{bmatrix} \begin{bmatrix} \rho \\ \dot{\rho} \end{bmatrix} + \begin{bmatrix} 0 \\ 1 \end{bmatrix} \mu_1 \tag{3.30}$$

Assuming that

$$\mu_1 = \omega_1 + g_{11}\dot{\rho} + g_{12}\rho \tag{3.31}$$

then

$$\begin{bmatrix} \dot{\rho} \\ \ddot{\rho} \end{bmatrix} = \begin{bmatrix} 0 & 1 \\ 0 & 0 \end{bmatrix} \begin{bmatrix} \rho \\ \dot{\rho} \end{bmatrix} + \begin{bmatrix} 0 \\ 1 \end{bmatrix} \omega_1 \tag{3.32}$$

hence, $\omega_1 = \ddot{\rho}$. It can be found that

$$\mu_1 = \ddot{\rho} + g_{11}\dot{\rho} + g_{12}\rho \tag{3.33}$$

It is concluded that a balance position of the double integrator is given by the conditions about ρ and its continual derivatives.

Hence, if a trajectory ρ_R which is secondary derivable over a range [0, T] is given, we can deduce:

$$\mu_{1R} = \ddot{\rho}_R + g_{11}\dot{\rho}_R + g_{12}\rho_R \tag{3.34}$$

Finally, the control law of the closed-loop double integrator is

$$\tau_{1without} = \ddot{\rho}_R - g_{11}[\dot{\rho} - \dot{\rho}_R] - g_{12}[\rho - \rho_R] \tag{3.35}$$

As known, $\rho = d'\theta_1$, the control law can be rewritten as

$$\tau_{1without} = d'\ddot{\theta}_{1R} - g_{11}d'[\dot{\theta}_1 - \dot{\theta}_{1R}] - g_{12}d'[\theta_1 - \theta_{1R}] \tag{3.36}$$

3.2.2. Determination of the feedback parameters for the first double integrator

In order to realize the control law: $\tau_1(t) = -G_1\left[\rho(t)\ \ \dot{\rho}(t)\right]^T$, the matrix of state feedback parameter $G_1 = [g_{12}\ \ g_{11}]$ should be obtained.

It is calculated by minimizing the index of performance *J* below:

$$J = \int_0^\infty \left[\begin{bmatrix} \rho(t) & \dot{\rho}(t) \end{bmatrix} Q_1 \begin{bmatrix} \rho(t) \\ \dot{\rho}(t) \end{bmatrix} + \tau_1^T(t) R_1 \tau_1(t) \right] dt \tag{3.37}$$

where

$R_1 = 1 > 0$

$$Q_1 = \left[T_{p1} \left(\int_0^{T_{p1}} e^{A_1 \tau} B_1 B_1^T e^{A_1^T \tau} d\tau \right) \right]^{-1} = \begin{bmatrix} \frac{12}{T_{p1}^4} & -\frac{6}{T_{p1}^3} \\ -\frac{6}{T_{p1}^3} & \frac{4}{T_{p1}^2} \end{bmatrix} > 0$$

Assuming that the symmetric matrix Σ_1 is the solution of Riccati equation

$$A_1^T \Sigma_1 + \Sigma_1 A_1 - \Sigma_1 B_1 R_1^{-1} B_1^T \Sigma_1 + Q_1 = 0 \tag{3.38}$$

where $\Sigma_1 = \begin{bmatrix} \sigma_1 & \sigma_2 \\ \sigma_2 & \sigma_3 \end{bmatrix}$ must be positive-definite, i.e. $\begin{cases} \sigma_1 > 0 \\ \sigma_1 \sigma_3 - \sigma_2^2 > 0 \end{cases}$

thus $\begin{cases} \sigma_1 = \sigma_2 \sigma_3 + \frac{6}{T_{p1}^3} > 0; \\ \sigma_2^2 = \frac{12}{T_{p1}^4} \Rightarrow \sigma_2 = \pm \frac{2\sqrt{3}}{T_{p1}^2}; \\ \sigma_3^2 = 2\sigma_2 + \frac{4}{T_{p1}^2} > 0. \end{cases}$

we obtain

$$\begin{cases} 2\sigma_2 + \frac{4}{T_{p1}^2} > 0 \Rightarrow \sigma_2 = \frac{2\sqrt{3}}{T_{p1}^2} \Rightarrow \sigma_3^2 = \frac{4(1+\sqrt{3})}{T_{p1}^2} \\ \sigma_2 \sigma_3 + \frac{6}{T_{p1}^3} > 0 \Rightarrow \sigma_3 = \frac{2\sqrt{1+\sqrt{3}}}{T_{p1}} \\ \sigma_1 = \sigma_2 \sigma_3 + \frac{6}{T_{p1}^3} = \frac{6 + 4\sqrt{3}\sqrt{1+\sqrt{3}}}{T_{p1}^3} \end{cases} \tag{3.39}$$

Hence, the expression of matrix Σ_1 is

$$\Sigma_1 = \begin{bmatrix} \dfrac{6+4\sqrt{3}\sqrt{1+\sqrt{3}}}{T_{p1}^3} & \dfrac{2\sqrt{3}}{T_{p1}^2} \\ \dfrac{2\sqrt{3}}{T_{p1}^2} & \dfrac{2\sqrt{1+\sqrt{3}}}{T_{p1}} \end{bmatrix} \tag{3.40}$$

As known, the matrix G_1 is noted as

$$G_1 = R_1^{-1} B_1^T \Sigma_1 \tag{3.41}$$

Then,

$$G_1 = \begin{bmatrix} \dfrac{2\sqrt{3}}{T_{p1}^2} & \dfrac{2\sqrt{1+\sqrt{3}}}{T_{p1}} \end{bmatrix} \tag{3.42}$$

As result, we obtain $g_{12} = \dfrac{2\sqrt{3}}{T_{p1}^2}$ and $g_{11} = \dfrac{2\sqrt{1+\sqrt{3}}}{T_{p1}}$.

The state model of the closed-loop system is written as follows

$$\begin{bmatrix} \dot{\rho} \\ \ddot{\rho} \end{bmatrix} = \left[A_1 - B_1 G_1\right] \begin{bmatrix} \rho \\ \dot{\rho} \end{bmatrix} = \begin{bmatrix} 0 & 1 \\ -\dfrac{2\sqrt{3}}{T_{p1}^2} & -\dfrac{2\sqrt{1+\sqrt{3}}}{T_{p1}} \end{bmatrix} \begin{bmatrix} \rho \\ \dot{\rho} \end{bmatrix} \tag{3.43}$$

The characteristic polynomial P(s) is given by

$$P(s) = |\, sI - A_1 + B_1 G_1 \,| = s^2 + \frac{2\sqrt{1+\sqrt{3}}}{T_{p1}} s + \frac{2\sqrt{3}}{T_{p1}^2} \tag{3.44}$$

If $P(s) = s^2 + 2\zeta\omega_n s + \omega_n^2$, we obtain $\omega_n = \dfrac{\sqrt{2\sqrt{3}}}{T_{p1}}$ and $\zeta = \dfrac{\sqrt{1+\sqrt{3}}}{\sqrt{2\sqrt{3}}} \approx 0.89$.

According to these results, the control law and feedback parameters of the second double integrator can be written as

$$\tau_{2without} = c'\ddot{\theta}_{2R} - g_{21}c'[\dot{\theta}_2 - \dot{\theta}_{2R}] - g_{22}c'[\theta_2 - \theta_{2R}] \tag{3.45}$$

where, $g_{22} = \dfrac{2\sqrt{3}}{T_{p2}^2}$ and $g_{21} = \dfrac{2\sqrt{1+\sqrt{3}}}{T_{p2}}$.

3.3. Dynamic analysis taking into account the payload

Based on the assumption above, we consider the link 2 and the payload as one object. Then,

$$M_2 = m_2 + m_p \tag{3.46}$$

$$L_{BS2r} = \frac{m_2}{M_2} L_{BS2} + \frac{m_p}{M_2} L_{BP} \tag{3.47}$$

$$I_{2+p} = I_2 + m_2(L_{BS2} - L_{BS2r})^2 + m_p(L_2 - L_{BS2r})^2 \tag{3.48}$$

where, M_2 is the total mass of link 2 and the payload; L_{BS2r} is the distance between the mass center of M_2 and the joint center B; L_{BP} is the distance between the joint center B and the end-effector; I_{2+p} is the total moment of inertia of link 2 and the payload.

Thus, according to the Lagrangian dynamics, the dynamic equations with payload are:

$$\begin{aligned}
\tau_{1with} &= \frac{d}{dt}\left(\frac{\partial L}{\partial \dot{\theta}_1}\right) - \frac{\partial L}{\partial \theta_1} \\
&= \ddot{\theta}_1[m_1 L_{AS1}^2 + I_{S1} + M_2 L_1^2 + M_2 L_{BS2r}^2 + 2M_2 L_1 L_{BS2r}\cos(\theta_2) + I_{2+P} \\
&\quad + m_3 L_1^2 + m_3 L_3^2 + m_3 L_{CS3}^2 - 2m_3 L_1 L_3 \cos(\theta_2) - 2m_3 L_1 L_{CS3}\cos(\theta_2) \\
&\quad + 2m_3 L_3 L_{CS3}\cos(2\theta_2) + I_{S3} + m_4(2L_3\cos(\theta_2) - L_1)^2 + I_{S4}] \\
&+ \ddot{\theta}_2[M_2 L_{BS2r}^2 + M_2 L_1 L_{BS2r}\cos(\theta_2) + I_{2+P} + m_3 L_3^2 - m_3 L_{CS3}^2 \\
&\quad - m_3 L_1 L_3 \cos(\theta_2) + m_3 L_1 L_{CS3}\cos(\theta_2) - I_{S3}] \\
&+ \dot{\theta}_1\dot{\theta}_2[-2M_2 L_1 L_{BS2r}\sin(\theta_2) + 2m_3 L_1 L_3 \sin(\theta_2) + 2m_3 L_1 L_{CS3}\sin(\theta_2) \\
&\quad - 4m_3 L_3 L_{CS3}\sin(2\theta_2) - 4m_4 L_3(2L_3\cos(\theta_2) - L_1)\sin(\theta_2)] \\
&+ \dot{\theta}_2^2[-M_2 L_1 L_{BS2r}\sin(\theta_2) + m_3 L_1 L_3 \sin(\theta_2) - m_3 L_1 L_{CS3}\sin(\theta_2)]
\end{aligned} \tag{3.49}$$

$$
\begin{aligned}
\tau_{2with} &= \frac{d}{dt}\left(\frac{\partial L}{\partial \dot{\theta}_2}\right) - \frac{\partial L}{\partial \theta_2} \\
&= \ddot{\theta}_1[M_2 L_{BS2r}^2 + 2M_2 L_1 L_{BS2r}\cos(\theta_2) + I_{2+p} + m_3 L_3^2 - m_3 L_{CS3}^2 \\
&\quad - m_3 L_1 L_3 \cos(\theta_2) + m_3 L_1 L_{CS3}\cos(\theta_2) - I_{S3}] \\
&+ \ddot{\theta}_2[M_2 L_{BS2r}^2 + I_{2+p} + m_3 L_3^2 + m_3 L_{CS3}^2 - 2m_3 L_3 L_{CS3}\cos(2\theta_2) + I_{S3} \\
&\quad + 4m_4 L_3^2 \sin^2(\theta_2)] \\
&+ \dot{\theta}_1^2[M_2 L_1 L_{BS2r}\sin(\theta_2) - m_3 L_1 L_3 \sin(\theta_2) - m_3 L_1 L_{CS3}\sin(\theta_2) \\
&\quad + 2m_3 L_3 L_{CS3}\sin(2\theta_2) + 2m_4 L_3(2L_3\cos(\theta_2) - L_1)\sin(\theta_2)] \\
&+ \dot{\theta}_2^2[2m_3 L_3 L_{CS3}\sin(2\theta_2) - 2m_4 L_3^2 \sin(2\theta_2)]
\end{aligned}
\tag{3.50}
$$

where, τ_{1with} and τ_{2with} are the output torque values of the first actuator and the second actuator respectively when taking into account the payload on the end-effector of the serial manipulator.

From equations (3.15), (3.16) and (3.47), we can obtain that

$$L_{CS3} = -\frac{m_4}{m_3} L_3 \tag{3.51}$$

$$L_{BS2r} = \frac{(m_3 + m_4)}{M_2} L_3 + \frac{m_p}{M_2} L_{BP} \tag{3.52}$$

Substituting these two equations into the dynamic equations (3.49) and (3.50), then they can be simplified as

$$
\begin{aligned}
\tau_{1with} &= \ddot{\theta}_1[I_{S1} + I_{2+p} + I_{S3} + I_{S4} + m_1 L_{AS1}^2 + M_2 L_1^2 + m_3 L_1^2 + m_4 L_1^2 \\
&\quad + \frac{[(m_3 + m_4)L_3 + m_p L_{BP}]^2}{M_2} + \frac{(m_3 + m_4)^2}{m_3} L_3^2 + 2m_p L_1 L_{BP}\cos(\theta_2)] \\
&\quad + \ddot{\theta}_2[I_{2+p} - I_{S3} + \frac{[(m_3 + m_4)L_3 + m_p L_2]^2}{M_2} + \frac{m_3^2 - m_4^2}{m_3} L_3^2] \\
&\quad + \ddot{\theta}_2[m_p L_1 L_{BP}\cos(\theta_2)] + \dot{\theta}_1\dot{\theta}_2[-2m_p L_1 L_{BP}\sin(\theta_2)] + \dot{\theta}_2^2[-m_p L_1 L_{BP}\sin(\theta_2)]
\end{aligned}
\tag{3.53}
$$

$$\begin{aligned}\tau_{2with} &= \ddot{\theta}_1[I_{2+p} - I_{S3} + \frac{[(m_3+m_4)L_3 + m_pL_{BP}]^2}{M_2} + \frac{m_3^2 - m_4^2}{m_3}L_3^2] \\ &+ \ddot{\theta}_2[I_{2+p} + I_{S3} + \frac{[(m_3+m_4)L_3 + m_pL_{BP}]^2}{M_2} + \frac{(m_3+m_4)^2}{m_3}L_3^2] \\ &+ \ddot{\theta}_1[m_pL_1L_{BP}\cos(\theta_2)] + \dot{\theta}_1^2[m_pL_{BP}]L_1\sin(\theta_2)\end{aligned} \tag{3.54}$$

Finally, replace the parameter I_{S3} and I_{2+p} by the equations (3.18) and (3.48), the dynamic equation with payload can be rewritten as

$$\begin{cases}\tau_{1with} = \ddot{\theta}_1[I_{S1} + 2I_{S2} + I_{S4} + m_1L_{AS1}^2 + (m_2+m_3+m_4)L_1^2 + 2\dfrac{(m_3+m_4)(m_2+m_3+m_4)}{m_2}L_3^2] \\ \quad + \ddot{\theta}_1[m_pL_1^2] + (\ddot{\theta}_1 + \ddot{\theta}_2)[\dfrac{[m_pL_{BP} + (m_3+m_4)L_3]^2}{M_2} - \dfrac{(m_3+m_4)^2}{m_2}L_3^2] \\ \quad + \ddot{\theta}_1[2m_pL_1L_{BP}]\cos\theta_2 + \ddot{\theta}_2[m_pL_1L_{BP}]\cos\theta_2 + \dot{\theta}_1\dot{\theta}_2[-2m_pL_1L_{BP}]\sin\theta_2 \\ \quad + \dot{\theta}_2^2[-m_pL_1L_{BP}]\sin\theta_2 \\ \tau_{2with} = 2\ddot{\theta}_2[I_{S2} + \dfrac{(m_3+m_4)(m_2+m_3+m_4)}{m_2}L_3^2] \\ \quad + (\ddot{\theta}_1 + \ddot{\theta}_2)[\dfrac{[m_pL_{BP} + (m_3+m_4)L_3]^2}{M_2} - \dfrac{(m_3+m_4)^2}{m_2}L_3^2] \\ \quad + \ddot{\theta}_1[m_pL_1L_{BP}]\cos\theta_2 + \dot{\theta}_1^2[m_pL_1L_{BP}]\sin\theta_2\end{cases} \tag{3.55}$$

Compare equation (3.55) with equation (3.19), the torques related to the payload can be found

$$\begin{cases}\Delta\tau_1 = \ddot{\theta}_1[m_pL_1^2] + (\ddot{\theta}_1 + \ddot{\theta}_2)[\dfrac{[m_pL_{BP} + (m_3+m_4)L_3]^2}{M_2} - \dfrac{(m_3+m_4)^2}{m_2}L_3^2] \\ \quad + \ddot{\theta}_1[2m_pL_1L_{BP}]\cos\theta_2 + \ddot{\theta}_2[m_pL_1L_{BP}]\cos\theta_2 + \dot{\theta}_1\dot{\theta}_2[-2m_pL_1L_{BP}]\sin\theta_2 \\ \quad + \dot{\theta}_2^2[-m_pL_1L_{BP}]\sin\theta_2 \\ \Delta\tau_2 = (\ddot{\theta}_1 + \ddot{\theta}_2)[\dfrac{[m_pL_{BP} + (m_3+m_4)L_3]^2}{M_2} - \dfrac{(m_3+m_4)^2}{m_2}L_3^2] \\ \quad + \ddot{\theta}_1[m_pL_1L_{BP}]\cos\theta_2 + \dot{\theta}_1^2[m_pL_1L_{BP}]\sin\theta_2\end{cases} \tag{3.56}$$

Hence, the dynamic equation with payload can be rewritten as

$$\begin{cases} \tau_{1with} = \tau_{1without} + \Delta\tau_1 \\ \tau_{2with} = \tau_{2without} + \Delta\tau_2 \end{cases} \tag{3.57}$$

As noted in the previous chapter, this part is referred as payload compensation. Extracting the payload compensation from the dynamic equation of the model taking into account the payload, then the model can be treated still as a dynamic decoupling model. Also, no matter there is payload or not, the simple linear control law can always be used.

3.4. Illustrative example with the SIMULINK block of MATLAB

For verifying the performance of this proposed dynamic decoupling method, a simulation model will be built in the SIMULINK block of MATLAB. We note that

$$\begin{aligned}
a_0 &= [m_1 L_{AS1}^2 + I_{S1} + M_2 L_1^2 + M_2 L_{BS2r}^2 + I_{2+p} + m_3 L_1^2 + m_3 L_3^2 \\
&\quad + m_3 L_{CS3}^2 + I_{S3} + I_{S4} + 4m_4 L_3^2 + m_4 L_1^2 + 2m_3 L_3 L_{CS3}] \\
a_1 &= [m_3 L_3 L_{CS3} + m_4 L_3^2] \\
a_2 &= [M_2 L_1 L_{BS2r} - m_3 L_1 L_3] \\
a_3 &= [M_2 L_{BS2r}^2 + I_{2+p} + m_3 L_3^2] \\
a_4 &= [m_3 L_{CS3}^2 + I_3] \\
a_5 &= [m_3 L_1 L_3] \\
a_6 &= [m_4 L_1 L_3] \\
a_7 &= [m_3 L_3 L_{CS3}]
\end{aligned} \tag{3.58}$$

then, the dynamic equations (3.49) and (3.50) can be rewritten as

$$\begin{aligned}
\tau_1 &= a_0\ddot{\theta}_1 + \ddot{\theta}_1[2a_2 - 2a_5 - 4a_6]\cos(\theta_2) + \ddot{\theta}_1[-4a_1]\sin^2(\theta_2) \\
&\quad + \ddot{\theta}_2[a_3 - a_4] + \ddot{\theta}_2[a_2 + a_5]\cos(\theta_2) + \dot{\theta}_1\dot{\theta}_2[-2a_2 + 2a_5 + 4a_6]\sin(\theta_2) \\
&\quad + \dot{\theta}_1\dot{\theta}_2[-8a_1]\sin(\theta_2)\cos(\theta_2) + \dot{\theta}_2^2[-a_2 - a_5]\sin(\theta_2)
\end{aligned} \tag{3.59}$$

$$\begin{aligned}\tau_2 &= \ddot{\theta}_1[a_3 - a_4] + \ddot{\theta}_1[a_2 + a_5]\cos(\theta_2) \\ &+ \ddot{\theta}_2[a_3 + a_4 - 2a_7] + \ddot{\theta}_2[4a_1]\sin^2(\theta_2) \\ &+ \dot{\theta}_1^2[a_2 - a_5 - 2a_6]\sin(\theta_2) + \dot{\theta}_1^2[4a_1]\sin(\theta_2)\cos(\theta_2) \\ &+ \dot{\theta}_2^2[4a_1]\sin(\theta_2)\cos(\theta_2)\end{aligned} \tag{3.60}$$

According to the form $A\ddot{\underline{q}} + C\dot{\underline{q}} = \underline{\tau}$,we can obtain the dynamic model equation as

$$\begin{bmatrix}\tau_1 \\ \tau_2\end{bmatrix} = \underbrace{\begin{bmatrix}a_0 + 2\alpha_1(\theta_2) - 4\beta_1(\theta_2) & a_3 - a_4 + \gamma_1(\theta_2) \\ a_3 - a_4 + \gamma_1(\theta_2) & a_3 + a_4 - 2\phi_7 + 4\beta_1(\theta_2)\end{bmatrix}}_{A}\underbrace{\begin{bmatrix}\ddot{\theta}_1 \\ \ddot{\theta}_2\end{bmatrix}}_{\ddot{q}} + \underbrace{\begin{bmatrix}\dot{\theta}_2[-2\alpha_2(\theta_2) - 8\beta_2(\theta_2)] & \dot{\theta}_2[-\gamma_2(\theta_2)] \\ \dot{\theta}_1[\alpha_2(\theta_2) + 4\beta_2(\theta_2)] & \dot{\theta}_2[4\beta_2(\theta_2)]\end{bmatrix}}_{C}\underbrace{\begin{bmatrix}\dot{\theta}_1 \\ \dot{\theta}_2\end{bmatrix}}_{\dot{q}} \tag{3.61}$$

where

$$\begin{aligned}\alpha_1(\theta_2) &= [a_2 - a_5 - a_6]\cos(\theta_2) \\ \alpha_2(\theta_2) &= [a_2 - a_5 - a_6]\sin(\theta_2) \\ \beta_1(\theta_2) &= a_1\sin^2(\theta_2) \\ \beta_2(\theta_2) &= a_1\sin(\theta_2)\cos(\theta_2) \\ \gamma_1(\theta_2) &= [a_2 + a_5]\cos(\theta_2) \\ \gamma_2(\theta_2) &= [a_2 + a_5]\sin(\theta_2)\end{aligned}$$

As the matrix A is positive and invertible, we deduce

$$A^{-1} = \frac{1}{\Delta(\theta_2)}\begin{bmatrix}a_3 + a_4 - 2a_7 + 4\beta_1(\theta_2) & -a_3 + a_4 - \gamma_1(\theta_2) \\ -a_3 + a_4 - \gamma_1(\theta_2) & a_0 + 2\alpha_1(\theta_2) - 4\beta_1(\theta_2)\end{bmatrix} \tag{3.62}$$

where

$$\Delta(\theta_2) = \left[a_0 + 2\alpha_1(\theta_2) - 4\beta_1(\theta_2)\right]\left[a_3 + a_4 - 2a_7 + 4\beta_1(\theta_2)\right] - \left[a_3 - a_4 + \gamma_1(\theta_2)\right]^2$$

Finally, the serial planar manipulator is modeled in MATLAB by using the following equations:

$$\begin{aligned}\ddot{\theta}_1 &= \frac{a_3+a_4-2a_7+4\beta_1(\theta_2)}{\Delta(\theta_2)}\tau_1+\frac{-a_3+a_4-\gamma_1(\theta_2)}{\Delta(\theta_2)}\tau_2\\ &+\frac{2[a_3+a_4-2a_7+4\beta_1(\theta_2)][\alpha_2(\theta_2)+4\beta_2(\theta_2)]}{\Delta(\theta_2)}\dot{\theta}_1\dot{\theta}_2\\ &-\frac{[-a_3+a_4-\gamma_1(\theta_2)][\alpha_2(\theta_2)+4\beta_2(\theta_2)]}{\Delta(\theta_2)}\dot{\theta}_1^2\\ &+\frac{[a_3+a_4-2a_7+4\beta_1(\theta_2)][\gamma_2(\theta_2)]}{\Delta(\theta_2)}\dot{\theta}_2^2-\frac{4[-a_3+a_4-\gamma_1(\theta_2)][\beta_2(\theta_2)]}{\Delta(\theta_2)}\dot{\theta}_2^2\end{aligned} \tag{3.63}$$

$$\begin{aligned}\ddot{\theta}_2 &= \frac{-a_3+a_4-\gamma_1(\theta_2)}{\Delta(\theta_2)}\tau_1+\frac{a_0+2\alpha_1(\theta_2)-4\beta_1(\theta_2)}{\Delta(\theta_2)}\tau_2\\ &+\frac{2[-a_3+a_4-\gamma_1(\theta_2)][\alpha_2(\theta_2)+4\beta_2(\theta_2)]}{\Delta(\theta_2)}\dot{\theta}_1\dot{\theta}_2\\ &-\frac{[a_0+2\alpha_1(\theta_2)-4\beta_1(\theta_2)][\alpha_2(\theta_2)+4\beta_2(\theta_2)]}{\Delta(\theta_2)}\dot{\theta}_1^2\\ &+\frac{[-a_3+a_4-\gamma_1(\theta_2)][\gamma_2(\theta_2)]}{\Delta(\theta_2)}\dot{\theta}_2^2-\frac{4[a_0+2\alpha_1(\theta_2)-4\beta_1(\theta_2)][\beta_2(\theta_2)]}{\Delta(\theta_2)}\dot{\theta}_2^2\end{aligned} \tag{3.64}$$

3.4.1. Simulation model of open-loop control system

First, the open-loop control system of the serial planar manipulator is built. It is constituted mainly by two parts, the controller part and the manipulator part. The controller part is described by the equations (3.19) and (3.56). And the manipulator part is described by equations (3.63) and (3.64), as shown in Fig. 3.2.

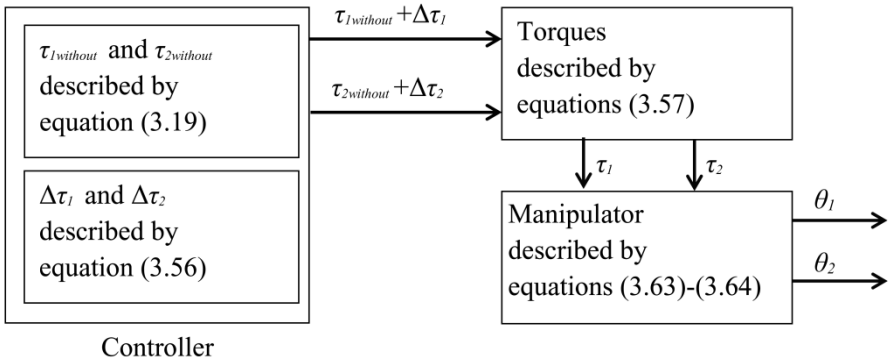

Figure 3.2. - The schema of the open-loop control system.

The parametric values of all the parts of the system is given in Tab. 3.1. It should be noted that the value of the length parameter L_{CS3} is negative. That is because a counterweight is added on the inverse extension line of link 3, when consider link 3 and the payload as one object, the total mass center moves along the inverse extension line of link 3 and finally located on the side of the joint C.

Table 3.1. - The parametric values of all the parts of the system.

mass (kg)		length (m)		moment of inertia ($kg \cdot m^2$)	
m_1	13.193	L_1/L_{AS1}	0.8/0.4	I_{S1}	0.77754
m_2	10.472	L_2/L_{BS2}	0.8/0.1738	I_{S2}	1.415
m_3	5.374	L_3/L_{CS3}	0.3/–0.0386	I_{S3}	2.2069
m_4	0.692	L_{BP}	0.5	I_{S4}	7.2×10^{-4}
m_p	5				

As discussed above, in order to simplify the dynamic model, link 2 and the payload are treated as one object. The parametric values of the composite object are shown in Tab. 3.2.

Table 3.2. - The composite parametric values of the system.

mass (kg)		length (m)		moment of inertia ($kg \cdot m^2$)	
M_2	15.472	L_{BS2r}	0.2792	I_{2+p}	1.7751

The initial and final simulation angles are given in Tab. 3.3.

Table 3.3. - The initial and final values of the desired trajectories.

Angle (°)		Velocity (m/s)		Acceleration (m/s^2)	
θ_{1I}	0	$\dot{\theta}_{1I}$	0	$\ddot{\theta}_{1I}$	0
θ_{1F}	40	$\dot{\theta}_{1F}$	0	$\ddot{\theta}_{1F}$	0
θ_{2I}	30	$\dot{\theta}_{2I}$	0	$\ddot{\theta}_{2I}$	0
θ_{2F}	80	$\dot{\theta}_{2F}$	0	$\ddot{\theta}_{2F}$	0

Different from the decoupled model that proposed in last chapter, there is no special requirement for choosing these angles, i.e. they can be arbitrary values. Here, for the desired trajectories, velocities and accelerations, the same expressions that described by equations (2.29) and (2.30) are used.

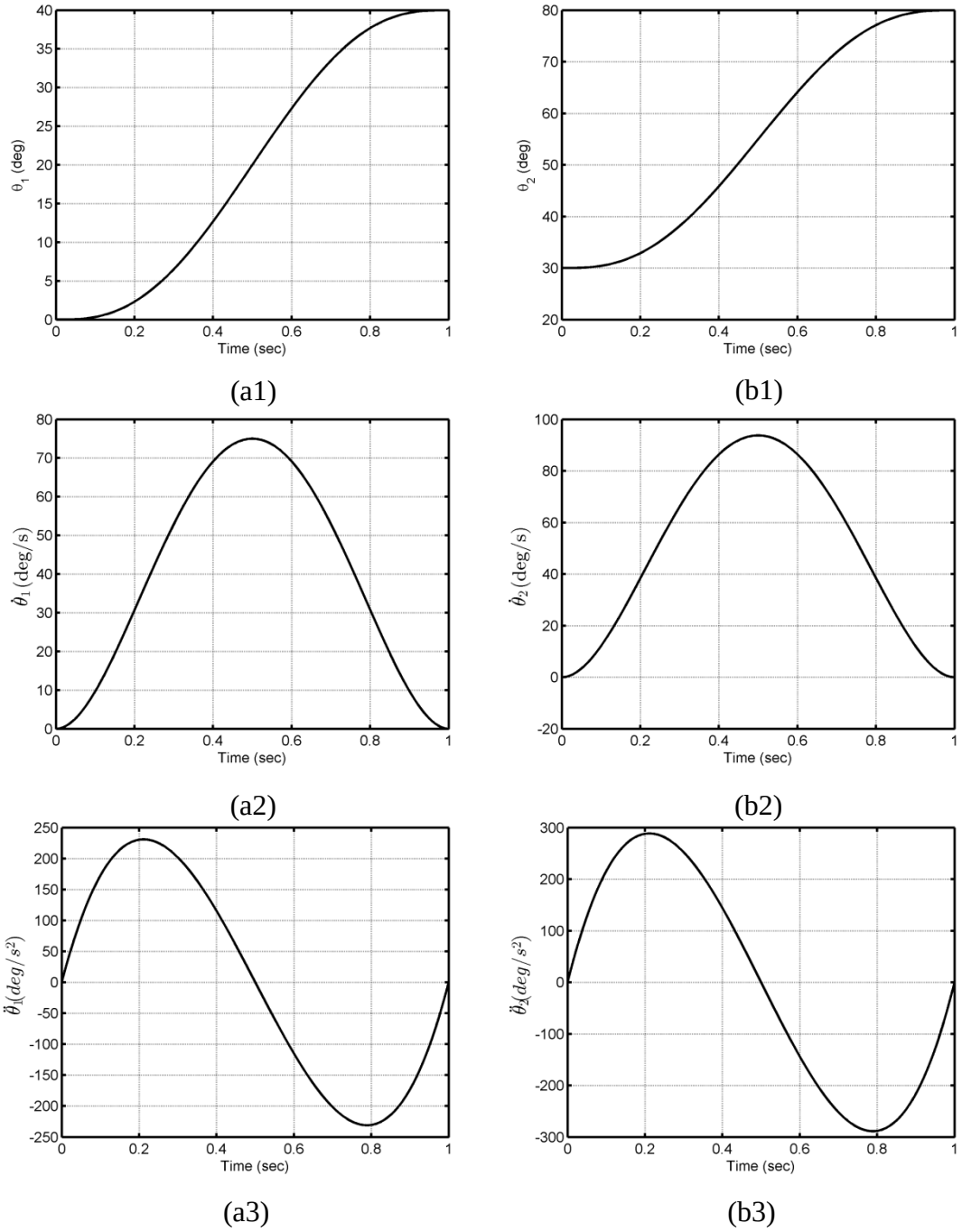

Figure 3.3. - Desired trajectories, velocities and accelerations of the two actuators.

As a result, they are shown in Fig. 3.3. Fig.3.3(a1)-(a3) are the curves of angular trajectory, angular velocity and angular acceleration of the first actuator. Fig.3.3(b1)-(b3) are the curves of angular trajectory, angular velocity and angular acceleration of the second actuator. It should be note that, the operation time is assumed as T=1s.

With all these conditions, the simulations of the open-loop system with a payload of 5 kg can be done. During the simulation, the required torque values are calculated firstly. As mentioned above, the controller can be divided into two parts: the dynamic decoupled model of the manipulator without payload and the payload compensation shown in Fig. 3.2. With the payload compensation, the expressions of the torques are derived exactly by the model of the manipulator. Thus, the desired torque values can be obtained, shown as the solid lines in Fig. 3.4. Meanwhile, the desired trajectories are achieved, shown as the solid lines in Fig. 3.5.

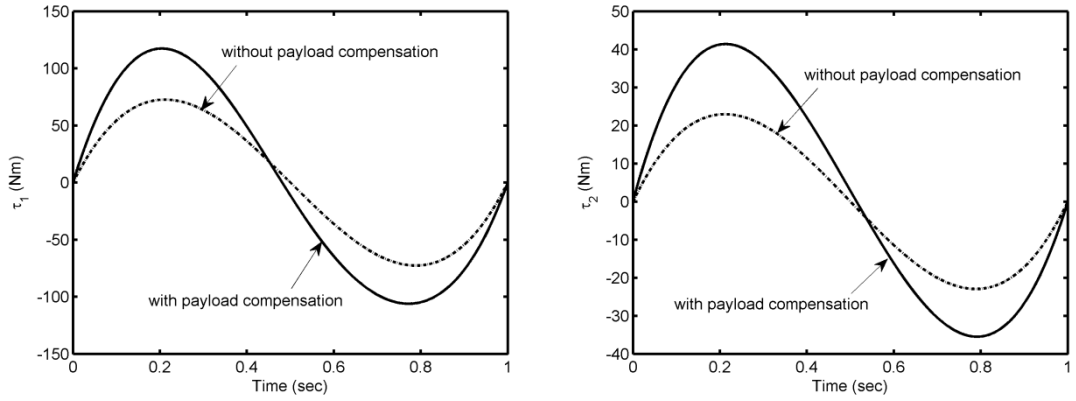

Figure 3.4. - Torques with payload compensation (solid line) and without it (dashed line) for the open-loop system.

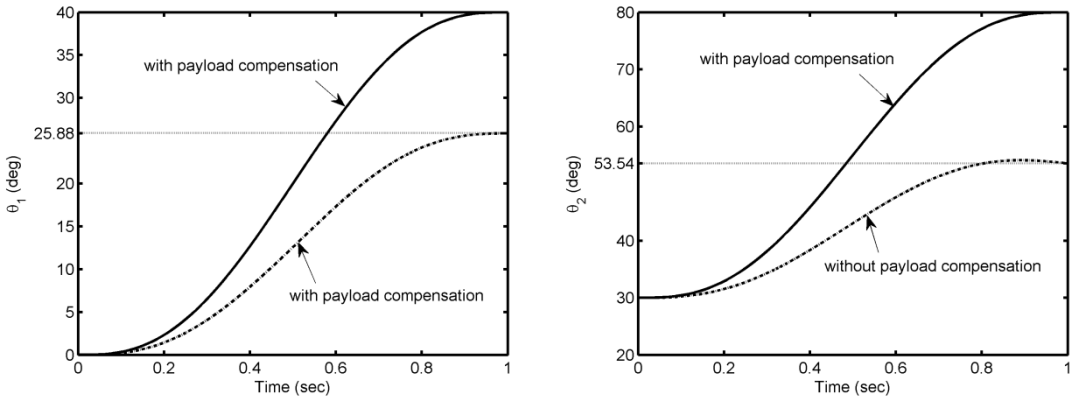

Figure 3.5. - Angular displacements of links with load compensation (solid line) and without it (dashed line) for the open-loop system.

When without the payload compensation, the torque expressions in the controller won't precisely reflect the model of the manipulator. Thus, under this situation, the torque values are different with the desired ones, shown as the dashed lines in Fig. 3.4. In other aspect, the payload compensation can be treated as the compensation of the inaccurate modeling of the manipulator. As known, the inaccurate modeling part is always exists more or less. Hence, without the payload compensation, a great difference will appear during the desired and the real trajectories (Fig. 3.5). The errors of angular displacements of link AB and BP are, respectively, 35.3% and 52.92%.

3.4.2. Simulation model of closed-loop control system

To deal with the unexpected disturbances or situations, such as the lack of the payload compensation, the closed-loop is added, shown in Fig. 3.6.

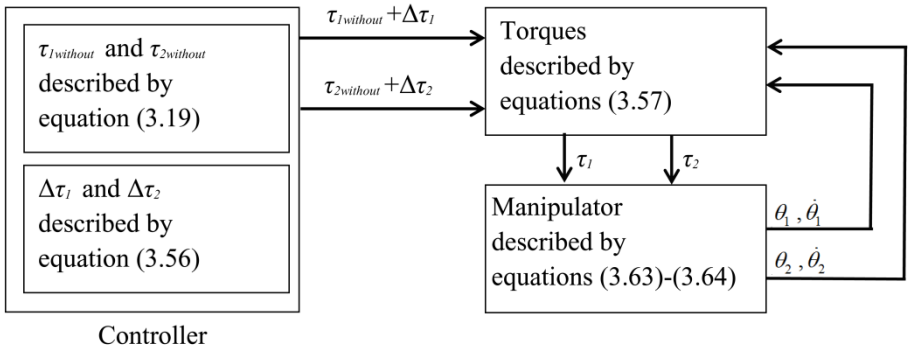

Figure 3.6. – The schema of the closed-loop control system.

The feedback factors are already obtained above, according to the schema of the closed-loop control system, the closed-loop control law can be written as

$$\begin{aligned}\tau_1(t) &= \tau_{1without} + \Delta\tau_1 \\ &\quad - g_{11}d'[\dot{\theta}_1 - \dot{\theta}_{1R}] - g_{12}d'[\theta_1 - \theta_{1R}] \\ \tau_2(t) &= \tau_{2without} + \Delta\tau_2 \\ &\quad - g_{21}c'[\dot{\theta}_2 - \dot{\theta}_{2R}] - g_{22}c'[\theta_2 - \theta_{2R}]\end{aligned} \tag{3.65}$$

where, $\tau_{1without}$ and $\tau_{2without}$ are given in equation (3.19); $\Delta\tau_1$ and $\Delta\tau_2$ are given in equation (3.56).

The simulation diagram in SIMULINK of MATLAB is shown in Appendix B. As known, the feedback loop works only when there is difference between the desired and

real trajectories. With the payload compensation, the desired torques allows an exact reproduction of the desired manipulator motions, i.e. the tracking curves overlaps completely with the desired trajectories, shown as the solid lines in Fig. 3.7 and Fig. 3.8. If the payload compensation is absent in the controller, it will lead to inaccurate torques, hence the incorrect tracking trajectories will be obtained. However, such a tracking error can be reduced because of the self-correcting performance of the feedback loop. It is obvious that, the tracking curves without payload compensation (the dashed lines in Fig. 3.8) are closer with the desired trajectories than the ones in open-loop system (the dashed lines in Fig. 3.5). As a result, the errors of angular displacements of link AB and BP are, respectively, 2.68% and 2.96%. Obviously, they are greatly diminished.

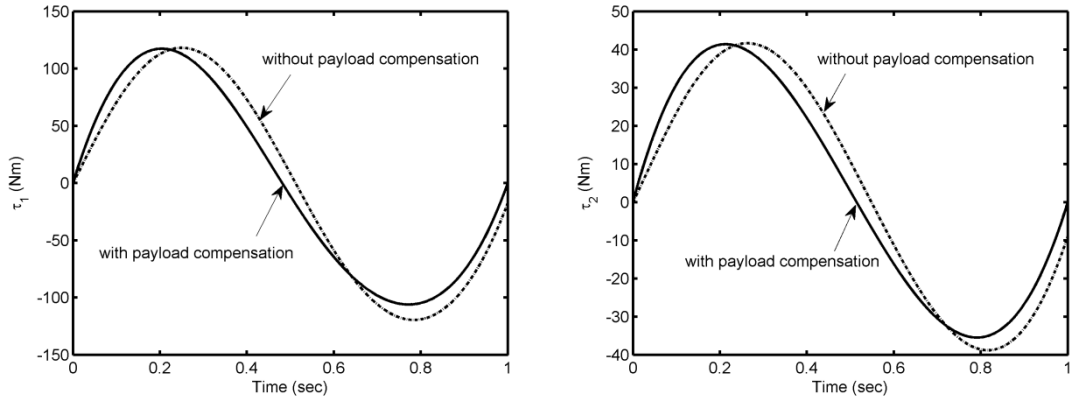

Figure 3.7. - Torques with payload compensation (solid line) and without it (dashed line) for the closed-loop system.

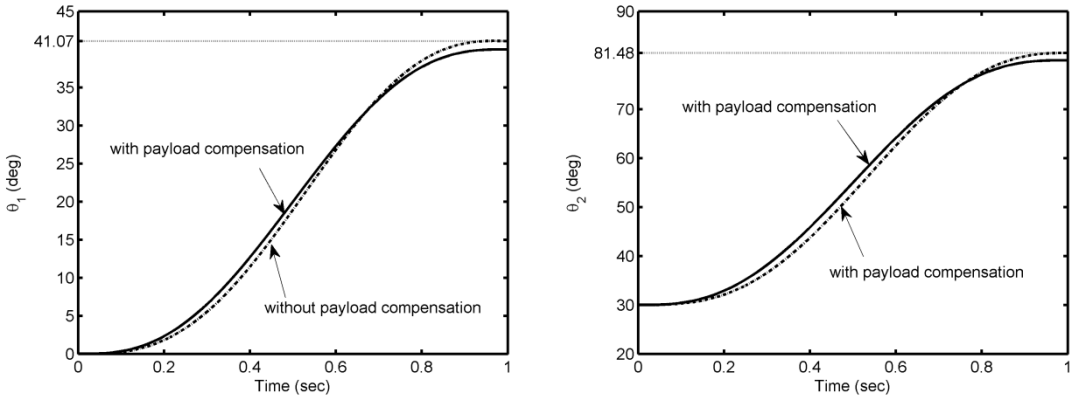

Figure 3.8. - Angular displacements of links with load compensation (solid line) and without it (dashed line) for the closed-loop system.

3.5. Summary

This chapter proposed a new dynamic decoupling principle, which involves connecting to a serial manipulator a two-link group forming a Scott-Russell mechanism with the initial links of the manipulator.

It has been carried out in two steps. At first, the dynamic decoupling of the serial manipulator is accomplished via the Scott-Russell mechanism properties and optimal redistribution of masses. Thus, the modification of the mass redistribution allows one to transform the original nonlinear system model into a fully linear system without using the feedback linearization technique. However, as it mentioned above, the changing payload leads to the perturbation of the dynamic decoupling of the manipulator. To ensure decoupled dynamics of the manipulator for any payload, an optimal control technique has been applied.

The perturbation of required motions of the manipulator with payload compensation and without has been illustrated via simulations. Two kinds of simulations are carried out with open-loop control system which is a non-feedback system and closed-loop control system. The obtained results showed the efficiency of the proposed solution.

Finally, it should be noted that the developed approach of dynamic decoupling can also be applied to the design of planar serial manipulators with three degrees of freedom.

Chapter 4

Tolerance analysis of serial manipulators with decoupled and coupled dynamics

This chapter deal with the robustness properties of serial manipulators with decoupled and coupled dynamics derived by tolerance analysis.

After having introduced some performance indices of the manipulators, the tolerance capabilities of four manipulators are analyzed. In order to quantify the influencing degree, two kinds of the indices are defined. They are angular error and position error.

Two kinds of simulation are designed here. The first kind of simulation is implemented by fixed parametric error. Then, the influencing degrees of all variables on the positioning accuracy of the manipulators are analyzed respectively.

In order to obtain the models closer to the practical situation, the random parametric errors are introduced in the second kind of simulation. Furthermore, the parametric errors of all the variables are added at the same time during one simulation.

The simulation results prove that the manipulators that decoupled by the mechatronic methods are more robust.

4.1. Performance indices of the manipulators

The performances of the manipulators such as the dexterity, load capacity, force transmission from the joint to the end-effector, and dynamic responsiveness etc. are investigated for optimize the design of the manipulators. Usually, in these researches, the performances are quantified by using some indices.

The dexterity indices for planar and spatial manipulators are presented in(Gosselin 1990). (Asada 1983) proposed the generalized inertia ellipsoid (GIE) as a quantitative method to measure the capability of changing end-effector's velocity in different directions for fixed kinetic energy. In the research of (Yoshikawa 1985), the dynamic manipulability ellipsoid (DME) is introduced for measuring the ease of changing the end-effector's configuration by a set of joint torques with fixed magnitude. Both of the two indices (GIE and DME) are based on the relationship between the generalized inertia force of the end-effector and the generalized inertia torques of joints. The dynamic conditioning index (DCI) which is defined as the least-square difference between the generalized inertia matrix and an isotropic matrix is used to measure the dynamic performance of a manipulator (Ma and Angeles 1990).

Besides the analysis of the performances above, the error tolerance analysis is also important for a manipulator. For applications in remote and/or hazardous environments where repair is not possible, the fault tolerance of the manipulators is necessary. Cause once the components failure, it will result in a robot's joint becoming immobilized, i.e., a locked joint failure mode (Ben-Gharbia et al. 2015). Hence, lots of researches such as to increase manipulator reliability (Cheng and Dhillon 2011) and to improve failure detection (Dixon et al. 2000).(Ben-Gharbia et al. 2011) are proposed. However, these applications are extreme ones. In normal application of the manipulators where repair is possible, there is another performance referred as error tolerance corresponds to fault tolerance needs to be considered.

Positioning inaccuracy can stem from a number of sources such as the dimensional error of the components, the assembly error, the deflection error, the clearance in the kinematic pair, the elastic deformation error, the friction and wear error and the measurement and control error etc. In addition, during the actual operation, the variation of the payload, acceleration and deceleration of the manipulator may cause the geometric deviation and the movement deviation of the manipulator. All of these can affect the positioning accuracy of the serial manipulators.

The error of serial manipulator can be divided into systematic error and random error. System error is the error in the manufacturing and assembly process of the

components. Usually, this kind of error is in the form of cumulative error, reverse error or periodic error. The error follows a certain mathematical model and can be compensated by control algorithm. Random error is the error that caused by uncertainty of the unpredictable disturbances, and therefore it is impossible to build a precise mathematical model for this error. The current effective way is to estimate the statistical processing of multiple measurements.

Considerable researches have been proposed for error analysis, error model derivation and calibration (Veitschegger and Wu 1986) (Wu 1983) (Veitschegger and Wu 1988). For the error model, some researches focus on the effects of manipulator joint errors (Waldron and Kumar 1979) (Benhabib et al. 1987), as well as the effects of link dimensional errors (Vaishnav and Magrab 1987) (Ferreira and Liu 1986). For instance, in the research of (Caro et al. 2005), two dimensional variations are discussed for a 2-DOF serial manipulator model.

4.2. The dynamic models of manipulators for tolerance capability comparison

The method mentioned in (Caro et al. 2005) is an efficient tolerance synthesis method. However, not just the length parameters, but also the parameters of mass and inertia are needed to be considered for tolerance analysis of the manipulators.

Hence, six main parameters of the serial manipulators are used here, they are:

- m_1, m_2 : the mass parameters of the two main links 1 and 2 respectively;
- I_{S1}, I_{S2} : the inertia parameters of the two main links 1 and 2 respectively;
- L_{AS1} : the distance between the center of mass of link 1 and joint A;
- L_{BS2} : the distance between the center of mass of link 2 and joint B.

In addition, four serial planar manipulators with two degrees of freedom are considered. They are:

- manipulator_0: a serial planar manipulator with non-decoupled dynamics, shown in Fig. 4.1.The simulation diagram in SIMULINK of MATLAB is shown in Appendix C.

- manipulator_1: a serial planar manipulator with decoupled dynamics (chapter 2), shown in Fig. 4.2.The simulation diagram in SIMULINK of MATLAB is shown in Appendix A.

- manipulator_2: the decoupled 2-DOF serial planar manipulator that proposed in chapter 3, shown in Fig. 4.3. The simulation diagram in SIMULINK of MATLAB is shown in Appendix B.

- manipulator_3: a decoupled 2-DOF serial planar manipulator that decoupled by feedback linearization (Fig. 4.4). The control schema of inverse dynamics control is shown in Fig. 4.5. And the simulation diagram in SIMULINK of MATLAB is shown in Appendix D.

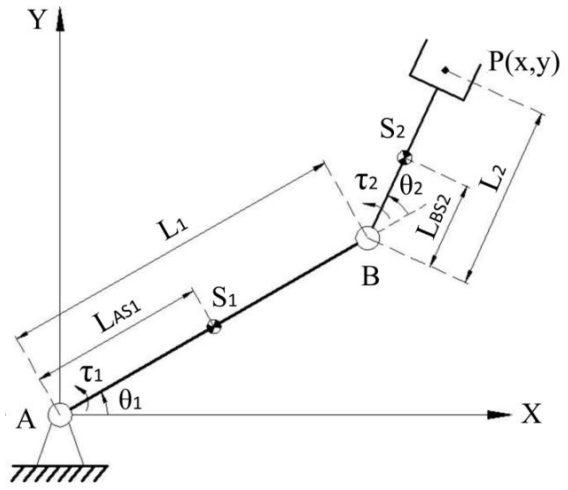

Figure 4.1. – The structure model of manipulator_0.

The dynamic equation of manipulator_0 without payload can be expressed as

$$\begin{cases} \tau_1 = \ddot{\theta}_1[a_{(0)} + b_{(0)} + 2m_2L_1L_{BS2}\cos\theta_2] + \ddot{\theta}_2[a_{(0)} + m_2L_1L_{BS2}\cos\theta_2] \\ \quad +\dot{\theta}_2^2[-m_2L_1L_{BS2}\sin\theta_2] + \dot{\theta}_1\dot{\theta}_2[-2m_2L_1L_{BS2}\sin\theta_2] \\ \tau_2 = \ddot{\theta}_1[a_{(0)} + m_2L_1L_{BS2}\cos\theta_2] + a_{(0)}\ddot{\theta}_2 \\ \quad +\dot{\theta}_1^2[m_2L_1L_{BS2}\sin\theta_2] \end{cases} \tag{4.1}$$

where

$$a_{(0)} = m_2 L_{BS2}^2 + I_{S2}$$
$$b_{(0)} = m_1 L_{AS1}^2 + m_2 L_1^2 + I_{S1}$$

Thus the structure model of manipulator_0 for the simulation is given as

$$\begin{cases} \ddot{\theta}_1 = \dfrac{\gamma_2}{\Delta(\theta_2)}\tau_1 - \dfrac{[\gamma_2 + \beta(\theta_2)]}{\Delta(\theta_2)}\tau_2 + \dfrac{\gamma_2\alpha(\theta_2)}{\Delta(\theta_2)}\dot{\theta}_1\dot{\theta}_2 \\ \quad + \dfrac{\alpha(\theta_2)[\gamma_2 + \beta(\theta_2)]}{\Delta(\theta_2)}\dot{\theta}_1^2 + \dfrac{\gamma_2\alpha(\theta_2)}{\Delta(\theta_2)}(\dot{\theta}_1 + \dot{\theta}_2)\dot{\theta}_2 \\ \ddot{\theta}_2 = -\dfrac{[\gamma_2 + \beta(\theta_2)]}{\Delta(\theta_2)}\tau_1 + \dfrac{\psi(\theta_2)}{\Delta(\theta_2)}\tau_2 - \dfrac{\alpha(\theta_2)[\gamma_2 + \beta(\theta_2)]}{\Delta(\theta_2)}\dot{\theta}_1\dot{\theta}_2 \\ \quad - \dfrac{\alpha(\theta_2)\psi(\theta_2)}{\Delta(\theta_2)}\dot{\theta}_1^2 - \dfrac{\alpha(\theta_2)[\gamma_2 + \beta(\theta_2)]}{\Delta(\theta_2)}(\dot{\theta}_1 + \dot{\theta}_2)\dot{\theta}_2 \end{cases} \tag{4.2}$$

where,

$$\alpha(\theta_2) = m_2 L_1 L_{BS2}\sin(\theta_2);$$
$$\beta(\theta_2) = m_2 L_1 L_{BS2}\cos(\theta_2);$$
$$\gamma_1 = I_{S1} + m_1 L_{AS1}^2;$$
$$\gamma_2 = I_{S2} + m_2 L_{BS2}^2;$$
$$\psi(\theta_2) = \gamma_1 + \gamma_2 + m_2 L_1^2 + 2\beta(\theta_2);$$
$$\Delta(\theta_2) = \gamma_1\gamma_2 + m_2 L_1^2 I_{S2} + [\alpha(\theta_2)]^2 > 0.$$

To establish the closed-loop control system, all the nonlinear terms in equation (4.1) are cancelled first, shown as equation (4.3).

$$\begin{cases} \tau_1 = (a_{(0)} + b_{(0)})\ddot{\theta}_1 + a_{(0)}\ddot{\theta}_2 \\ \tau_2 = a_{(0)}\ddot{\theta}_1 + a_{(0)}\ddot{\theta}_2 \end{cases} \tag{4.3}$$

Then, we obtain

$$\begin{cases} \ddot{\theta}_1 = \dfrac{1}{b_{(0)}}\tau_1 - \dfrac{1}{b_{(0)}}\tau_2 \\ \ddot{\theta}_2 = -\dfrac{1}{b_{(0)}}\tau_1 + (\dfrac{1}{a_{(0)}} + \dfrac{1}{b_{(0)}})\tau_2 \end{cases} \tag{4.4}$$

According to the same derivation process in chapter 2, the closed-loop control law of manipulator_0 can be deduced as

$$\begin{cases} \tau_1 = [a_{(0)} + b_{(0)}]\ddot{\theta}_{1R} + a_{(0)}\ddot{\theta}_{2R} \\ \quad -g_{11}[(a_{(0)} + b_{(0)})[\dot{\theta}_1 - \dot{\theta}_{1R}] + a_{(0)}[\dot{\theta}_2 - \dot{\theta}_{2R}]] \\ \quad -g_{12}[(a_{(0)} + b_{(0)})[\theta_1 - \theta_{1R}] + a_{(0)}[\theta_2 - \theta_{2R}]] \\ \tau_2 = a_{(0)}\ddot{\theta}_{1R} + a_{(0)}\ddot{\theta}_{2R} \\ \quad -g_{21}[a_{(0)}[\dot{\theta}_1 - \dot{\theta}_{1R}] + a_{(0)}[\dot{\theta}_2 - \dot{\theta}_{2R}]] \\ \quad -g_{22}[a_{(0)}[\theta_1 - \theta_{1R}] + a_{(0)}[\theta_2 - \theta_{2R}]] \end{cases} \tag{4.5}$$

where, the feedback factors are: $g_{11} = g_{21} = \dfrac{2\sqrt{1+\sqrt{3}}}{T_p}$ and $g_{12} = g_{22} = \dfrac{2\sqrt{3}}{T_p^2}$.

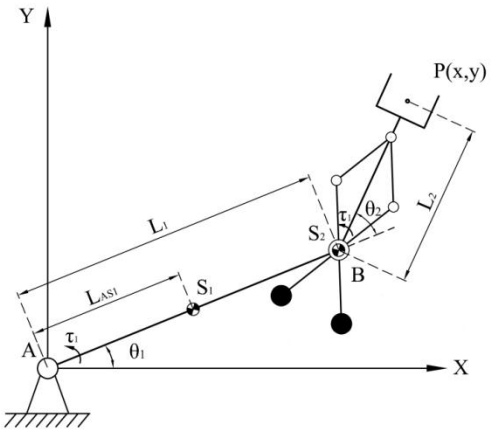

Figure 4.2. – The structure model of manipulator_1.

According to the results in chapter 2, the dynamic equation of manipulator_1 without payload is expressed as

$$\begin{cases} \tau_1 = (a_{(1)} + b_{(1)})\ddot{\theta}_1 + a_{(1)}\ddot{\theta}_2 \\ \tau_2 = a_{(1)}\ddot{\theta}_1 + a_{(1)}\ddot{\theta}_2 \end{cases} \tag{4.6}$$

where,

$$a_{(1)} = I_{S2} + I_{SR} + m_2 L_{BS2}^2 + m_{SR} L_{BS2}^2 + m_{cw} L_{cw}^2$$
$$b_{(1)} = m_1 L_{AS1}^2 + I_{S1} + m_{2+SR+cw} L_1^2$$

The structure model of manipulator_1 for the simulation is given as

$$\begin{cases} \ddot{\theta}_1 = \dfrac{\gamma_2}{\Delta(\theta_2)}\tau_1 - \dfrac{[\gamma_2 + \beta(\theta_2)]}{\Delta(\theta_2)}\tau_2 + \dfrac{\gamma_2\alpha(\theta_2)}{\Delta(\theta_2)}\dot{\theta}_1\dot{\theta}_2 \\ \quad + \dfrac{\alpha(\theta_2)[\gamma_2 + \beta(\theta_2)]}{\Delta(\theta_2)}\dot{\theta}_1^2 + \dfrac{\gamma_2\alpha(\theta_2)}{\Delta(\theta_2)}(\dot{\theta}_1 + \dot{\theta}_2)\dot{\theta}_2 \\ \ddot{\theta}_2 = -\dfrac{[\gamma_2 + \beta(\theta_2)]}{\Delta(\theta_2)}\tau_1 + \dfrac{\psi(\theta_2)}{\Delta(\theta_2)}\tau_2 - \dfrac{\alpha(\theta_2)[\gamma_2 + \beta(\theta_2)]}{\Delta(\theta_2)}\dot{\theta}_1\dot{\theta}_2 \\ \quad - \dfrac{\alpha(\theta_2)\psi(\theta_2)}{\Delta(\theta_2)}\dot{\theta}_1^2 - \dfrac{\alpha(\theta_2)[\gamma_2 + \beta(\theta_2)]}{\Delta(\theta_2)}(\dot{\theta}_1 + \dot{\theta}_2)\dot{\theta}_2 \end{cases} \tag{4.7}$$

where

$$\alpha(\theta_2) = m_{2+SR+cw} L_1 L_{BS2r} \sin(\theta_2);$$
$$\beta(\theta_2) = m_{2+SR+cw} L_1 L_{BS2r} \cos(\theta_2);$$
$$\gamma_1 = I_{S1} + m_1 L_{AS1}^2;$$
$$\gamma_2 = I_{S2+SR+cw} + m_{2+SR+cw} L_{BS2r}^2;$$
$$\psi(\theta_2) = \gamma_1 + \gamma_2 + m_{2+SR+cw} L_1^2 + 2\beta(\theta_2);$$
$$\Delta(\theta_2) = \gamma_1\gamma_2 + m_{2+SR+cw} L_1^2 I_{S2} + [\alpha(\theta_2)]^2 > 0.$$

To establish the closed-loop system of manipulator_1, the equation (4.6) is reformed as

$$\begin{cases} \ddot{\theta}_1 = \dfrac{1}{b_{(1)}}\tau_1 - \dfrac{1}{b_{(1)}}\tau_2 \\ \ddot{\theta}_2 = -\dfrac{1}{b_{(1)}}\tau_1 + (\dfrac{1}{a_{(1)}} + \dfrac{1}{b_{(1)}})\tau_2 \end{cases} \tag{4.8}$$

According to the results in chapter 2, the closed-loop control law of manipulator_1 can be written as

$$\begin{cases} \tau_1 = (a_{(1)} + b_{(1)})\ddot{\theta}_{1R} + a_{(1)}\ddot{\theta}_{2R} - g_{11}[(a_{(1)} + b_{(1)})[\dot{\theta}_1 - \dot{\theta}_{1R}] + a_{(1)}[\dot{\theta}_2 - \dot{\theta}_{2R}]] \\ \quad -g_{12}[(a_{(1)} + b_{(1)})[\theta_1 - \theta_{1R}] + a_{(1)}[\theta_2 - \theta_{2R}]] \\ \tau_2 = a_{(1)}\ddot{\theta}_{1R} + a_{(1)}\ddot{\theta}_{2R} - g_{21}[a_{(1)}[\dot{\theta}_1 - \dot{\theta}_{1R}] + a_{(1)}[\dot{\theta}_2 - \dot{\theta}_{2R}]] \\ \quad -g_{22}[a_{(1)}[\theta_1 - \theta_{1R}] + a_{(1)}[\theta_2 - \theta_{2R}]] \end{cases} \tag{4.9}$$

where, the feedback factors are: $g_{11} = g_{21} = \dfrac{2\sqrt{1+\sqrt{3}}}{T_p}$ and $g_{12} = g_{22} = \dfrac{2\sqrt{3}}{T_p^2}$.

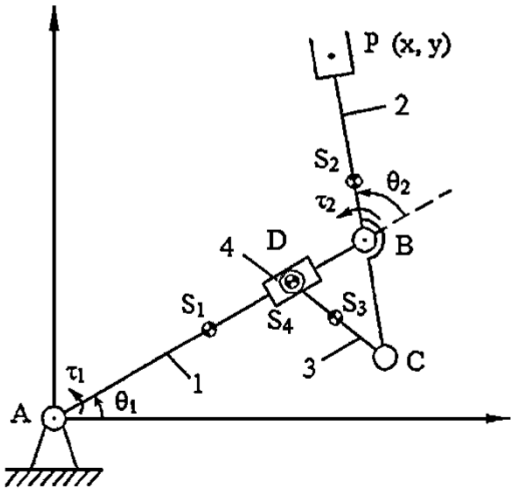

Figure 4.3. – The structure model of manipulator_2.

According to the results in chapter 3, the dynamic equation of manipulator_2 without payload is expressed as

$$\begin{cases} \tau_1 = a_{(2)}\ddot{\theta}_1 \\ \tau_2 = b_{(2)}\ddot{\theta}_2 \end{cases} \tag{4.10}$$

where,

$$a_{(2)} = I_{S1} + 2I_{S2} + I_{S4} + m_1 L_{AS1}^2 + (m_2 + m_3 + m_4)L_1^2 + 2\frac{(m_3 + m_4)(m_2 + m_3 + m_4)}{m_2} L_3^2$$

$$b_{(2)} = 2[I_{S2} + \frac{(m_3 + m_4)(m_2 + m_3 + m_4)}{m_2} L_3^2]$$

Thus the structure model of manipulator_2 can be described as equations (4.11) and (4.12).

$$\begin{aligned}\ddot{\theta}_1 = {} & \frac{a_3 + a_4 - 2a_7 + 4\beta_1(\theta_2)}{\Delta(\theta_2)}\tau_1 + \frac{-a_3 + a_4 - \gamma_1(\theta_2)}{\Delta(\theta_2)}\tau_2 \\ & + \frac{2[a_3 + a_4 - 2a_7 + 4\beta_1(\theta_2)][\alpha_2(\theta_2) + 4\beta_2(\theta_2)]}{\Delta(\theta_2)}\dot{\theta}_1\dot{\theta}_2 \\ & - \frac{[-a_3 + a_4 - \gamma_1(\theta_2)][\alpha_2(\theta_2) + 4\beta_2(\theta_2)]}{\Delta(\theta_2)}\dot{\theta}_1^2 \\ & + \frac{[a_3 + a_4 - 2a_7 + 4\beta_1(\theta_2)][\gamma_2(\theta_2)]}{\Delta(\theta_2)}\dot{\theta}_2^2 - \frac{4[-a_3 + a_4 - \gamma_1(\theta_2)][\beta_2(\theta_2)]}{\Delta(\theta_2)}\dot{\theta}_2^2\end{aligned} \tag{4.11}$$

$$\begin{aligned}\ddot{\theta}_2 = {} & \frac{-a_3 + a_4 - \gamma_1(\theta_2)}{\Delta(\theta_2)}\tau_1 + \frac{a_0 + 2\alpha_1(\theta_2) - 4\beta_1(\theta_2)}{\Delta(\theta_2)}\tau_2 \\ & + \frac{2[-a_3 + a_4 - \gamma_1(\theta_2)][\alpha_2(\theta_2) + 4\beta_2(\theta_2)]}{\Delta(\theta_2)}\dot{\theta}_1\dot{\theta}_2 \\ & - \frac{[a_0 + 2\alpha_1(\theta_2) - 4\beta_1(\theta_2)][\alpha_2(\theta_2) + 4\beta_2(\theta_2)]}{\Delta(\theta_2)}\dot{\theta}_1^2 \\ & + \frac{[-a_3 + a_4 - \gamma_1(\theta_2)][\gamma_2(\theta_2)]}{\Delta(\theta_2)}\dot{\theta}_2^2 - \frac{4[a_0 + 2\alpha_1(\theta_2) - 4\beta_1(\theta_2)][\beta_2(\theta_2)]}{\Delta(\theta_2)}\dot{\theta}_2^2\end{aligned} \tag{4.12}$$

where

$$a_0 = [m_1 L_{AS1}^2 + I_{S1} + M_2 L_1^2 + M_2 L_{BS2r}^2 + I_{2+p} + m_3 L_1^2 + m_3 L_3^2 + m_3 L_{CS3}^2 + I_{S3} + I_{S4} + 4m_4 L_3^2 + m_4 L_1^2 + 2m_3 L_3 L_{CS3}];$$

$$a_1 = [m_3 L_3 L_{CS3} + m_4 L_3^2];$$

$$a_2 = [M_2 L_1 L_{BS2r} - m_3 L_1 L_3];$$

$$a_3 = [M_2 L_{BS2r}^2 + I_{2+p} + m_3 L_3^2];$$

$$a_4 = [m_3 L_{CS3}^2 + I_3];$$

$$a_5 = m_3 L_1 L_3;$$

$$a_6 = m_4 L_1 L_3;$$

$$a_7 = m_3 L_3 L_{CS3};$$

$$\alpha_1(\theta_2) = [a_2 - a_5 - a_6]\cos(\theta_2);$$

$$\alpha_2(\theta_2) = [a_2 - a_5 - a_6]\sin(\theta_2);$$

$$\beta_1(\theta_2) = a_1 \sin^2(\theta_2);$$

$$\beta_2(\theta_2) = a_1 \sin(\theta_2)\cos(\theta_2);$$

$$\gamma_1(\theta_2) = [a_2 + a_5]\cos(\theta_2);$$

$$\gamma_2(\theta_2) = [a_2 + a_5]\sin(\theta_2).$$

As the same, to establish the closed-loop control of manipulator_2, the equation (4.10) is reformed as

$$\begin{cases} \ddot{\theta}_1 = \dfrac{1}{a_{(2)}}\tau_1 \\ \ddot{\theta}_2 = \dfrac{1}{b_{(2)}}\tau_2 \end{cases} \tag{4.13}$$

According to the results in chapter 3, the closed-loop control law of manipulator_2 can be written as

$$\begin{cases} \tau_1 = a_{(2)}\ddot{\theta}_{1R} - g_{11}a_{(2)}[\dot{\theta}_1 - \dot{\theta}_{1R}] - g_{12}a_{(2)}[\theta_1 - \theta_{1R}] \\ \tau_2 = b_{(2)}\ddot{\theta}_{2R} - g_{21}b_{(2)}[\dot{\theta}_2 - \dot{\theta}_{2R}] - g_{22}b_{(2)}[\theta_2 - \theta_{2R}] \end{cases} \tag{4.14}$$

where, the feedback factors are: $g_{11} = g_{21} = \dfrac{2\sqrt{1+\sqrt{3}}}{T_p}$ and $g_{12} = g_{22} = \dfrac{2\sqrt{3}}{T_p^2}$.

The manipulator_3 has the same structure as manipulator_0 (Fig. 4.4), however, it is linearized and decoupled by feedback linearization which is shown in Fig 4.5.

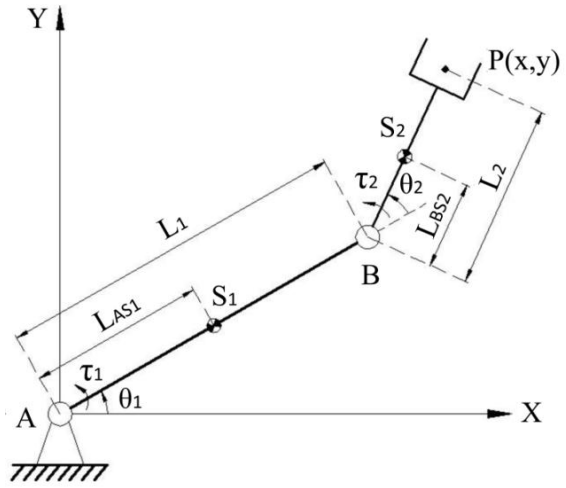

Figure 4.4. – The structure model of manipulator_3.

The dynamic model of manipulator_3 can be expressed as

$$\tau = A(\theta)\ddot{\theta} + C(\theta,\dot{\theta})\dot{\theta} \tag{4.15}$$

The decoupling law is written as

$$\tau = \hat{A}(\theta)v + C(\theta,\dot{\theta})\dot{\theta} \tag{4.16}$$

where, $\hat{A}(\theta)$ is referred to as the inertia matrix that be formed by nominal parameters; $\hat{C}(\theta,\dot{\theta})$ is referred to as Coriolis and centrifugal effects that be formed by nominal parameters.

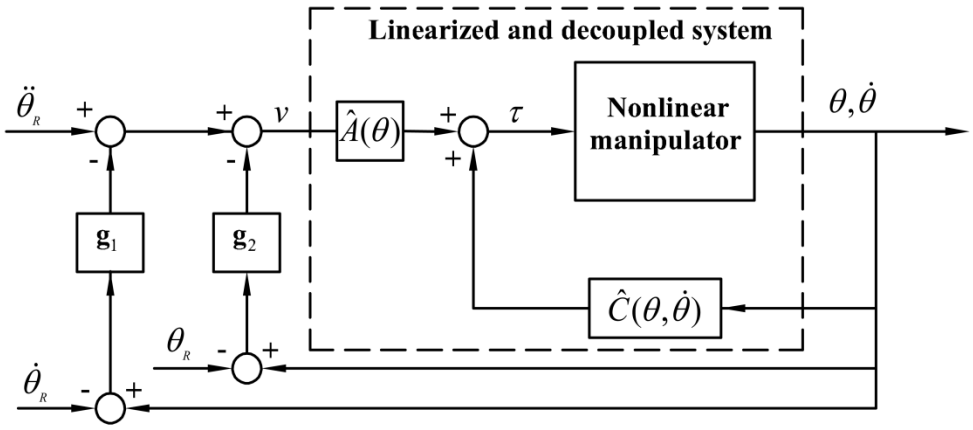

Figure 4.5. – The control schema of inverse dynamics control for manipulator_3.

If $\hat{A}(\theta) = A(\theta)$ and $\hat{C}(\theta, \dot{\theta}) = C(\theta, \dot{\theta})$, then we obtain

$$A(\theta)v = A(\theta)\ddot{\theta} \tag{4.17}$$

In addition, the inertia matrix $A(\theta)$ is reversible, thus

$$v(t) = \ddot{\theta}(t) \tag{4.18}$$

Substituting equations (4.15) and (4.18) into equation (4.1), then the equation of the torque can be rewritten as

$$\begin{cases} \tau_1 = [a_{(0)} + b_{(0)} + 2m_2 L_1 L_{BS2} \cos\theta_2]v_1 + [a_{(0)} + m_2 L_1 L_{BS2} \cos\theta_2]v_2 \\ \quad + [-m_2 L_1 L_{BS2} \sin\theta_2]\dot{\theta}_2^2 + [-2m_2 L_1 L_{BS2} \sin\theta_2]\dot{\theta}_1\dot{\theta}_2 \\ \tau_2 = [a_{(0)} + m_2 L_1 L_{BS2} \cos\theta_2]v_1 + a_{(0)}v_2 \\ \quad + [m_2 L_1 L_{BS2} \sin\theta_2]\dot{\theta}_1^2 \end{cases} \tag{4.19}$$

Replacing τ_1 and τ_2 of the equation (4.1) by equation (4.19), finally, we can obtain

$$\begin{bmatrix} \ddot{\theta}_1(t) \\ \ddot{\theta}_2(t) \end{bmatrix} = \begin{bmatrix} v_1(t) \\ v_2(t) \end{bmatrix} \tag{4.20}$$

Now, as shown in Fig. 4.5, the nonlinear manipulator which is described by equation (4.2) becomes linearized and decoupled.

Based on this linear and decoupled model, the closed-loop control system can be furthermore established. Because that this model is similar to manipulator_2, according to the same derivation process, the closed-loop control law and the feedback factors can be obtained

$$\begin{cases} v_1(t) = \ddot{\theta}_{1R}(t) - g_{11}[\dot{\theta}_1(t) - \dot{\theta}_{1R}(t)] - g_{12}[\theta_1(t) - \theta_{1R}(t)] \\ v_2(t) = \ddot{\theta}_{2R}(t) - g_{21}[\dot{\theta}_2(t) - \dot{\theta}_{2R}(t)] - g_{22}[\theta_2(t) - \theta_{2R}(t)] \end{cases} \tag{4.21}$$

where, the feedback factors are: $g_{11} = g_{21} = \dfrac{2\sqrt{1+\sqrt{3}}}{T_p}$ and $g_{12} = g_{22} = \dfrac{2\sqrt{3}}{T_p^2}$.

Through the comparisons among the closed-loop control law of these four manipulators, it is found that, the manipulator_0 is similar to manipulator_1, and the manipulator_2 is similar to manipulator_3. However, in the aspect of the structure model, the manipulator_1 and manipulator_2 are much simpler than manipulator_0 and manipulator_3.

Next, in order to compare the robustness of these manipulators, the error tolerance capability analysis is introduced. In addition, to make meaningful comparisons between different manipulators, it is useful to quantify the system capability in terms of a representative numerical index. This also allows one to optimize the design with respect to the physical parameters such as the mass distribution, actuator location or link dimensions. Hence, here in order to quantitatively describe the tolerance capability against the parametric variation, two kinds of indices referred as angular error and position error are identified.

The angular error is defined as the ratio of the absolute angular variation to the desired overall angular displacement $\Delta\theta_i$. It is calculated as

$$\varepsilon_{\theta i} = \left| \frac{\delta\theta_i}{\Delta\theta_i} \right| \times 100\% \quad (i = 1, 2) \tag{4.22}$$

where, $\Delta\theta_i = \theta_{iF} - \theta_{iI}$. θ_{iI} represents the desired initial angle of the *ith* actuator, θ_{iF} represents the desired final angle of the *ith* actuator.

According to the kinematic of the manipulators, the position vector of the end-effector of the serial manipulator in the Cartesian coordinate that attached on the first joint can be written as

$$P = \begin{bmatrix} \cos\theta_1 & \cos(\theta_1 + \theta_2) \\ \sin\theta_1 & \sin(\theta_1 + \theta_2) \end{bmatrix} \begin{bmatrix} L_1 \\ L_2 \end{bmatrix} \tag{4.23}$$

where, $P = \begin{bmatrix} x_P \\ y_P \end{bmatrix}$.

The position error is defined as the norm of the position vector variation that caused by the variation of the angular displacement of the actuators. The expression is described as

$$\varepsilon_P = \sqrt{\delta x_P^2 + \delta y_P^2} \qquad (mm) \tag{4.24}$$

with,

$$\begin{aligned} \delta x_P &= L_{1N}\cos\theta_{1N} + L_{2N}\cos(\theta_{1N}+\theta_{2N}) - L_{1R}\cos\theta_{1R} - L_{2R}\cos(\theta_{1R}+\theta_{2R}) \\ \delta y_P &= L_{1N}\sin\theta_{1N} + L_{2N}\sin(\theta_{1N}+\theta_{2N}) - L_{1R}\sin\theta_{1R} - L_{2R}\sin(\theta_{1R}+\theta_{2R}) \end{aligned} \tag{4.25}$$

where, $\delta x_P, \delta y_P$ are the components of the position vector variation on the x axis and y axis of the Cartesian coordinate respectively; $L_{1N}, L_{2N}, \theta_{1N}, \theta_{2N}$ are the nominal parameters ; $L_{1R}, L_{2R}, \theta_{1R}, \theta_{2R}$ are the real parameters.

4.3. Tolerance capability comparison among the manipulators

For the comparison, the main parameters are needed to be uniformed, shown as in (Tab. 4.1). As the special condition of reverse rotations of the two main links is necessary for the dynamic decoupling of manipulator_1, the initial and final angular positions of the manipulators are given as in (Tab. 4.2).

Table 4.1. – The parametric values of the open-loop control system.

mass (kg)		length (m)		moment of inertia ($kg \cdot m^2$)	
m_1	13.193	L_1/L_{AS1}	0.8/0.4	I_{S1}	0.77754
m_2	8.477	L_2/L_{BS2}	0.5/0.25	I_{S2}	0.20744

Table 4.2. – The initial and final values of the desired trajectories.

Angle ($^\circ$)		Velocity (m/s)		Acceleration (m/s^2)	
θ_{1I}	60	$\dot{\theta}_{1I}$	0	$\ddot{\theta}_{1I}$	0
θ_{1F}	0	$\dot{\theta}_{1F}$	0	$\ddot{\theta}_{1F}$	0
θ_{2I}	20	$\dot{\theta}_{2I}$	0	$\ddot{\theta}_{2I}$	0
θ_{2F}	80	$\dot{\theta}_{2F}$	0	$\ddot{\theta}_{2F}$	0

The desired trajectories of the two links are produced by equation (2.29) and (2.30). With these simulation conditions, two kinds of comparison methods are designed, they are implemented by the introduction of fixed and random parametric errors respectively. All the simulations are taken under the close-loop systems.

4.3.1. Tolerance capability comparison by introducing the fixed parametric error

In this section, to provide insight to the tolerance capability, a set of simulations are designed for the main independent variables. In each simulation, the error is added to one and only one parameter, the value of error is assumed to vary from -20% to 20% in step of 5%. Here, δm_1, δm_2, δI_{S1}, δI_{S2}, δL_{AS1} and δL_{BS2} are noted as the diviation of the variables m_1, m_2, I_{S1}, I_{S2} and L_{AS1} respectivily.

During these simulations, the angular error $\varepsilon_{\theta i}$ and the position error ε_P are calculated according to the equations (4.22) and (4.24).

The simulations with 20% parametric errors of the variables are shown in Fig. 4.6 to compare the tracking accuracy among the four manipulators during the whole process. Each figure shows the influence on the angular accuracy of one link by introducing one kind of variable error for the four manipulators.

Fig. 4.6(a1) shows the curves of absolut deviation of θ_1 that influenced by δm_1 during the whole process. Obviously, for the coupled manipulator_0, there are three peaks of wave, for all the three dynamic decoupled models (manipulator_1, manipulator_2, manipulator_3,), there are two peaks of wave. Moreover, they are much lower than the peaks of wave in the coupled manipulator_0. It should be noted that, during the coupled manipulators, the angular error curves of manipulator_1 and manipulator_2 are similar and both of theirs peaks of wave are lower than the ones of manipulator_3 which is dynamic decoupled by the control method. However, with the increase of operation time, for all the manipulators, the difference between the desired trajectory and the real trajectory became smaller and smaller, and then became a constant.

From this aspect, the rates of convergence of the decoupled manipulators are similar and faster than the coupled manipulator_0. The similar phenomenon also exists in Fig. 4.6(a2) and Fig. 4.6(a3). The robust of the decoupled manipulators for tracking the desired trajectory also displayed in Fig. 4.6(a5) and Fig. 4.6(a6), especially in Fig. 4.6(a4). It shows that, during the whole process, the parametric error of variable I_{S2} has no influence on the tracking accuracy of link 1.

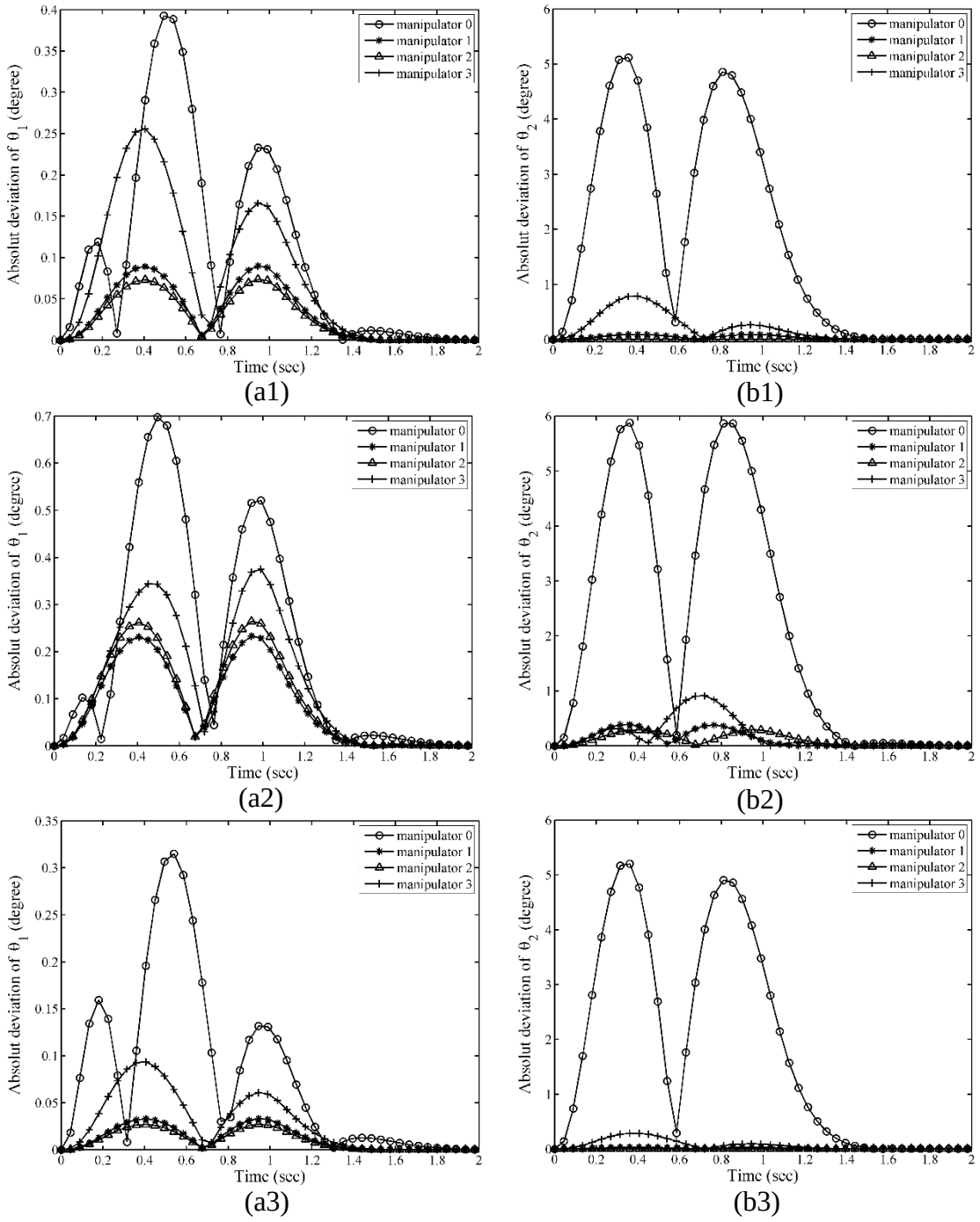

Figure 4.6. – The absolut deviation of the two links that influenced by introducing 20% parametric errors of the variables during the whole process of the four manipulators. (a1)-(a6) show the angular errors of link 1 that influenced by δm_1, δm_2, δI_{S1}, δI_{S2}, δL_{AS1}, δL_{BS2}, respectively. (b1)-(b6) show the angular errors of link 2 that influenced by δm_1, δm_2, δI_{S1}, δI_{S2}, δL_{AS1}, δL_{BS2} respectively.

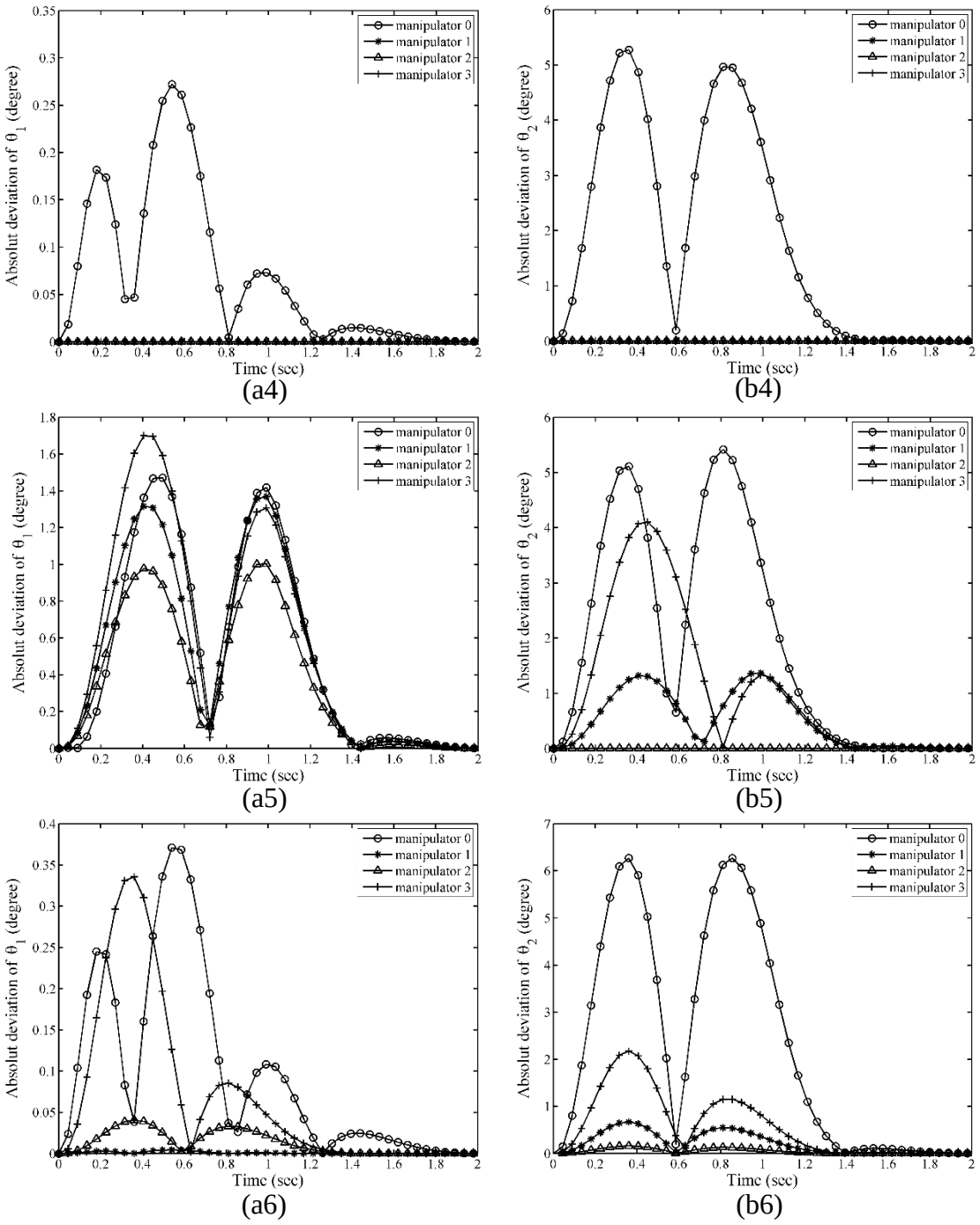

Figure 4.6. – The absolut deviation of the two links that influenced by introducing 20% parametric errors of the variables during the whole process of the four manipulators. (a1)-(a6) show the angular errors of link 1 that influenced by δm_1, δm_2, δI_{S1}, δI_{S2}, δL_{AS1}, δL_{BS2}, respectively. (b1)-(b6) show the angular errors of link 2 that influenced by δm_1, δm_2, δI_{S1}, δI_{S2}, δL_{AS1}, δL_{BS2} respectively. (Continued).

Figure 4.6(b1)-(b6) show the curves of angular error of link 2 that influenced by δm_1, δm_2, δI_{S1}, δI_{S2}, δL_{AS1}, δL_{BS2} during the whole process respectively. All of them strongly proved that the decoupled manipulators can track the desired trajectory more precise and less sensitive to the variable errors during the whole process. In addition, it also can be found that, the tracking accuracies of manipulator_1 and manipulator_2 are higher than the ones of manipulator_3.

Moreover, according to the final tracking results, the highter robust performance of the decoupled also been proved (Tab. 4.3, Tab.4.4, Tab. 4.5 and Tab. 4.6).

Table 4.3 shows the influence on the positioning accuracy of manipulator_0. As mentioned above, in order to establish the closed-loop control, all the nonlinear terms in the dynamic equations are cancelled. This causes the discordance between the control model and the real manipulator. The result is that, even not any parametric error is introduced, the positioning error still exists. For all kinds of variables, along with the increase of the parametric error, both the angular error and the position error become larger.

Table 4.3. – The influence on the positioning accuracy of manipulator_0 by introducing fixed errors.

		-20%	-15%	-10%	-5%	0	5%	10%	15%	20%
	$\varepsilon_{\theta 1}$	0,000246	0,000239	0,000236	0,000238	0,000243	0,000252	0,000265	0,000281	0,000299
δm_1	$\varepsilon_{\theta 2}$	0,000748	0,000823	0,000892	0,000955	0,001012	0,001063	0,001109	0,001148	0,001183
	ε_p	0,005916	0,006228	0,006550	0,006879	0,007212	0,007548	0,007885	0,008223	0,008562
	$\varepsilon_{\theta 1}$	0,000313	0,000270	0,000249	0,000242	0,000243	0,000244	0,000239	0,000220	0,000183
δm_2	$\varepsilon_{\theta 2}$	0,001112	0,000516	0,000048	0,000563	0,001012	0,001376	0,001638	0,001782	0,001797
	ε_p	0,004534	0,002403	0,002807	0,004988	0,007212	0,009068	0,010363	0,010955	0,010744
	$\varepsilon_{\theta 1}$	0,000237	0,000237	0,000239	0,000241	0,000243	0,000246	0,000250	0,000253	0,000258
δI_{S1}	$\varepsilon_{\theta 2}$	0,000926	0,000949	0,000971	0,000992	0,001012	0,001032	0,001050	0,001068	0,001085
	ε_p	0,006723	0,006844	0,006966	0,007089	0,007212	0,007335	0,007459	0,007583	0,007707
	$\varepsilon_{\theta 1}$	0,000308	0,000292	0,000276	0,000260	0,000243	0,000226	0,000209	0,000191	0,000173
δI_{S2}	$\varepsilon_{\theta 2}$	0,000477	0,000629	0,000769	0,000897	0,001012	0,001115	0,001203	0,001278	0,001339
	ε_p	0,005219	0,005777	0,006302	0,006783	0,007212	0,007581	0,007887	0,008124	0,008290
	$\varepsilon_{\theta 1}$	0,001533	0,000893	0,000463	0,000252	0,000243	0,000390	0,000629	0,000911	0,001290
δL_{AS1}	$\varepsilon_{\theta 2}$	0,002217	0,001119	0,000195	0,000521	0,001012	0,001285	0,001380	0,001364	0,001290
	ε_p	159,996477	119,998832	80,001383	40,003990	0,007212	39,991362	79,989642	119,988269	159,986697
	$\varepsilon_{\theta 1}$	0,000309	0,000317	0,000312	0,000289	0,000243	0,000168	0,000057	0,000092	0,000281
δL_{BS2}	$\varepsilon_{\theta 2}$	0,001955	0,001206	0,000411	0,000361	0,001012	0,001408	0,001379	0,000730	0,000730
	ε_p	99,997451	74,997385	49,997426	24,997614	0,007212	25,001386	50,000473	74,999237	99,997679

Table 4.4. – The influence on the positioning accuracy of manipulator_1 by introducing fixed errors.

		-20%	-15%	-10%	-5%	0	5%	10%	15%	20%
	$\varepsilon_{\theta 1}$	0,000053	0,000041	0,000029	0,000015	0	0,000016	0,000034	0,000053	0,000073
δm_1	$\varepsilon_{\theta 2}$	0,000053	0,000041	0,000029	0,000015	0	0,000016	0,000034	0,000053	0,000073
	ε_p	0,000440	0,000348	0,000243	0,000127	0	0,000138	0,000286	0,000445	0,000613
	$\varepsilon_{\theta 1}$	0,000084	0,000079	0,000063	0,000036	0	0,000045	0,000098	0,000158	0,000224
δm_2	$\varepsilon_{\theta 2}$	0,000024	0,000011	0,000003	0,000001	0	0,000004	0,000011	0,000020	0,000030
	ε_p	0,000983	0,000876	0,000675	0,000381	0	0,000464	0,001004	0,001614	0,002287
	$\varepsilon_{\theta 1}$	0,000022	0,000017	0,000011	0,000006	0	0,000006	0,000012	0,000018	0,000025
δI_{S1}	$\varepsilon_{\theta 2}$	0,000022	0,000017	0,000011	0,000006	0	0,000006	0,000012	0,000018	0,000025
	ε_p	0,000183	0,000140	0,000095	0,000048	0	0,000050	0,000101	0,000153	0,000207
	$\varepsilon_{\theta 1}$	0	0	0	0	0	0	0	0	0
δI_{S2}	$\varepsilon_{\theta 2}$	0	0	0	0	0	0	0	0	0
	ε_p	0	0	0	0	0	0	0	0	0
	$\varepsilon_{\theta 1}$	0,001302	0,000576	0,000107	0,000083	0	0,000317	0,000796	0,001365	0,002036
δL_{AS1}	$\varepsilon_{\theta 2}$	0,001302	0,000576	0,000107	0,000083	0	0,000317	0,000796	0,001365	0,002036
	ε_p	160,000000	120,000000	80,000000	40,000000	0	40,000000	80,000000	120,000001	160,000001
	$\varepsilon_{\theta 1}$	0,000003	0,000001	0,000001	0	0	0	0,000001	0,000002	0,000003
δL_{BS2}	$\varepsilon_{\theta 2}$	0,000169	0,000126	0,000083	0,000042	0	0,000042	0,000084	0,000128	0,000173
	ε_p	99,999979	74,999988	49,999995	24,999999	0	25,000001	50,000006	75,000013	100,000022

Table 4.5. – The influence on the positioning accuracy of manipulator_2 by introducing fixed errors.

		-20%	-15%	-10%	-5%	0	5%	10%	15%	20%
	$\varepsilon_{\theta 1}$	0,000045	0,000035	0,000024	0,000013	0	0,000013	0,000028	0,000043	0,000059
δm_1	$\varepsilon_{\theta 2}$	0	0	0	0	0	0	0	0	0
	ε_p	0,000475	0,000371	0,000257	0,000133	0	0,000142	0,000294	0,000454	0,000622
	$\varepsilon_{\theta 1}$	0,000087	0,000084	0,000068	0,000040	0	0,000051	0,000112	0,000183	0,000262
δm_2	$\varepsilon_{\theta 2}$	0,000087	0,000085	0,000070	0,000042	0	0,000055	0,000124	0,000205	0,000298
	ε_p	0,000732	0,000704	0,000570	0,000333	0	0,000424	0,000933	0,001518	0,002172
	$\varepsilon_{\theta 1}$	0,000018	0,000014	0,000009	0,000005	0	0,000005	0,000010	0,000015	0,000020
δI_{S1}	$\varepsilon_{\theta 2}$	0	0	0	0	0	0	0	0	0
	ε_p	0,000193	0,000147	0,000099	0,000050	0	0,000051	0,000104	0,000158	0,000213
	$\varepsilon_{\theta 1}$	0	0	0	0	0	0	0	0	0
δI_{S2}	$\varepsilon_{\theta 2}$	0	0	0	0	0	0	0	0	0
	ε_p	0	0	0	0	0	0	0	0	0
	$\varepsilon_{\theta 1}$	0,000507	0,000172	0,000030	0,000087	0	0,000219	0,000544	0,000942	0,001389
δL_{AS1}	$\varepsilon_{\theta 2}$	0	0	0	0	0	0	0	0	0
	ε_p	160,002617	120,000886	79,999848	39,999552	0	39,998872	79,997197	119,995142	159,992838
	$\varepsilon_{\theta 1}$	0,000008	0,000006	0,000005	0,000002	0	0,000003	0,000005	0,000008	0,000012
δL_{BS2}	$\varepsilon_{\theta 2}$	0,000034	0,000026	0,000018	0,000010	0	0,000010	0,000021	0,000033	0,000044
	ε_p	100,000065	75,000052	50,000037	25,000020	0	25,000022	50,000045	75,000070	100,000096

Table 4.6. – The influence on the positioning accuracy of manipulator_3 by introducing fixed errors.

		-20%	-15%	-10%	-5%	0	5%	10%	15%	20%
	$\varepsilon_{\theta 1}$	0,000079	0,000067	0,000049	0,000027	0	0,000031	0,000066	0,000105	0,000147
δm_1	$\varepsilon_{\theta 2}$	0,000124	0,000103	0,000075	0,000040	0	0,000046	0,000098	0,000155	0,000217
	ε_p	0,000664	0,000557	0,000409	0,000223	0	0,000258	0,000549	0,000871	0,001222
	$\varepsilon_{\theta 1}$	0,000033	0,000076	0,000083	0,000056	0	0,000083	0,000190	0,000317	0,000461
δm_2	$\varepsilon_{\theta 2}$	0,000072	0,000057	0,000043	0,000026	0	0,000043	0,000111	0,000214	0,000364
	ε_p	0,000311	0,000657	0,000754	0,000522	0	0,000763	0,001714	0,002802	0,003987
	$\varepsilon_{\theta 1}$	0,000038	0,000029	0,000020	0,000010	0	0,000011	0,000022	0,000034	0,000047
δI_{S1}	$\varepsilon_{\theta 2}$	0,000058	0,000044	0,000030	0,000016	0	0,000016	0,000034	0,000052	0,000070
	ε_p	0,000316	0,000244	0,000168	0,000086	0	0,000091	0,000187	0,000287	0,000392
	$\varepsilon_{\theta 1}$	0	0	0	0	0	0	0	0	0
δI_{S2}	$\varepsilon_{\theta 2}$	0	0	0	0	0	0	0	0	0
	ε_p	0	0	0	0	0	0	0	0	0
	$\varepsilon_{\theta 1}$	0,001144	0,000497	0,000080	0,000085	0	0,000305	0,000774	0,001353	0,002063
δL_{AS1}	$\varepsilon_{\theta 2}$	0,001345	0,000594	0,000106	0,000093	0	0,000354	0,000903	0,001584	0,002423
	ε_p	159,998964	119,999496	79,999870	40,000044	0	40,000251	80,000666	120,001192	160,001856
	$\varepsilon_{\theta 1}$	0,000010	0,000008	0,000006	0,000004	0	0,000004	0,000008	0,000011	0,000011
δL_{BS2}	$\varepsilon_{\theta 2}$	0,000294	0,000083	0,000030	0,000052	0	0,000089	0,000156	0,000110	0,000170
	ε_p	99,999920	74,999931	49,999948	24,999971	0	24,999966	49,999932	74,999908	99,999907

Table 4.4, 4.5 and 4.6 shows the influences on the positioning accuracies of manipulator_1, manipulator_2 and manipulator_3 respectively. They are all linearized and decoupled models. Through the comparison between the linear model and the nonlinear model, the biggest difference is that, there is no positioning error in the simulations of the linear models with the nominal parametric values.

In addition, compared with the values of both angular error and position error which are caused by introducing δm_1, δm_2, δI_{S1}, and δI_{S2} respectively in the coupled manipulator_0, the values of the corresponding ones in the decoupled manipulators are an order of magnitude. Especially, the positioning errors that caused by δI_{S2} in the manipulator_1, manipulator_2 and manipulator_3 are all zero, that is, the inertia deviation of link 2 has no influence on the positioning error in the decoupled manipulators. Moreover, it can be found that, the angular accuracy of link 2 can't be affected by the variable deviations of link 1 (δm_1, δI_{S1}, δL_{AS1}), this is also confirmed in Fig. 4.6(4a) and 4.6(4b) above.

Compared with other kinds of variables, the parametric errors of the length variables lead to the biggest influences on the positioning accuracy. It seems that the control system here cannot compensate the position error that caused by the variation of length variable. Besides, the effects of the mass variables are weaker. And the third impact factor for positioning accuracy is the inertia variable.

4.3.2. Tolerance capability comparison by introducing the random parametric error

In last section, the influencing degrees on the angular error and position error that caused by the six variables are analyzed respectively. In order to closer the practical situation, the variations of all the variables are added to the nominal models at the same time. As the control method cannot compensate the positon errors that caused by the length variables, only the mass diviations (δm_1, δm_2) and inertia diviations (δI_{S1}, δI_{S2}) are investigated in this section.

Thus, the positioning accuracy of the manipulator is influenced by the parametric errors of all the variables together.

There are totally eleven simulations for each manipulator. One of them is implemented with nominal parametric values. The rest ten simulations are implemented by adding the parametric errors of the four variables in the same time. In order to let the parametric values closer to the practical situation, ten sets of random values are created in MATLAB first, shown as

$$Ran = \begin{bmatrix} 0,814724 & 0,157613 & 0,655741 & 0,706046 \\ 0,905792 & 0,970593 & 0,035712 & 0,031833 \\ 0,126987 & 0,957167 & 0,849129 & 0,276923 \\ 0,913376 & 0,485376 & 0,933993 & 0,046171 \\ 0,632359 & 0,80028 & 0,678735 & 0,097132 \\ 0,09754 & 0,141886 & 0,75774 & 0,823458 \\ 0,278498 & 0,421761 & 0,743132 & 0,694829 \\ 0,546882 & 0,915736 & 0,392227 & 0,317099 \\ 0,957507 & 0,792207 & 0,655478 & 0,950222 \\ 0,964889 & 0,959492 & 0,171187 & 0,034446 \end{bmatrix} \tag{4.26}$$

In order to make sure that the variation range of the variable is still from -20% to 20%. the equations (4.27)-(4.30) are used to calculate the real parametric values for all the simulations.

$$m_{1r} = m_{1n} \times (0.8 + 0.4 \times Ran(i,1)) \tag{4.27}$$

$$m_{2r} = m_{2n} \times (0.8 + 0.4 \times Ran(i,2)) \tag{4.28}$$

$$I_{S1r} = I_{S1n} \times (0.8 + 0.4 \times Ran(i,3)) \tag{4.29}$$

$$I_{S2r} = I_{S2n} \times (0.8 + 0.4 \times Ran(i,4)) \tag{4.30}$$

where, m_{1r}, m_{2r} I_{S1r} and I_{S2r} represent the real parametric values ; m_{1n}, m_{2n} I_{S1n} and I_{S2n} represent the nominal parametric values.

Finally, the real parametric values for all the simulations can obtained, shown in Tab. 4.7. In this table, Sim_i means the *i*th simulation. It should be note that, all the parametric values are nominal value in the first simulation (Sim_1). In the rest simulations (from Sim_2 to Sim_11), the parametric values are all added with errors.

Based on these simulations, the total tolerance capability of all the models can be compared. Fig. 4.7 shows the angular errors of the link 1. It shows that, in Sim_1, all the angular errors of link 1 of the decoupled manipulators (manipulator_1, manipulator_2 and manipulator_3) are zero. On the contrary, for the coupled manipulator_0, there is the angular error. As discussed in the last section, this is because the 'mismatch' between the control model and the actual model in coupled manipulator_0. This phenomenon also exists for the angular error of link 2 and the positioning error of the end-effector, shown in Fig. 4.8 and Fig.4.9.

When the parametric errors are added, the angular errors appear. It shows that the angular errors of link 1 of manipulator_1 and manipulator_2 are close and smaller than the ones of manipulator_0 and manipulator_3. Meanwhile the range of variation of the angular errors of link 1 are also smaller than the ones in manipulator_0 and manipulator_3.

Table 4.7. – The real parametric values for the 10 simulations.

	m_{1r}	m_{2r}	I_{S1r}	I_{S2r}
Sim_1	13.193	8.477	0.77754	0.20744
Sim_2	14,85386	7,316034	0,825978	0,224537
Sim_3	15,33445	10,07269	0,633139	0,168593
Sim_4	11,22453	10,02716	0,886125	0,18893
Sim_5	15,37447	8,427412	0,912519	0,169783
Sim_6	13,89149	9,495191	0,833129	0,174012
Sim_7	11,06914	7,262708	0,857701	0,234279
Sim_8	12,02409	8,211708	0,853158	0,223606
Sim_9	13,4404	9,886676	0,744021	0,192264
Sim_10	15,60736	9,467817	0,825896	0,244798
Sim_11	15,64631	10,03505	0,675274	0,16881

The angular errors of link 2 that caused by the parametric errors of all the variables together are shown in Fig. 4.8. Obviously, the angular error of the coupled manipulator_0 is much higher than the ones of the decoupled manipulators. Among the three coupled manipulator, it is difficult to say which is better. This is difference with the phenomenon in Fig. 4.7.

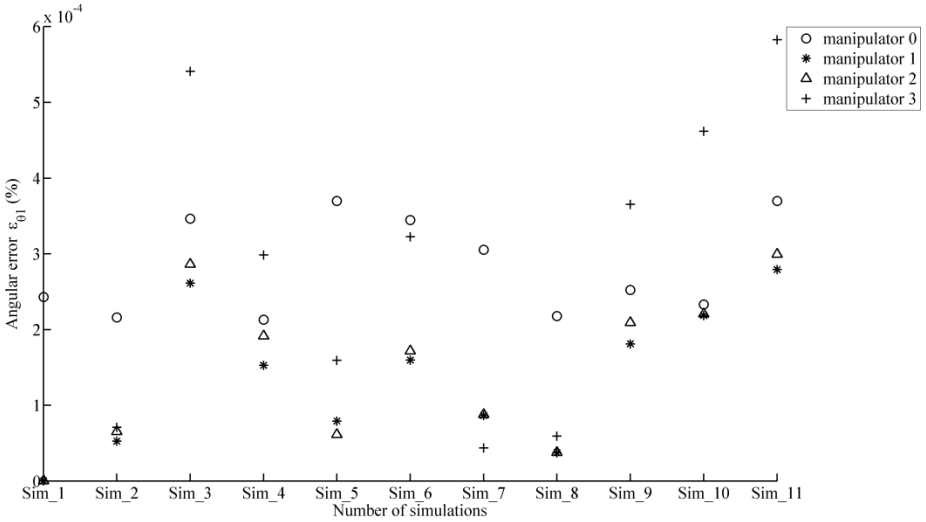

Figure 4.7. – The angular error of link 1 with the parametric errors of all the variables.

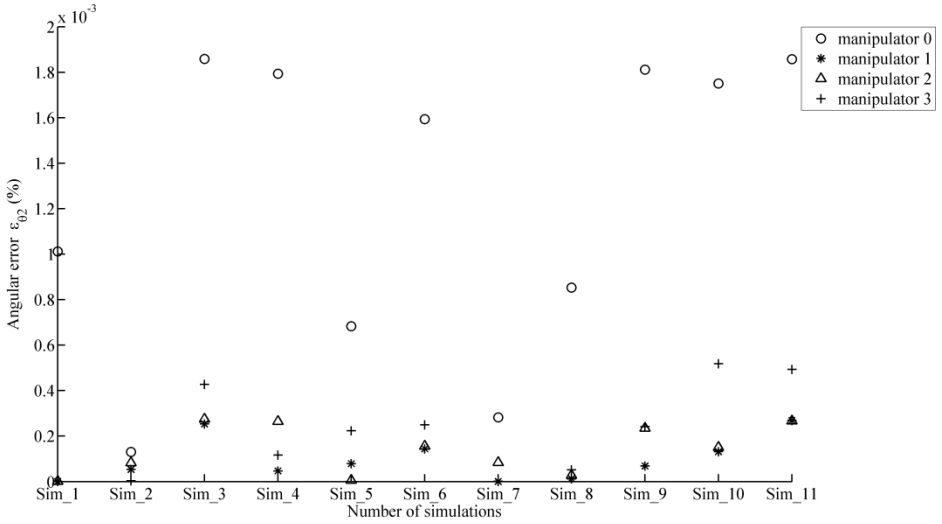

Figure 4.8. – The angular error of link 2 with the parametric errors of all the variables.

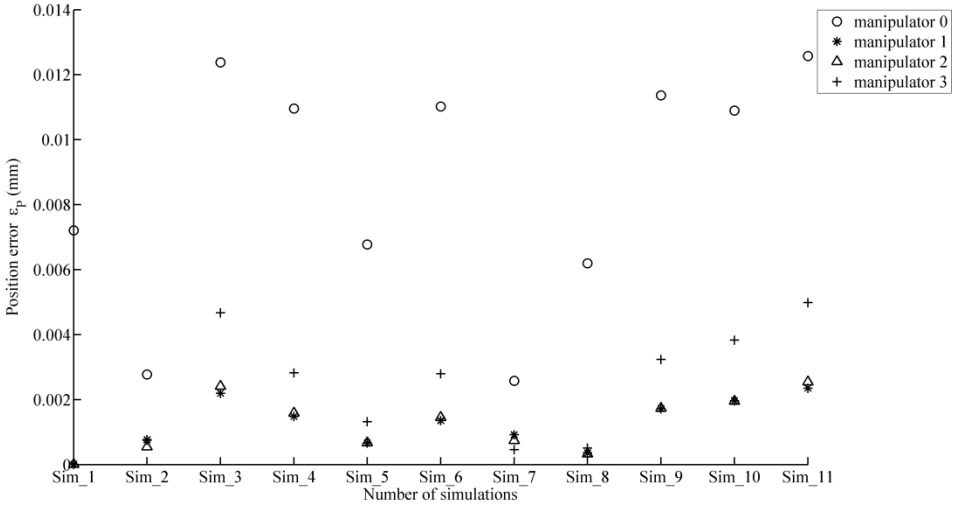

Figure 4.9. – The position error of the end-effector with the parametric errors of all the variables.

In Fig. 4.9, the position errors of the end-effector of all the models are represented. A clear tendency appears that the position error of the end-effector in the coupled manipulator_0 is the highest. In addition, the position errors of the end-effectors in manipulator_1 and manipulator_2 are close and they are smaller than the ones in manipulator_3. In other words, the tolerance capability of manipulator_1 and manipulator_2 which are decoupled by the mechatronic methods that proposed in this thesis are similar. And these two manipulators are more robust than manipulator_3 which is decoupled by the control method. Of course, all these three decoupled manipulators are much more robust than the coupled manipulator.

4.4. Summary

In this chapter, the tolerance capabilities of four models are analyzed. Two kinds of indices are proposed to quantify the positioning accuracy of the manipulator. They are angular error of the actuators and the position error of the end-effector.

First, in order to analysis the influencing degree of each variable of the manipulator on the positioning accuracy, the fixed parametric errors are introduced. According to the quantitative analysis, it shows that the positioning accuracy is more sensitive with the

variation of the length variables. The second influencing factors are the mass parameters. And the influences of the inertia parameters on the positioning accuracy are the lowest.

In addition, it can be also found that, during the whole process, the tracking trajectories of the decoupled manipulators, especially in manipulator_1 and manipulator_2, are more precise and less sensitive to the variable errors.

Then, in order to obtain the models closer to the practical situation, the random parametric errors are introduced. Furthermore, the parametric errors of all the variables are added at the same time during one simulation. According to the results, the advantages of the coupled manipulators (manipulator_1 and manipulator_2) appear. The tolerance capabilities of these two manipulators are higher than the ones of manipulator_3 which is decoupled by feedback linearization and the coupled manipulator.

Discussion

Serial manipulators are principally designed by revolute or prismatic joints. In the chapters above, the serial manipulators with revolute joints has been discussed. The dynamic decoupling of serial manipulator with prismatic joints is a very complicated problem. In this discussion, an attempt is made to carry out the dynamic decoupling of serial manipulators with prismatic joints by using the same approaches, which was applied to serial manipulators with revolute joints.

The Scott-Russell mechanism has been successfully used in previous chapters for achieving the dynamic decoupling of the serial manipulators with revolute joints. In the present section, the rhomboid pantograph mechanism having the same properties as the Scott-Russell mechanism is considered for the simplification of dynamic equations of the serial manipulators with prismatic joints.

First, a proper manipulator model with a prismatic joint is examined. Then, the rhomboid pantograph mechanism is introduced. Finally, the dynamics of the model is analyzed.

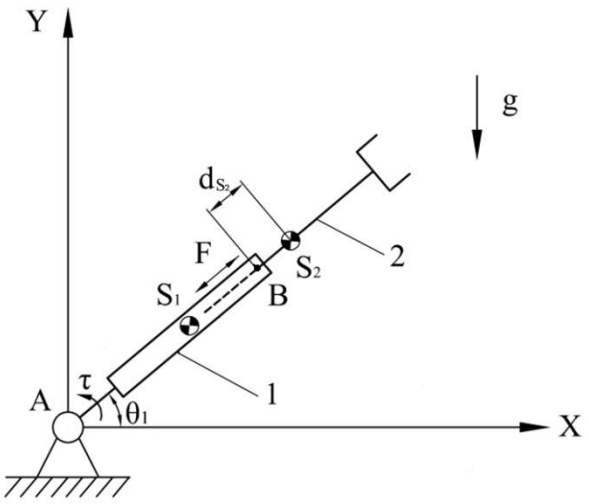

Figure 5.1. – Planar serial manipulator with a prismatic joint.

Let us consider a planar serial manipulator with two degrees of freedom shown in (Fig. 5.1). This is a planar serial manipulator with revolute and prismatic joints. Link 1 of the manipulator is connected with the base of the manipulator by a revolute joint and link 2 is connected with link 1 by a prismatic joint.

As in the previous cases, the Lagrangian formalism is still used for the dynamic modeling.

First, the Lagrangian is calculated as

$$L = E - P = E_1 + E_2 - P_1 - P_2 \tag{5.1}$$

where,

$$E_1 = \frac{1}{2} m_1 L_{AS1}^2 \dot{\theta}_1^2 + \frac{1}{2} I_{S1} \dot{\theta}_1^2$$

$$E_2 = \frac{1}{2} m_2 [\dot{d}_{S2}^2 + (L_1 + d_{S2})^2 \dot{\theta}_1^2] + \frac{1}{2} I_{S2} \dot{\theta}_1^2$$

$$P_1 = m_1 g L_{AS1} \sin\theta_1$$

$$P_2 = m_2 g (L_1 + d_{S2}) \sin\theta_1$$

Thus, the Lagrangian dynamic equations of the manipulator can be obtained as

$$\begin{aligned} \tau &= \frac{d}{dt}\left(\frac{\partial L}{\partial \dot{\theta}_1}\right) - \frac{\partial L}{\partial \theta_1} \\ &= m_1 L_{AS1}^2 \ddot{\theta}_1 + I_{S1} \ddot{\theta}_1 + m_2 (L_1 + d_{S2})^2 \ddot{\theta}_1 + 2 m_2 (L_1 + d_{S2}) \dot{\theta}_1 \dot{d} + I_{S2} \ddot{\theta}_1 \\ &\quad + m_1 g L_{AS1} \cos\theta_1 + m_2 g (L_1 + d_{S2}) \cos\theta_1 \end{aligned} \tag{5.2}$$

$$\begin{aligned} F &= \frac{d}{dt}\left(\frac{\partial L}{\partial \dot{d}_{S2}}\right) - \frac{\partial L}{\partial d_{S2}} \\ &= m_2 \ddot{d}_{S2} - m_2 (L_1 + d_{S2}) \dot{\theta}_1^2 + m_2 g \sin\theta_1 \end{aligned} \tag{5.3}$$

Rewriting these equations, we obtain

$$\begin{aligned} \tau &= [m_1 L_{AS1}^2 + I_{S1} + m_2 (L_1 + d_{S2})^2 + I_{S2}] \ddot{\theta}_1 + 2 m_2 (L_1 + d_{S2}) \dot{\theta}_1 \dot{d} \\ &\quad + m_1 g L_{AS1} \cos\theta_1 + m_2 g (L_1 + d_{S2}) \cos\theta_1 \\ F &= m_2 \ddot{d}_{S2} - m_2 (L_1 + d_{S2}) \dot{\theta}_1^2 + m_2 g \sin\theta_1 \end{aligned} \tag{5.4}$$

where, m_1, m_2 are the masses of link 1 and 2, respectively; I_{S1}, I_{S2} are the moments of inertia of links 1 and 2, respectively; L_1, L_2 are the lengths of links 1 and 2, respectively; L_{AS1} is the distance between the center of mass S_1 of link 1 and joint center *A*; d_{S2} is the distance between the center of mass S_2 of link 2 and joint center *B*; θ_1 is angular displacement of link 1 relative to the base; $\dot{\theta}_1$ is angular velocity of link 1 relative to the base; $\dot{d}_{S2}$ is velocity of center of mass S_2 of link 2 relative to joint center *B*; $\ddot{\theta}_1$ is the angular acceleration of link 1 relative to the base; $\ddot{d}_{S2}$ is acceleration of center of mass S_2 of link 2 relative to joint center *B*; τ is the input torque and F is the input force, g is the gravity acceleration.

Obviously, this is a coupled and nonlinear dynamic model. Now, the rhomboid pantograph mechanism will be added in order to examine the decoupling conditions in such a structure.

Figure 5.2 shows the examined serial manipulator with the added rhomboid pantograph mechanism having the same properties as the Scott-Russell mechanism.

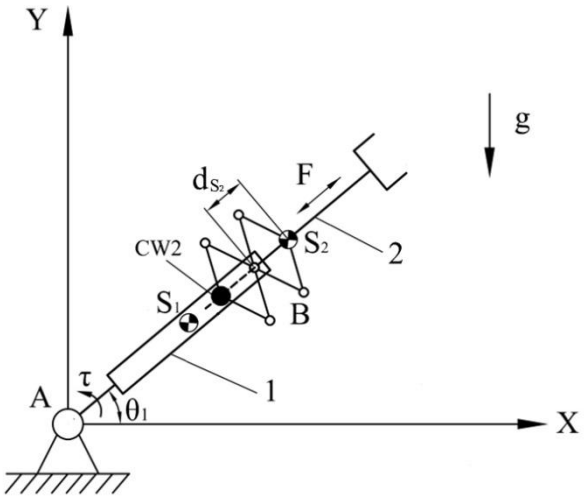

Figure 5.2. – Serial manipulator with the added rhomboid pantograph mechanism.

In the modified structure, one end of the added mechanism is attached on the center of mass of link 2. The other end of the mechanism is connected with the counterweight CW2. Thus the counterweight CW2 copies the movement of the center of mass S_2 in the opposite direction.

Assuming that

$$m_{CW2}L_{CW2} = m_2 d_{S2} \tag{5.5}$$

where, m_{CW2} is the mass of the counterweight CW2 that attached on one end of the rhomboid pantograph mechanism, L_{CW2} is the distance between the mass of the counterweight CW2 and the center of joint B.

Further, in order to simply the following calculation, we will consider that the loops of the rhomboid pantograph mechanism are similar, i.e.

$$\begin{aligned} m_{CW2} &= m_2 \\ L_{CW2} &= d_{S2} \end{aligned} \tag{5.6}$$

Now, let us rewrite the Lagrangian factor taking into account the added structure

$$L = E_1 + E_2 + E_3 - P_1 - P_2 - P_3 \tag{5.7}$$

where,

$$E_1 = \frac{1}{2} m_1 L_{AS1}^2 \dot{\theta}_1^2 + \frac{1}{2} I_{S1} \dot{\theta}_1^2$$

$$E_2 = \frac{1}{2} m_2 [\dot{d}_{S2}^2 + (L_1 + d_{S2})^2 \dot{\theta}_1^2] + \frac{1}{2} I_{S2} \dot{\theta}_1^2$$

$$E_3 = \frac{1}{2} m_2 [\dot{d}_{S2}^2 + (L_1 - d_{S2})^2 \dot{\theta}_1^2]$$

$$P_1 = m_1 g L_{AS1} \sin\theta_1$$

$$P_2 = m_2 g (L_1 + d_{S2}) \sin\theta_1$$

$$P_3 = m_2 g (L_1 - d_{S2}) \sin\theta_1$$

Thus, we get:

$$\begin{aligned} \tau &= \frac{d}{dt}\left(\frac{\partial L}{\partial \dot{\theta}_1}\right) - \frac{\partial L}{\partial \theta_1} \\ &= m_1 L_{AS1}^2 \ddot{\theta}_1 + I_{S1} \ddot{\theta}_1 + m_2 (L_1 + d_{S2})^2 \ddot{\theta}_1 + 2 m_2 (L_1 + d_{S2}) \dot{\theta}_1 \dot{d}_{S2} + I_{S2} \ddot{\theta}_1 \\ &+ m_2 (L_1 - d_{S2})^2 \ddot{\theta}_1 - 2 m_2 (L_1 - d_{S2}) \dot{\theta}_1 \dot{d}_{S2} \\ &+ m_1 g L_{AS1} \cos\theta_1 + m_2 g (L_1 + d_{S2}) \cos\theta_1 + m_2 g (L_1 - d_{S2}) \cos\theta_1 \end{aligned} \tag{5.8}$$

$$F = \frac{d}{dt}\left(\frac{\partial L}{\partial \dot{d}_{S2}}\right) - \frac{\partial L}{\partial d_{S2}} \qquad (5.9)$$
$$= m_2\ddot{d}_{S2} + m_2\ddot{d}_{S2} - m_2(L_1 + d_{S2})\dot{\theta}_1^2 + m_2(L_1 - d_{S2})\dot{\theta}_1^2$$

Rewriting these equations, we obtain

$$\begin{aligned} \tau &= [m_1 L_{AS1}^2 + I_{S1} + 2m_2 L_1^2 + 2m_2 d_{S2}^2 + I_{S2}]\ddot{\theta}_1 + 4m_2 d_{S2}\dot{\theta}_1 \dot{d}_{S2} \\ &\quad + m_1 g L_{AS1}\cos\theta_1 + 2m_2 g L_1 \cos\theta_1 \\ F &= 2m_2\ddot{d}_{S2} - 2m_2 d_{S2}\dot{\theta}_1^2 \end{aligned} \qquad (5.10)$$

From equation (5.10) it can be seen that the gravity terms in the second equation is cancelled. To cancel the gravity term in the first equation, another counterweight should be added to link 1.

The static moment of the added counterweight CW1 can be found by the expression

$$m_{CW1} L_{CW1} = m_1 L_{AS1} + m_2(L_1 + d_{S2}) + m_2(L_1 - d_{S2}) \qquad (5.11)$$

where, m_{CW1} is the mass of the added counterweight CW1 mounted on the link 1, L_{CW1} is the distance between the center of mass of the counterweight CW1 and the center of the revolute joint A.

Finally, we obtain

$$\begin{aligned} \tau &= [m_1 L_{AS1}^2 + I_{S1} + 2m_2 L_1^2 + 2m_2 d_{S2}^2 + I_{S2} + m_{CW1} L_{CW1}^2]\ddot{\theta}_1 + 4m_2 d_{S2}\dot{\theta}_1 \dot{d}_{S2} \\ F &= 2m_2\ddot{d}_{S2} - 2m_2 d_{S2}\dot{\theta}_1^2 \end{aligned} \qquad (5.12)$$

It is obvious that, the added rhomboid pantograph mechanism allows one to carry out a partial decoupling. It ensures only the cancellation of the terms related to gravity.

In conclusion, it should be noted that the application of the rhomboid pantograph mechanism having the same properties as the Scott-Russell mechanism on the serial planar manipulator with a prismatic joint allows a partial cancellation of the coupled terms of the dynamic equations. The given analysis showed that only terms due to gravity have been cancelled. The problem of dynamic decoupling of serial manipulators with prismatic joints remains quite complicated.

Conclusion

The critical review given in the first chapter showed that the known mechanical solutions can only be reached by a considerably more complicated design of the initial structure of the manipulator. The complexity of mechanical solutions is in the fact that the dynamic decoupling can be achieved via the opposite rotation of links and their optimal redistribution of masses. In the known design concepts such a solution is carried out by the connection of gears to the oscillating links. The gears added to the oscillating links of the manipulator are sources of shocks between teeth that lead to the perturbation of the operation of the manipulator, the noise and other negative effects. It is obvious that mechanical solutions for adjustment of nonlinear terms of dynamic equations due to the changing payload can be reached by unreasonably complicated design.

On the other hand, dynamic decoupling via optimal control of a manipulator with a nonlinear system model and a changing payload is also rather complex task. A number of procedures for the synthesis of control systems ensuring high quality control of manipulators have been elaborated. Applicability of these approximation solutions depends on the neglected interaction dynamics, which can be viewed as modeling errors. It is obvious that the robustness analysis can be applied to determine their impact. This problem is more complicated and unpredictable when it is necessary to take into account a variable payload. In this case, the nonlinearity due to the variable load adds to the nonlinearity of the manipulator structure.

Considering the mentioned problems related to the dynamic decoupling of manipulators, in the thesis are proposed new solutions combining both mechanical and control solutions.

Chapter 2 deals with the design concept of adjustable serial manipulators with linearized and decoupled dynamics taking into account the changing payload. The novelty of the developed method consist in the fact that the opposite rotation for dynamic decoupling is achieved not by including gears in the existing system but by opposite rotation of the links themselves. At first, the dynamic decoupling of the serial manipulator with adjustable lengths of links is accomplished via an opposite rotation of links and optimal redistribution of masses. Thus, the proposed mechanical solution allows one to transform the original nonlinear system model into a fully linear system without using the feedback linearization technique. However, as mentioned above, the

changing payload creates the variable forces on the actuators, which are also nonlinear. Thus, the changing payload leads to the perturbation of the dynamic decoupling of the manipulator. To ensure linearized and decoupled dynamics of the manipulator for any payload, an optimal control technique is applied. It should be noted that the linearized dynamic of the manipulator via opposite rotation of manipulator's links leads to relatively simple equations, which are easier to analyze for further dynamic decoupling taking into account the changing payload.

Chapter 3 deals with a new dynamic decoupling principle, which involves connecting to a serial manipulator a two-link group forming a Scott-Russell mechanism with the initial links of the manipulator. The opposite motion of links in the Scott-Russell mechanism combined with optimal redistribution of masses allows the cancellation of the coefficients of nonlinear terms in the manipulator's kinetic and potential energy equations. Then, by using the optimal control design, the dynamic decoupling due to the changing payload is achieved. The proposed approach, which is a symbiosis of mechanical and control solutions, improves the known design concepts permitting the dynamic decoupling of serial manipulators.

In chapter 4, the tolerance capabilities of the two dynamic decoupling manipulators (referred to as manipulator_1 and manipulator_2) are investigated through the comparison with a coupled manipulator (referred to as manipulator_0) and one other manipulator which is decoupled by command (referred to as manipulator_3). Two kinds of indices are proposed to quantify the positioning accuracy of the manipulator. They are angular error of the actuators and the position error of the end-effector. And two kinds of simulations are implemented for complete analysis. Through the results, it is obvious that, during the whole process, the tracking trajectories of the decoupled manipulators, especially in manipulator_1 and manipulator_2, are more precise and less sensitive to the variable errors. In the aspect of the final positioning accuracy, according to the quantitative analysis, it also shows that the tolerance capabilities of the two manipulators that dynamic decoupled by the mechatronic method are higher than the ones of the coupled model and the dynamic decoupled model by command. In brief, no matter the behavior during the whole process or the final positioning accuracy, both of these aspects prove that the manipulators that decoupled by the mechatronic method in this thesis are more robust.

All suggested design methodologies and control techniques are illustrated by simulations carried out using ADAMS and MATLAB software, which have confirmed the efficiency of the developed approaches.

Finally, it should be noted that in the thesis an attempt is made to carry out the dynamic decoupling of serial manipulators with prismatic joints by using the same approaches, which was applied to serial manipulators with revolute joints. The obtained results showed that only terms due to gravity has been cancelled. The problem of dynamic decoupling of serial manipulators with prismatic joints remains quite complicated.

We would like to mention that these works have been presented in several articles that listed in Appendix E.

Résumé étendu en Français

CONCEPTION ET ETUDE DES MANIPULATEURS SERIELS A DYNAMIQUE DECOUPLEE PRENANT EN COMPTE LA CHARGE EMBARQUEE

Les manipulateurs sériels composés de chaines cinématiques ouvertes sont des systèmes multi entrées et multi sorties représentés par des équations différentielles couplées et non linéaires. Ces équations différentielles se complexifient si l'on tient compte de la charge embarquée. Dans ce contexte, l'utilisation d'une commande classique de type PID, pour des applications nécessitant des mouvements rapides et précis, n'est pas efficace. En effet, les forces non linéaires qui interviennent dans les manipulateurs sériels induisent des erreurs de réponse en position lors de mouvements très rapides. Même à vitesse lente, les erreurs en position ne sont pas négligeables.

Afin d'améliorer la précision de positionnement de ces manipulateurs, il a été proposé à partir des années 90 d'appliquer une commande par découplage non linéaire (nommée «feedback linearization», «inverse dynamics» ou «computer torque control»). Cette commande, envisageable suite au développement fulgurant des technologies des microprocesseurs, consiste à obtenir un système découplé et linéarisé par compensation des termes non linéaires couplés issus du modèle dynamique du manipulateur grâce à une boucle de retour dite interne. Une condition préalable à l'utilisation de la commande par découplage non linéaire est l'identification du modèle dynamique issu du lagrangien dont l'inverse doit être calculé dans un intervalle de temps inférieur au pas d'acquisition des mesures nécessaires à la commande du système découplé et linéarisé grâce à une boucle de retour dite externe. La figure suivante présente la structure de commande par découplage non linéaire.

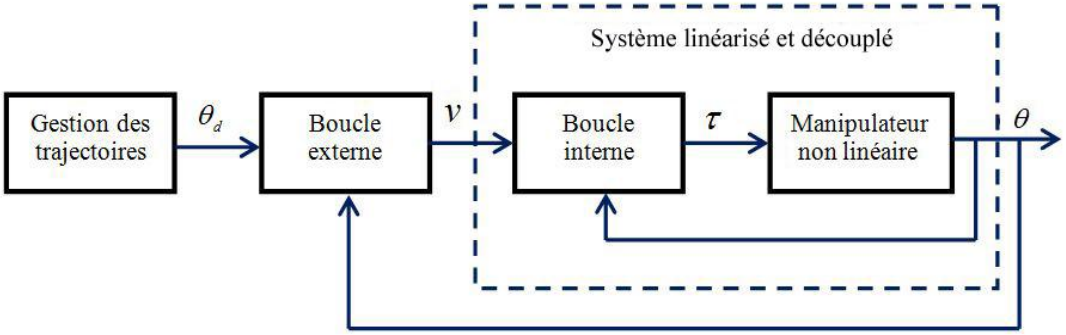

Structure de commande par découplage non linéaire.

Sans l'utilisation de microprocesseurs puissants, la contrainte de temps est difficile à satisfaire lorsque le modèle dynamique du robot est complexe. Ce type de commande conduit généralement à une solution coûteuse qui est peu attractive d'un point de vue industriel.

Pour satisfaire le temps de calcul nécessaire à la boucle de commande dite externe, il est proposé dans ce mémoire une recherche de solutions mécaniques susceptibles de simplifier le modèle dynamique du manipulateur sériel. Dans le cadre de ce travail, l'objectif fixé est le découplage total des équations de la dynamique du manipulateur par des solutions combinées au niveau de la mécanique et de la commande en tenant compte de la charge embarquée. Le cas ultime du découplage total conduit à la suppression de la boucle dite interne. Sur le plan mécanique, les solutions envisagées pour simplifier les modèles dynamiques ne doivent pas conduire à augmenter considérablement les masses en mouvement et à ajouter des complexités structurelles supplémentaires trop importantes.

Chapitre 1 : Conception des manipulateurs à dynamique simplifiée

Après un bref historique de l'évolution des manipulateurs sériels et des applications industrielles, ce chapitre est dédié d'une part, aux méthodes mécaniques actuelles de linéarisation et de découplage des équations dynamiques et d'autre part, à la synthèse de la loi de commande, issue de la commande optimale à horizon infini, du modèle simplifié obtenu par découplage non linéaire (avec la boucle dite interne).

Au niveau de la mécanique, les méthodes consacrées à la linéarisation et au découplage des équations dynamiques des robots sériels peuvent s'inscrire dans l'une des trois tendances principales suivantes :

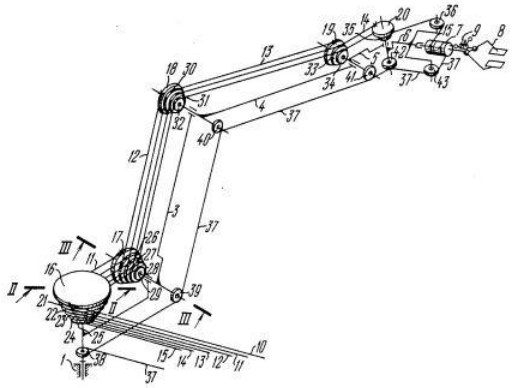

Figure 1.1. - Linéarisation et découplage par délocalisation de l'actionneur.

1) La linéarisation et le découplage des équations dynamiques par la délocalisation de l'actionneur. Cela consiste à découpler la cinématique du mouvement quand la rotation de chaque élément est due à un seul actionneur. En d'autres termes, on

doit s'assurer que les déplacements de l'actionneur correspondent à un ensemble de coordonnées généralisées indépendantes qui permettent de localiser sans aucune ambiguïté le manipulateur. La figure 1.1 montre l'exemple présenté en 1981 par Belyanin, Konstantin, Aron et Alfred.

Ce principe de conception n'est pas optimal du point de vue de la reproduction précise du mouvement car il accumule les erreurs dues aux jeux et à l'élasticité de la courroie de transmission utilisée habituellement pour le découplage, ainsi que les erreurs dues à la fabrication.

2) La linéarisation et le découplage des équations dynamiques par la redistribution optimale des inerties. Cela consiste à obtenir des tenseurs d'inertie diagonaux qui doivent être indépendants de la configuration du manipulateur. La figure 1.2 montre un robot KUKA avec telle redistribution des masses afin de simplifier les équations dynamiques.

Figure 1.2. - Robot KUKA avec redistribution des masses.

Une telle approche est efficace pour les manipulateurs sériels si les axes des liaisons ne sont pas parallèles.

3) La linéarisation et le découplage des équations dynamiques par la mise en place d'éléments auxiliaires. La figure 1.3 montre l'exemple présenté en 2012 par Arakelian et Sargsyan.

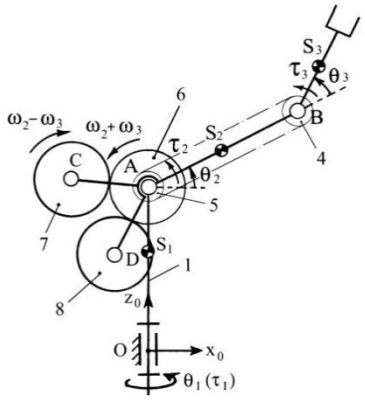

Figure 1.3. - Manipulateur découplé par un groupe d'engrenages.

La modification de la structure du manipulateur permet d'atteindre le découplage dynamique. Cette nouvelle tendance, dans la conception de robots sériels, est certainement prometteuse. Elle devrait aboutir au développement de nouveaux manipulateurs découplés sans grande difficulté. Cependant, la méthodologie de conception proposée dans diverses études conduit inévitablement à l'augmentation de la masse totale du manipulateur suite aux éléments ajoutés au niveau de chaque lien.

Les solutions connues sur le plan mécanique conduisent souvent à une conception compliquée et à une augmentation inévitable de la masse totale du manipulateur. En conséquence, les couples à appliquer deviennent importants et ils ne tiennent pas compte de la charge embarquée.

Au niveau de la commande, le chapitre 1 présente les commandes par retour d'état statique et par retour d'état dynamique (rejet asymptotique d'une perturbation constante) d'un double intégrateur. En effet, que ce soit par découplage non linéaire par la commande ou par découplage du manipulateur par la mécanique, on aboutit toujours à des doubles intégrateurs (par obtention de la forme canonique, si nécessaire). La figure 1.4 présente la commande par retour d'état statique du double intégrateur.

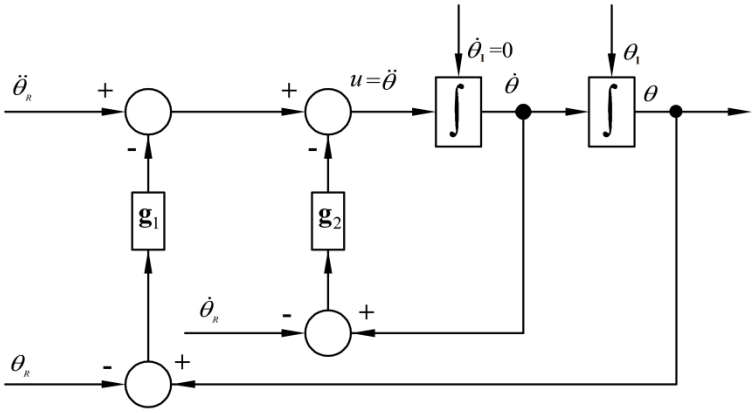

Figure 1.4. - Commande par retour d'état statique.

Si l'on se donne une trajectoire θ_R, 2 fois dérivable sur un intervalle $[0 \quad T]$, vérifiant les conditions initiales et finales, la loi de commande s'écrit :

$$u = \ddot{\theta}_R - g_1[\theta - \theta_R] - g_2[\dot{\theta} - \dot{\theta}_R]$$

Le retour statique (g_1 et g_2) est déterminé de telle manière que la commande u minimise le critère de performance à horizon infini suivant :

$$J = \int_0^\infty \left[\begin{pmatrix} \theta & \dot{\theta} \end{pmatrix} \left[T_p G_{RC}(0, T_p) \right]^{-1} \begin{pmatrix} \theta \\ \dot{\theta} \end{pmatrix} + u^2 \right] dt$$

où $G_{RC}\left(0,T_p\right)$ est le grammien transitoire de commandabilité sur un horizon de poursuite T_P capable de régler les modes dominants du système en boucle fermée.

En ce qui concerne la commande robuste par retour d'état dynamique du double intégrateur, un reconstructeur est mis en place dans la boucle afin d'obtenir $\hat{\theta}, \hat{\dot{\theta}}$ et $\hat{d}$ (estimation de la perturbation fictive constante d qui permet de générer de l'intégration implicite). La figure 1.5 présente la commande par retour d'état dynamique du double intégrateur où les gains g_1 et g_2 sont identiques à ceux déterminés précédemment (principe de séparation). La loi de commande est : $u = \ddot{\theta}_R - g_1[\hat{\theta} - \theta_R] - g_2[\dot{\theta} - \dot{\theta}_R] - \hat{d}$.

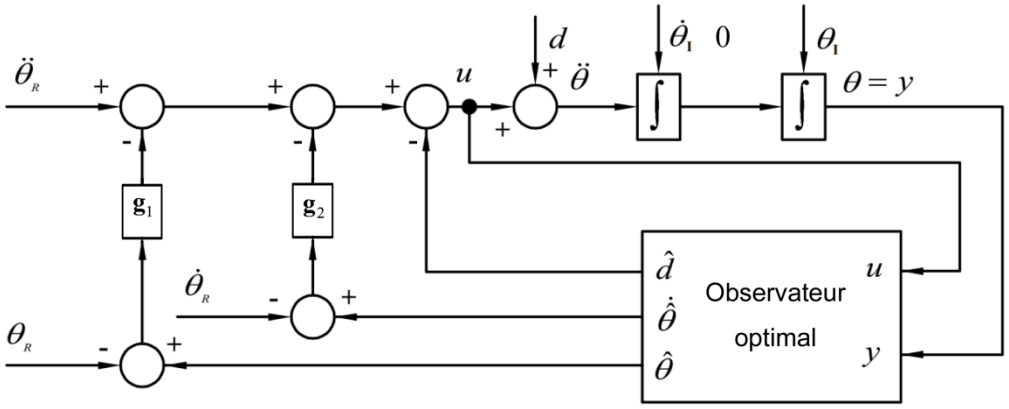

Figure 1.5. - Commande par retour d'état dynamique.

La synthèse du reconstructeur est basée sur le grammien transitoire d'observabilité sur un horizon de régulation T_R capable de régler les modes du reconstructeur.

Dans les chapitres 2 et 3 de la thèse, les solutions proposées permettent d'améliorer la conception des manipulateurs sériels découplés, par une augmentation relativement faible de la masse totale des éléments en mouvement et, en prenant en compte la charge embarquée afin d'obtenir une bonne précision de positionnement.

Chapitre 2 : Manipulateur sériel reconfigurable à dynamique découplée

La structure du manipulateur reconfigurable à dynamique découplée, sans charge embarquée, est présentée à la figure 2.1. Le manipulateur est composé de deux bras et de deux liaisons rotoïdes motorisées. Les effets de la gravité sont compensés par construction mécanique.

Les longueurs $L_1 = L_{AB}$ et $L_2 = L_{BP}$ des bras 1 (composé de 1a et 1b) et 2 (composé de 2a et 2b) sont variables et peuvent être modifiées selon la trajectoire désirée pour le préhenseur. La présence de deux mécanismes Scott-Russel permet d'obtenir l'équilibrage statique du bras 2 pour toutes les configurations possibles du manipulateur (en fonction de 2b). Le modèle géométrique inverse du manipulateur permet d'obtenir les angles θ_1 et θ_2 en fonction de la trajectoire du préhenseur $P(x, y)$:

$$\theta_1 = \tan^{-1}\left[\frac{y\left(L_1 + L_2\cos\theta_2\right) - xL_2\sin\theta_2}{x\left(L_1 + L_2\cos\theta_2\right) + yL_2\sin\theta_2}\right] \text{ et } \theta_2 = \pm\cos^{-1}\left[\frac{x^2 + y^2 - L_1^2 - L_2^2}{2L_1L_2}\right]$$

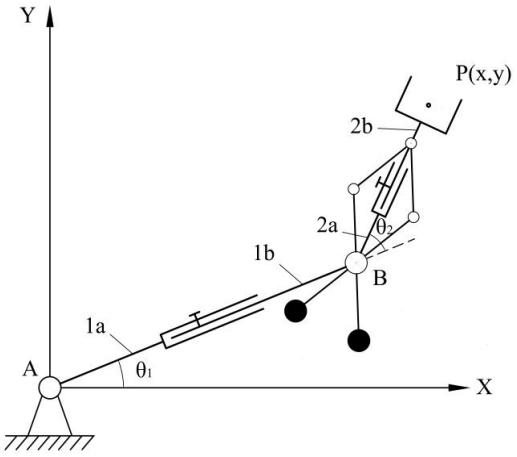

Figure 2.1. - Structure du manipulateur.

Deux solutions sont possibles et correspondent à deux postures différentes nommées «coude bas», notée avec l'index (1) sur la figure 2.2, et coude haut, notée avec l'index (2). En effet, la figure 2.2 montre deux configurations du manipulateur pour une position initiale P^i («coude bas») et une position finale P^f («coude haut») du préhenseur. L'autre solution, pour une position initiale P^i («coude haut») et une position finale P^f («coude bas») du préhenseur, n'apparait pas sur la figure 2.2.

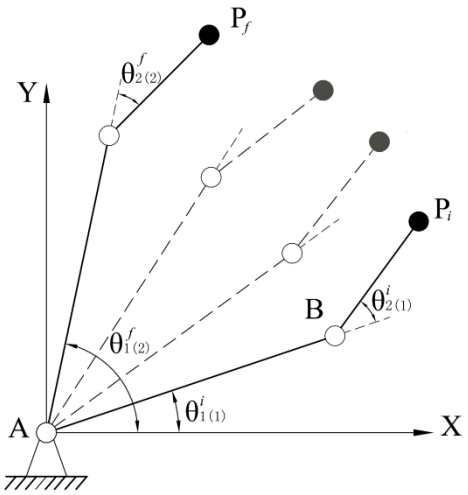

Figure 2.2. - Les configurations initiale et finale du manipulateur.

Le manipulateur étant statiquement équilibré (le centre de masse du bras 2 est en B), le modèle dynamique devient linéaire mais est couplé, c'est-à-dire :

$$\begin{bmatrix} \tau_1 \\ \tau_2 \end{bmatrix} = \begin{bmatrix} I_{S2} + I_{S1} + m_1 L_{AS1}^2 + m_2 L_1^2 & I_{S2} \\ I_{S2} & I_{S2} \end{bmatrix} \begin{bmatrix} \ddot{\theta}_1 \\ \ddot{\theta}_2 \end{bmatrix}$$

où τ_1 et τ_2 : les couples en A et B ; I_{S1} et I_{S2} : les moments d'inertie des bras 1 et 2 ; m_1 et m_2 : les masses des bras 1 et 2 ; $\ddot{\theta}_1$ et $\ddot{\theta}_2$: les accélérations angulaires en A et B ; L_{AS1} : la distance du centre de masse du bras 1 par rapport au point A.

Pour découpler le modèle linéaire, il faut assurer les rotations opposées des bras 1 et 2 avec les accélérations angulaires telles que : $\ddot{\theta}_1 = -\ddot{\theta}_2$. Dans ce cas, on obtient :

$$\tau_1 = \left(I_{S2} + I_{S1} + m_1 L_{AS1}^2 + m_2 L_1^2 \right) \ddot{\theta}_1 \quad ; \quad \tau_2 = 0$$

Les conditions qui conduisent à $\ddot{\theta}_1 = -\ddot{\theta}_2$, consiste à calculer les longueurs L_1 et L_2 en fonction des conditions initiales et finales des angles θ_1 *et* θ_2 qui doivent vérifier :

$$\left| \theta^f_{1(2)} - \theta^i_{1(1)} \right| = - \left| \theta^f_{2(2)} - \theta^i_{2(1)} \right|$$

A partir des équations géométriques du manipulateur et pour les positions initiale (coude bas) $P^i\left(x_i, y_i\right)$ et finale (coude haut) $P^f\left(x_f, y_f\right)$ et pour $\Delta\theta_1 = \theta^f_{1(2)} - \theta^f_{1(1)}$, on en déduit :

$$L_1 = \frac{x_f^2 + y_f^2 - x_i^2 - y_i^2}{2L_2(\cos\theta_{2(2)}^f - \cos\theta_{2(1)}^i)} \quad ; \quad L_2 = \left[\frac{-\xi - (\xi^2 - 4\chi)^{1/2}}{2}\right]^{1/2}$$

où

$$\xi = \left[2(\chi)^{1/2}\cos\theta_{2(1)}^i - x_i^2 - y_i^2\right] \; ; \; \chi = \left[\frac{x_f^2 + y_f^2 - x_i^2 - y_i^2}{2(\cos\theta_{2(2)}^f - \cos\theta_{2(1)}^i)}\right]^2 \; ; \; \theta_{2(2)}^f = -(\Delta\theta_1 - \theta_{2(1)}^i)$$

En tenant compte de la charge embarquée (masse m_p), les équations différentielles couplées et non linéaires du manipulateur à l'étude se complexifient. Ces équations complexes seront utilisées, après inversion, pour créer le modèle du manipulateur sous l'environnement MATLAB/SIMULINK.

Sous l'hypothèse des rotations opposées $\left(\ddot{\theta}_1 = -\ddot{\theta}_2\right)$, les équations se simplifient et deviennent alors exploitables pour compenser par anticipation la charge embarquée. Dans ce cas, on obtient :

$$\tau_1 = \left(I_{S2} + I_{S1} + m_1 L_{AS1}^2 + m_2 L_1^2\right)\ddot{\theta}_1 + m_P L_1\left(L_1 + L_2\cos(\theta_2)\right)\ddot{\theta}_1 - m_P L_1\left(L_2\sin(\theta_2)\right)\dot{\theta}_1\dot{\theta}_2$$

$$\tau_2 = 0 + m_P L_1\left(L_2\cos(\theta_2)\right)\ddot{\theta}_1 + m_P L_1\left(L_2\sin(\theta_2)\right)\dot{\theta}_1^2$$

Si $m_p = 0$ (pas de charge embarquée), on retrouve les équations des couples τ_1 et τ_2 déterminées précédemment.

Pour les simulations, les trajectoires angulaires de θ_{1R} et θ_{2R} sont construites par interpolation polynômiale (polynômes du cinquième ordre qui vérifient les conditions initiales et finales). Pour les valeurs nominales du manipulateur, quatre simulations (avec et sans compensation de la charge embarquée) sont effectuées.

La première simulation, en boucle ouverte avec compensation de la charge, fournit des résultats identiques aux trajectoires désirées qui sont présentées à la figure 2.3. La deuxième simulation, en boucle ouverte sans compensation de la charge, fournit des résultats qui divergent car le système est instable. Il ne peut pas rejeter la perturbation (charge embarquée).

La troisième simulation, en boucle fermée avec compensation de la charge, fournit des résultats identiques aux trajectoires désirées qui sont présentées à la figure 2.3. La quatrième simulation, en boucle fermée sans compensation de la charge, fournit des résultats qui convergent car le système est asymptotiquement stable mais présente des écarts en régime permanent pour θ_1 et θ_2 qui sont liés à la charge embarquée.

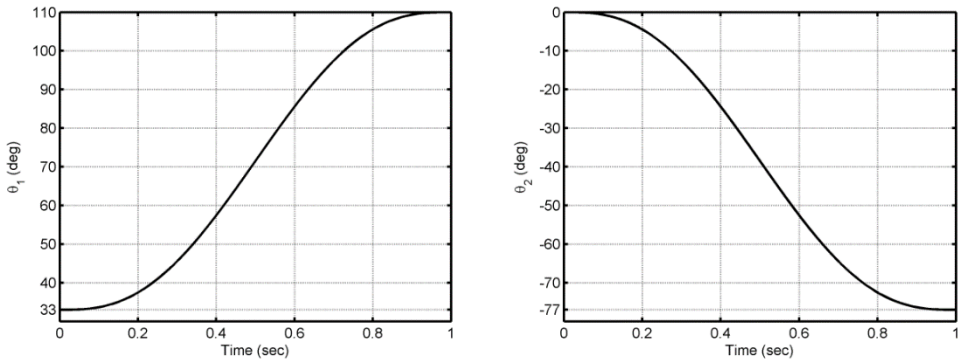

Figure 2.3. - Les trajectoires désirées pour θ_1 et θ_2.

Les résultats obtenus attestent de l'efficacité et de la pertinence de la solution proposée dans ce chapitre 2 qui tient compte de la charge embarquée.

Chapitre 3 : Découplage des manipulateurs sériels à liaisons rotoïdes

Le manipulateur sériel à dynamique découplée, sans charge embarquée, est présenté à la figure 3.1. Le manipulateur est composé de deux bras principaux (1 et 2), de deux liaisons rotoïdes (A et B) motorisées (deux degrés de liberté) et d'un bras auxiliaire (3) connecté à un glisseur (4) par l'intermédiaire d'une liaison pivot glissant en D et au bras 2 grâce à une liaison pivot (rotoïde) en C.

Le mécanisme Scott-Russel, constitué des éléments BC, CD et du glisseur, permet un mouvement rectiligne parallèle au bras 1 et génère des accélérations angulaires identiques des bras 2 et 3.

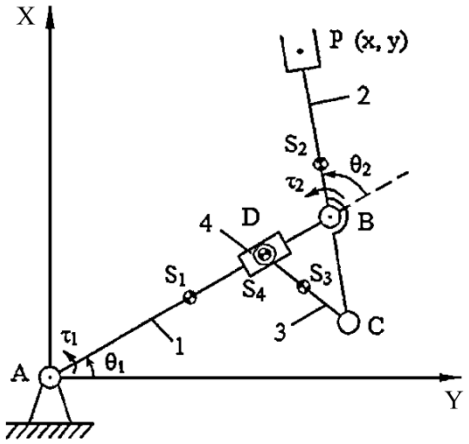

Figure 3.1. - Structure du manipulateur.

Le manipulateur est statiquement équilibré si l'on vérifie les relations suivantes :

$$m_3 L_{CS3} + m_4 L_3 = 0 \ ; \ (m_3 + m_4) L_3 - m_2 L_{BS2} = 0$$

où m_2, m_3 et m_4 : les masses des bras 2 et 3 et du glisseur 4 ; L_3 : longueur du bras 3 ; L_{BS2} : la distance du centre de masse du bras 2 par rapport au point B ; L_{CS3} : la distance du centre de masse du bras 3 par rapport au point C.

Ces deux conditions permettent d'obtenir un modèle dynamique linéaire couplé. Pour effectuer le découplage, le moment d'inertie du bras 3 doit être égal à :

$$I_{S3} = I_{S2} + \left[\frac{(m_3 + m_4)^2}{m_2} + \frac{m_3^2 - m_4^2}{m_3} \right] L_3^2$$

où I_{S2} et I_{S3} : les moments d'inertie des bras 2 et 3.

Dans ce cas, on obtient :

$$\tau_1 = \left(I_{S1} + 2I_{S2} + I_{S4} + m_1 L_{AS1}^2 + (m_2 + m_3 + m_4) L_1^2 + 2 \frac{(m_3 + m_4)(m_2 + m_3 + m_4)}{m_2} L_3^2 \right) \ddot{\theta}_1$$

$$\tau_2 = 2 \left(I_{S2} + \frac{(m_3 + m_4)(m_2 + m_3 + m_4)}{m_2} L_3^2 \right) \ddot{\theta}_2$$

où τ_1 et τ_2 : les couples en A et B ; I_{S1} et I_{S4} : les moments d'inertie du bras 1 et du glisseur 4 ; m_1 : la masse du bras 1 ; L_1 : la longueur du bras 1 ; L_{AS1} : la distance du centre de masse du bras 1 par rapport au point A.

En tenant compte de la charge embarquée (masse m_p), les équations différentielles couplées et non linéaires du manipulateur à l'étude se complexifient terriblement. Ces équations très complexes seront utilisées, après inversion, pour créer le modèle du manipulateur sous l'environnement MATLAB/SIMULINK.

Sous l'hypothèse des deux conditions réalisées, les équations se simplifient et deviennent alors exploitables pour compenser par anticipation la charge embarquée. Les couples à appliquer deviennent :

$$\begin{aligned} \tau_1 = & \left(I_{S1} + 2I_{S2} + I_{S4} + m_1 L_{AS1}^2 + (m_2 + m_3 + m_4) L_1^2 + 2 \frac{(m_3 + m_4)(m_2 + m_3 + m_4)}{m_2} L_3^2 \right) \ddot{\theta}_1 \\ & + m_p L_1 \left(L_1 + 2 L_{BP} \cos\theta_2 \right) \ddot{\theta}_1 + m_p L_1 L_{BP} \left(\ddot{\theta}_2 \cos\theta_2 - 2\dot{\theta}_1 \dot{\theta}_2 \sin\theta_2 - \dot{\theta}_2^2 \sin\theta_2 \right) \\ & + \left(\frac{\left(m_p L_{BP} + (m_3 + m_4) L_3 \right)^2}{m_2 + m_p} - \frac{(m_3 + m_4)^2 L_3^2}{m_2} \right) (\ddot{\theta}_1 + \ddot{\theta}_2) \end{aligned}$$

$$\tau_2 = 2\left(I_{S2} + \frac{(m_3+m_4)(m_2+m_3+m_4)}{m_2} L_3^2 \right) \ddot{\theta}_2 + m_p L_1 L_{BP} \left(\ddot{\theta}_1 \cos\theta_2 + \dot{\theta}_1^2 \sin\theta_2 \right)$$
$$+ \left(\frac{\left(m_p L_{BP} + (m_3+m_4) L_3 \right)^2}{m_2 + m_p} - \frac{(m_3+m_4)^2 L_3^2}{m_2} \right) (\ddot{\theta}_1 + \ddot{\theta}_2)$$

où L_{BP} : la distance du préhenseur par rapport au point B.

Si $m_p = 0$ (pas de charge embarquée), on retrouve les équations des couples τ_1 et τ_2 déterminées précédemment.

Pour les simulations, les trajectoires angulaires de θ_{1R} et θ_{2R} sont construites par interpolation polynômiale (polynômes du cinquième ordre qui vérifient les conditions et finales). Pour les valeurs nominales du manipulateur, quatre simulations (avec et sans compensation de la charge embarquée) sont effectuées.

La première simulation, en boucle ouverte avec compensation de la charge, fournit des résultats identiques aux trajectoires désirées qui sont présentées à la figure 3.2. La deuxième simulation, en boucle ouverte sans compensation de la charge, fournit des résultats qui divergent car le système est instable. Il ne peut pas rejeter la perturbation (charge embarquée).

La troisième simulation, en boucle fermée avec compensation de la charge, fournit des résultats identiques aux trajectoires désirées qui sont présentées à la figure 3.2. La quatrième simulation, en boucle fermée sans compensation de la charge, fournit des résultats qui convergent car le système est asymptotiquement stable mais présente des écarts en régime permanent pour θ_1 et θ_2 qui sont liés à la charge embarquée.

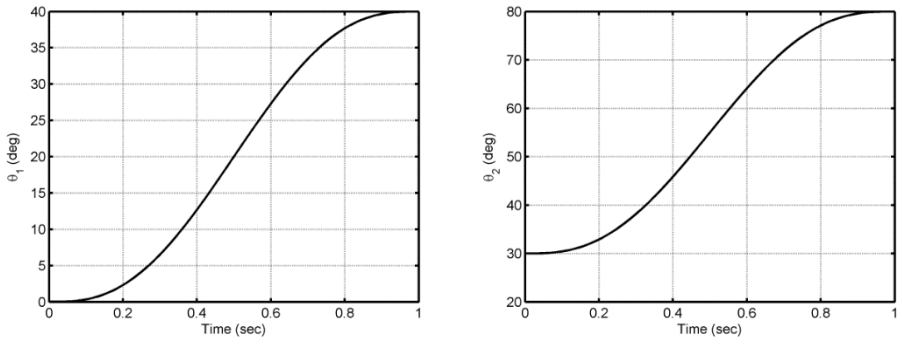

Figure 3.2. - Les trajectoires désirées pour θ_1 et θ_2.

Les résultats obtenus attestent de l'efficacité et de la pertinence de la solution proposée dans ce chapitre 3 qui tient compte de la charge embarquée.

Chapitre 4 : Analyse de la tolérance des manipulateurs sériels à dynamique couplée et découplée

Le chapitre 4 est dédié à deux études qualitatives, par simulation, sur la robustesse de quatre modèles de manipulateurs planaires et sériels, à deux degrés de liberté, pour la même loi de commande en boucle fermée (la boucle de retour externe). Il s'agit de simuler les comportements en régime transitoire et en régime permanent des quatre systèmes, sans charge embarquée, lorsque les paramètres des modèles des manipulateurs varient par rapport à leurs valeurs nominales. Les manipulateurs sont les suivants :

- Le manipulateur_0 à dynamique non découplée, présenté à la figure 4.1.
- Le manipulateur_1 du chapitre 2 (figure 2.1) à dynamique découplée.
- Le manipulateur_2 du chapitre 3 (figure 3.1) à dynamique découplée.
- Le manipulateur_3 à dynamique découplée par la commande par l'intermédiaire de la boucle de retour interne (obtention des doubles intégrateurs).

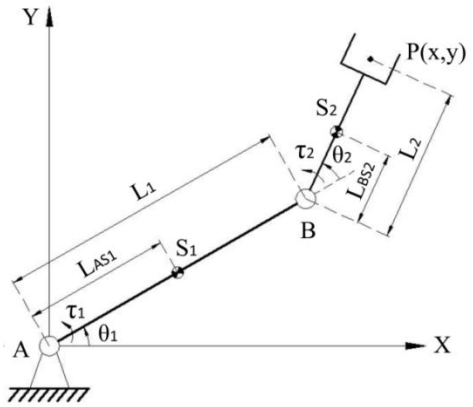

Figure 4.1. - Structure du manipulateur.

Pour établir la loi de commande du manipulateur_0 de la figure 4.1, le modèle linéaire et découplé est obtenu en négligeant les forces centrifuges, de Coriolis et les influences mutuelles de la matrice d'inertie pour la rendre constante et diagonale.

La première étude qualitative consiste à observer les valeurs absolues des erreurs, dans le plan articulaire, en régime transitoire. Les paramètres variables concernent les masses m_1 (bras 1) et m_2 (bras 2), les moments d'inertie I_{S1} (bras 1) et I_{S2} (bras 2) et

les distances L_{AS1} (centre de masse du bras 1 par rapport au point A) et L_{BS2} (centre de masse du bras 2 par rapport au point B). Pour chaque simulation, un seul des six paramètres définis est modifié (variation de $\pm 20\%$ par pas de 5%). La figure 4.2 présente les résultats pour une variation de $+20\%$ de la masse m_1.

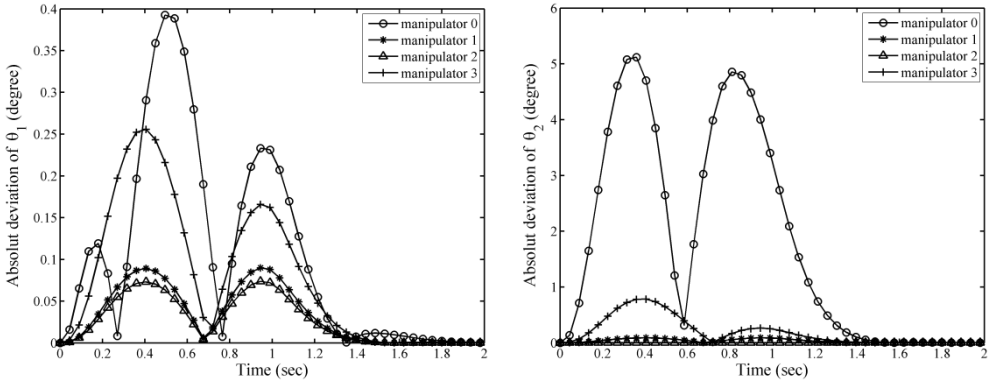

Figure 4.2. - Valeurs absolues des erreurs sur θ_1 et θ_2.

Tous les autres résultats présentés dans le mémoire sont en concordance avec ceux de la figure 4.2 et permettent d'en tirer la conclusion suivante : les amplitudes des variations des valeurs absolues des erreurs sur θ_1 et θ_2 sont nettement plus faibles pour les manipulateurs des chapitres 2 et 3 à dynamique linéarisée et découplée que celles du manipulateur_3 (découplage par la boucle interne) et surtout celles du manipulateur_0 à dynamique non découplée.

La deuxième étude qualitative consiste à observer les écarts en régime permanent dans les plans articulaire et cartésien. Les paramètres variables concernent les masses m_1 (bras 1) et m_2 (bras 2), les moments d'inertie I_{S1} (bras 1) et I_{S2} (bras 2) et les distances L_{AS1} (centre de masse du bras 1 par rapport au point A) et L_{BS2} (centre de masse du bras 2 par rapport au point B). Pour chaque simulation, les six paramètres définis précédemment sont tous modifiés en même temps par tirage des valeurs, à l'aide d'un générateur pseudo-aléatoire, dans une plage de $\pm 20\%$ de leurs valeurs nominales. La figure 4.3 présente les résultats des écarts en régime permanent dans le plan cartésien.

Les résultats en régime permanent, dans le plan articulaire, qui sont présentés dans le mémoire sont en concordance avec ceux de la figure 4.3 et permettent d'en tirer la conclusion suivante : les écarts en position sur θ_1 et θ_2, dans l'espace articulaire et les écarts en position du préhenseur, dans l'espace cartésien, sont beaucoup plus faibles pour les manipulateurs des chapitres 2 et 3 à dynamique linéarisée et découplée que ceux du manipulateur_3 (découplage par la boucle interne) et surtout ceux du manipulateur_0 à dynamique non découplée.

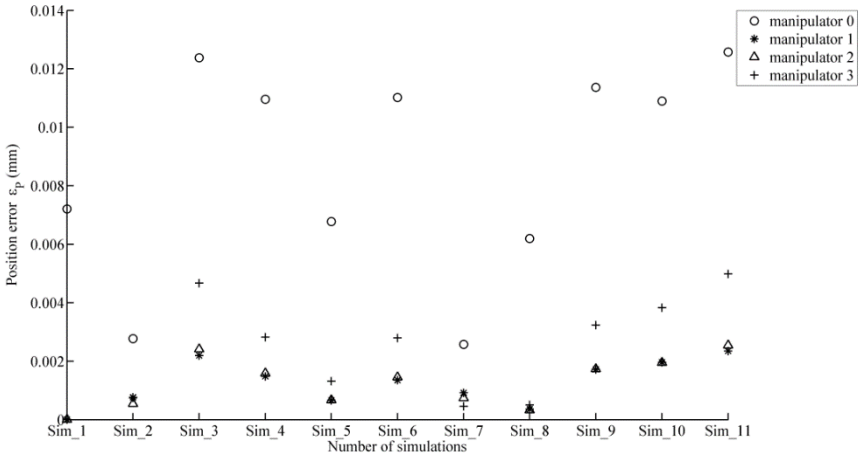

Figure 4.3. - Ecarts en régime permanent du préhenseur.

En conclusion, les résultats de simulation montrent (pour une même loi de commande en boucle fermée) une meilleure robustesse (vis-à-vis des variations des paramètres) des modèles des manipulateurs planaires et sériels, développés aux chapitres 2 et 3. Ceci est dû à la pertinence des modèles utilisés, proches des modèles réels, pour générer la loi de commande.

Discussion :

En général, les manipulateurs sériels font apparaitre des liaisons rotoïdes et des liaisons prismatiques. Dans les chapitres 2 et 3, les manipulateurs développés possèdent uniquement des liaisons rotoïdes et aucune liaison prismatique. Dans le cadre des liaisons rotoïdes, c'est l'utilisation du mécanisme Scott-Russel qui a permis le découplage partiel et total des équations dynamiques des manipulateurs étudiés.

Dans le cadre d'une simple discussion, le découplage dynamique d'un manipulateur sériel, soumis à la gravitation, avec une liaison rotoïde et une liaison prismatique est mis à l'étude. Le modèle est non linéaire et couplé. Pour examiner les conditions de découplage des équations du manipulateur présenté à la figure 5.1, un pantographe rhomboïdal est mis en place. Ce type de mécanisme présente les mêmes propriétés que le mécanisme Scott-Russel. Une extrémité du pantographe rhomboïdal est attachée au centre de masse S_2 du bras 2 qui est connecté au bras 1 par une liaison prismatique. L'autre extrémité du pantographe est connectée au contrepoids $CW2$ qui copie le mouvement du centre de masse S_2 dans la direction opposée. Enfin, le bras 1 est connecté à la base du manipulateur par une liaison rotoïde.

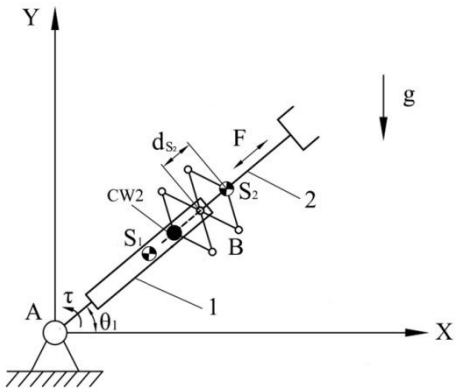

Figure 5.1. - Structure du manipulateur.

Si l'on rajoute un contrepoids au niveau du bras 1, les équations du couple τ et de la force F se simplifient mais restent non linéaires et couplées. Cependant les termes dus à la gravité n'apparaissent plus dans les équations finales.

Cet exemple simple montre la difficulté très importante à surmonter lorsque l'on souhaite découpler un manipulateur sériel avec une liaison prismatique.

Conclusion :

Les solutions originales, développées aux chapitres 2 et 3, pour linéariser et découpler la dynamique d'un manipulateur planaire et sériel à deux degrés de liberté sont très prometteuses. Elles permettent de mettre en place une commande optimale qui tient compte de la charge embarquée (très utile dans le cadre d'opérations du type « pick and place »). La pertinence des solutions retenues confère une très bonne robustesse vis-à-vis des variations des paramètres des modèles. Enfin, travailler sur un modèle linéaire permet d'envisager, par exemple, la mise en place de lois de commande à énergie minimale, à temps minimal, etc.

Par rapport à la commande par découplage non linéaire, les commandes proposées s'affranchissent de la boucle interne et autorisent des cadences élevées (réduction du temps de calcul). La précision est également améliorée car elles permettent un calcul précis des couples nécessaires au mouvement du manipulateur.

L'ensemble du travail réalisé est illustré par les simulations réalisées sur les progiciels ADAMS et MATLAB.

Pour l'avenir, des démonstrateurs seraient évidemment les bienvenus pour valider les résultats obtenus. De même, une ouverture vers les manipulateurs parallèles est à considérer.

Bibliography

Abdel-Rahman, T. M., and Elbestawi, M. A. (1991). "Synthesis and dynamics of statically balanced direct-drive manipulators with decoupled inertia tensors." *Mechanism and Machine Theory*, 26(4), 389–402.

Angeles, J. (2013). "Design Challenges in the Development of Fast Pick-and-place Robots." *Romansy 19 – Robot Design, Dynamics and Control*, CISM International Centre for Mechanical Sciences, V. Padois, P. Bidaud, and O. Khatib, eds., Springer Vienna, 61–68.

Arakelian, V., Aoustin, Y., and Chevallereau, C. (2016a). "On the Design of the Exoskeleton Arm with Decoupled Dynamics." *New Trends in Medical and Service Robots*, Springer, 143–150.

Arakelian, V., and Dahan, M. (1995). "Equilibrage optimal des mécanismes pour manipulateurs." *Actes du 12e Congrès Français de Mécanique, Strasbourg*, 4, 373–6.

Arakelian, V., Jatsun, S., Sargsyan, S., and Jatsun, A. (2011). "On the design of serial manipulators with linearized dynamics." *Proceedings of the ASME 2011 International Design Engineering Technical Conferences & Computers and Information in Engineering Conference IDETC/CIE*, 1–6.

Arakelian, V., Le Baron, J.-P., and Mkrtchyan, M. (2016b). "Design of Scotch yoke mechanisms with improved driving dynamics." *Proceedings of the Institution of Mechanical Engineers, Part K: Journal of Multi-body Dynamics*, 230(4), 379–386.

Arakelian, V., and Sargsyan, S. (2012). "On the design of serial manipulators with decoupled dynamics." *Mechatronics*, 22(6), 904–909.

Armstrong, B., Khatib, O., and Burdick, J. (1986). "The explicit dynamic model and inertial parameters of the PUMA 560 arm." *Robotics and Automation. Proceedings. 1986 IEEE International Conference on*, IEEE, 510–518.

Asada, H. (1983). "A geometrical representation of manipulator dynamics and its application to arm design." *Journal of dynamic systems, measurement, and control*, 105(3), 131–142.

Asada, H., and Slotine, J.-J. (1986a). *Robot analysis and control*. John Wiley & Sons.

Asada, H., and Slotine, J.-J. E. (1986b). *Robot Analysis and Control*. John Wiley & Sons.

Asada, H., and Youcef-Toumi, K. (1984a). "Decoupling of manipulator inertia tensor by mass redistribution." *Proceedings of the Design Engineering Technical Conference, Cambridge*.

Asada, H., and Youcef-Toumi, K. (1984b). "Analysis and Design of a Direct-Drive Arm With a Five-Bar-Link Parallel Drive Mechanism." *Journal of Dynamic Systems, Measurement, and Control*, 106(3), 225–230.

Atashzar, S. F., Talebi, H. A., and Towhidkhah, F. (2010). "A robust feedback linearization approach for tracking control of flexible-link manipulators using an EKF disturbance estimator." IEEE, 1791–1796.

Bejczy, A., Tarn, T., Yun, X., and Han, S. (1985). "Nonlinear feedback control of PUMA 560 robot arm by computer." IEEE, 1680–1688.

Belyanin, P. N., Konstantin, F., Aron, K., and Alfred, K. (1981). "Mechanical arm."

Ben-Gharbia, K. M., Maciejewski, A. A., and Roberts, R. G. (2015). "Modifying the kinematic structure of an anthropomorphic arm to improve fault tolerance." *2015 IEEE International Conference on Robotics and Automation (ICRA)*, 1455–1460.

Ben-Gharbia, K. M., Roberts, R. G., and Maciejewski, A. A. (2011). "Examples of planar robot kinematic designs from optimally fault-tolerant Jacobians." *2011 IEEE International Conference on Robotics and Automation*, 4710–4715.

Benhabib, B., Fenton, R., and Goldenberg, A. (1987). "Computer-aided joint error analysis of robots." *IEEE Journal on Robotics and Automation*, 3(4), 317–322.

Bhat, S. P., Bernstein, D. S., and others. (1998). “Continuous finite-time stabilization of the translational and rotational double integrators.” *IEEE Transactions on Automatic Control*, 43(5), 678–682.

Bobrow, J. E., Dubowsky, S., and Gibson, J. S. (1985). “Time-optimal control of robotic manipulators along specified paths.” *The international journal of robotics research*, 4(3), 3–17.

Caro, S., Bennis, F., and Wenger, P. (2005). “Tolerance Synthesis of Mechanisms: A Robust Design Approach.” *Journal of Mechanical Design*, 127(1), 86–94.

Chen Ken, Lin Jian-Ya, and Lu Yong Xiang. (1988). “Fuzzy Control of Robot Manipulator.” IEEE, 1210–1212.

Chen, Y., and Desrochers, A. A. (1989). “Structure of minimum-time control law for robotic manipulators with constrained paths.” *Robotics and Automation, 1989. Proceedings., 1989 IEEE International Conference on*, IEEE, 971–976.

Cheng, F.-T., Hour, T.-L., Sun, Y.-Y., and Chen, T.-H. (1997). “Study and resolution of singularities for a 6-DOF PUMA manipulator.” *IEEE Transactions on Systems, Man, and Cybernetics, Part B (Cybernetics)*, 27(2), 332–343.

Cheng, S., and Dhillon, B. S. (2011). “Reliability and availability analysis of a robot-safety system.” *Journal of Quality in Maintenance Engineering*, 17(2), 203–232.

Coelho, T. A. H., Yong, L., and Alves, V. F. A. (2004). “Decoupling of dynamic equations by means of adaptive balancing of 2-dof open-loop mechanisms.” *Mechanism and Machine Theory*, 39(8), 871–881.

Corke, P. I. (1991). *Operational Details of the Unimation Puma servo system,"*. Tech. Rep. MTM-226, CSIRO Div. Manufacturing Technology.

Craig, J. J. (2005). *Introduction to robotics: mechanics and control*. Pearson Prentice Hall Upper Saddle River.

De Silva, C. W., and MacFarlane, A. G. J. (1989). “Knowledge-based control approach for robotic manipulators.” *International Journal of Control*, 50(1), 249–273.

Denkena, B., and Lepper, T. (2015). “Enabling an industrial robot for metal cutting operations.” *Procedia CIRP*, 35, 79–84.

Descusse, J., Lafay, J. F., and Malabre, M. (1988). “Solution to Morgan’s problem.” *IEEE Transactions on Automatic Control*, 33(8), 732–739.

Dixon, W. E., Walker, I. D., Dawson, D. M., and Hartranft, J. P. (2000). “Fault detection for robot manipulators with parametric uncertainty: a prediction-error-based approach.” *IEEE Transactions on Robotics and Automation*, 16(6), 689–699.

Dukkipati, R. V. (2007). *Mechanism and Machine Theory*. bohem press.

Elgazzar, S. (1985). “Efficient kinematic transformations for the PUMA 560 robot.” *IEEE Journal on Robotics and Automation*, 1(3), 142–151.

Ferreira, P. M., and Liu, C. R. (1986). “An analytical quadratic model for the geometric error of a machine tool.” *Journal of Manufacturing Systems*, 5(1), 51–63.

Filaretov, V. F., and Vukobratović, M. K. (1993). “Static balancing and dynamic decoupling of the motion of manipulation robots.” *Mechatronics*, 3(6), 767–782.

Gebizlioğlu, Ö. E. (2003). “External Control of PUMA 700 Series Robot Based on the Communication Protocols LUN and DDCMP.” Middle East Technical University.

George C, D., Jr. (1961). “Programmed article transfer.” Brookside Drive, Greenwich.

Gompertz, R. S., and Yang, D. C. (1989). “Performance evaluation of dynamically linearized and kinematically redundant planar manipulators.” *Robotics and computer-integrated manufacturing*, 5(4), 321–331.

Gosselin, C. M. (1990). “Dexterity indices for planar and spatial robotic manipulators.” *Robotics and Automation, 1990. Proceedings., 1990 IEEE International Conference on*, IEEE, 650–655.

Guillo, M., and Dubourg, L. (2016). “Impact & improvement of tool deviation in friction stir welding: Weld quality & real-time compensation on an industrial robot.” *Robotics and Computer-Integrated Manufacturing*, 39, 22–31.

Guo, Y., Dong, H., Wang, G., and Ke, Y. (2016). “Vibration analysis and suppression in robotic boring process.” *International Journal of Machine Tools and Manufacture*, 101, 102–110.

Gupta, K. K., and Guo, Z. (1991). “A practical motion planner for PUMA 560.” IEEE, 258–261.

Hocking, L. M. (1991). *Optimal Control: An Introduction to the Theory with Applications*. Clarendon Press.

Jin, Y. (1998). “Decentralized adaptive fuzzy control of robot manipulators.” *IEEE Transactions on Systems, Man, and Cybernetics, Part B (Cybernetics)*, 28(1), 47–57.

Kiam Heong Ang, Chong, G., and Yun Li. (2005). “PID control system analysis, design, and technology.” *IEEE Transactions on Control Systems Technology*, 13(4), 559–576.

Kircanski, M. V., and Boric, M. D. (1992). “Symbolical singular value decomposition for PUMA robot and its application to robot control.” Proceedings of the International Symposium on Industrial Robots, International Federation of Robotics & Robotic Industries, 255–255.

Kolhe, J. P., Shaheed, M., Chandar, T. s., and Talole, S. e. (2013). “Robust control of robot manipulators based on uncertainty and disturbance estimation.” *International Journal of Robust and Nonlinear Control*, 23(1), 104–122.

Kuc, T.-Y., Nam, K., and Lee, J. S. (1991). “An iterative learning control of robot manipulators.” *IEEE Transactions on Robotics and Automation*, 7(6), 835–842.

Lasalle, J. P. (1961). *Lefschetz, Stability by Lyapunov’s Direct Method*. Academic Press New York;

Leahy, M. B. (1989). “Experimental analysis of robot control: a performance standard for the PUMA-560.” IEEE Comput. Soc. Press, 257–264.

Leali, F., Pellicciari, M., Pini, F., Berselli, G., and Vergnano, A. (2013). “An offline programming method for the robotic deburring of aerospace components.” *Robotics in Smart Manufacturing*, Springer, 1–13.

Levine, W. S. (1996). *The Control Handbook*. CRC Press.

Li, W., Chang, X. G., Wahl, F. M., and Farrell, J. (2001). “Tracking control of a manipulator under uncertainty by FUZZY P+ ID controller.” *Fuzzy Sets and Systems*, 122(1), 125–137.

Liao, Y. G. (2011). “Design and Analysis of a Modified Scott Russell Straight-Line Mechanism for a Robot End-Effector.” *Journal of Applied science and Engineering Technology*, 42–49.

Lin, F., and Brandt, R. D. (1998). “An optimal control approach to robust control of robot manipulators.” *IEEE Transactions on Robotics and Automation*, 14(1), 69–77.

Ma, O., and Angeles, J. (1990). “The concept of dynamic isotropy and its applications to inverse kinematics and trajectory planning.” IEEE Comput. Soc. Press, 481–486.

Matsuoka, S., Shimizu, K., Yamazaki, N., and Oki, Y. (1999). “High-speed end milling of an articulated robot and its characteristics.” *Journal of materials processing technology*, 95(1), 83–89.

Mendes, N., Neto, P., Simão, M. A., Loureiro, A., and Pires, J. N. (2016). “A novel friction stir welding robotic platform: welding polymeric materials.” *The International Journal of Advanced Manufacturing Technology*, 85(1–4), 37–46.

Minotti, P., and Pracht, P. (1992). “Design of robots driven by linear servo systems.” *Robotica*, 10(04), 361–368.

Moradi, M., Nikoobin, A., and Azadi, S. (2010). “Adaptive decoupling for open chain planar robots.” *Scientia Iranica: Transaction B, Mechanical Engineering*, 17(5), 376–86.

Nawrocka, A., Kot, A., and Nawrocki, M. (2016). “Neural network control of nonlinear objects.” IEEE, 517–522.

Nof, S. Y. (1999). *Handbook of Industrial Robotics*. John Wiley & Sons.

Olsson, T., Haage, M., Kihlman, H., Johansson, R., Nilsson, K., Robertsson, A., Björkman, M., Isaksson, R., Ossbahr, G., and Brog\a ardh, T. (2010). “Cost-efficient drilling using industrial robots with high-bandwidth force feedback.” *Robotics and Computer-Integrated Manufacturing*, 26(1), 24–38.

Ouyang, P. R., Pano, V., and Dam, T. (2015). “PID position domain control for contour tracking.” *International Journal of Systems Science*, 46(1), 111–124.

Ouyang, P. R., Zhang, W. J., and Gupta, M. M. (2006). “An adaptive switching learning control method for trajectory tracking of robot manipulators.” *Mechatronics*, 16(1), 51–61.

Petrov, M., Ganchev, I., and Taneva, A. (2002). “Fuzzy PID control of nonlinear plants.” *Intelligent Systems, 2002. Proceedings. 2002 First International IEEE Symposium*, IEEE, 30–35.

Piltan, F., Sulaiman, N., Zargari, A., Keshavarz, M., and Badri, A. (2011). “Design PID-Like Fuzzy Controller With Minimum Rule Base and Mathematical Proposed On-line Tunable Gain: Applied to Robot Manipulator.” *International Journal of Artificial intelligence and expert system*, 2(4), 184–195.

Rao, V. G., and Bernstein, D. S. (2001). “Naive control of the double integrator.” *IEEE Control Systems*, 21(5), 86–97.

Rocco, P. (1996). “Stability of PID control for industrial robot arms.” *IEEE Transactions on Robotics and Automation*, 12(4), 606–614.

Santibanez, V., and Kelly, R. (1998). “A class of nonlinear PID global regulators for robot manipulators.” IEEE, 3601–3606.

Senthil Kumar, J., and Karthigai Amutha, E. (2014). “Control and tracking of robotic manipulator using PID controller and hardware in Loop Simulation.” IEEE, 1–3.

Siciliano, B., and Khatib, O. (2016). “Robotics and the Handbook.” *Springer Handbook of Robotics*, B. Siciliano and O. Khatib, eds., Springer International Publishing, 1–10.

Slotine, J.-J. E., and Li, W. (1987). “On the Adaptive Control of Robot Manipulators.” *The International Journal of Robotics Research*, 6(3), 49–59.

Slotine, J.-J. E., Li, W., and others. (1991). *Applied nonlinear control*. prentice-Hall Englewood Cliffs, NJ.

Su, Y., Zheng, C., and Mullerz, P. C. (2007). “Global Asymptotic Stability of PID Controller for Robotic Manipulators.” *2007 International Conference on Mechatronics and Automation*, 3244–3249.

Sugie, T., and Ono, T. (1991). “An iterative learning control law for dynamical systems.” *Automatica*, 27(4), 729–732.

Sun, C., He, W., and Hong, J. (2016). “Neural Network Control of a Flexible Robotic Manipulator Using the Lumped Spring-Mass Model.” *IEEE Transactions on Systems, Man, and Cybernetics: Systems*, 1–12.

Sun, D., and Mills, J. K. (1999). “Performance Improvement of Industrial Robot Trajectory Tracking Using Adaptive-Learning Scheme.” *Journal of Dynamic Systems, Measurement, and Control*, 121(2), 285–292.

Tran, T. T., Ge, S. S., and He, W. (2015). “Adaptive control for a robotic manipulator with uncertainties and input saturations.” *2015 IEEE International Conference on Mechatronics and Automation (ICMA)*, 1525–1530.

Tran, T.-T., Ge, S. S., and He, W. (2016). “Adaptive control for an uncertain robotic manipulator with input saturations.” *Control Theory and Technology*, 14(2), 113–121.

Vaishnav, R. N., and Magrab, E. B. (1987). “A general procedure to evaluate robot positioning errors.” *The International journal of robotics research*, 6(1), 59–74.

Veitschegger, W. K., and Wu, C.-H. (1988). “Robot calibration and compensation.” *IEEE Journal on Robotics and Automation*, 4(6), 643–656.

Veitschegger, W., and Wu, C.-H. (1986). “Robot accuracy analysis based on kinematics.” *IEEE Journal on Robotics and Automation*, 2(3), 171–179.

Vosniakos, G.-C., and Matsas, E. (2010). “Improving feasibility of robotic milling through robot placement optimisation.” *Robotics and Computer-Integrated Manufacturing*, 26(5), 517–525.

Waldron, K. J., and Kumar, A. (1979). “Development of a Theory of Errors for Manipulators.” *Proceedings of the Fifth World Congress on the Theory of Machines and Mechanisms*, 821–826.

Waurzyniak, P. (2015). “Fast, lightweight robots help factories go faster.” *Manufacturing Engineering*, 154(3), 55–64.

Wu, C. h. (1983). “The Kinematic Error Model for the Design of Robot Manipulator.” *1983 American Control Conference*, 497–502.

Xu, Y., Paul, R. P., and Shum, H.-Y. (1991). “Fuzzy control of robot and compliant wrist system.” IEEE, 1431–1437.

Yang, D. C. H., and Tzeng, S. W. (1985). “Simplification and linearization of manipulator dynamics by design.” *Proc. of the 9th Applied Mechanics Conference*.

Yang, D. C. H., and Tzeng, S. W. (1986). “Simplification and linearization of manipulator dynamics by the design of inertia distribution.” *The International journal of robotics research*, 5(3), 120–128.

Yang, H. S., and Slotine, J.-J. E. (1994). “Fast Algorithms for Near-Minimum-Time Control of Robot Manipulators Communication.” *The International Journal of Robotics Research*, 13(6), 521–532.

Yoo, B. K., and Ham, W. C. (2000). “Adaptive control of robot manipulator using fuzzy compensator.” *IEEE Transactions on fuzzy systems*, 8(2), 186–199.

Yoshikawa, T. (1985). “Dynamic manipulability of robot manipulators.” *Robotics and Automation. Proceedings. 1985 IEEE International Conference on*, IEEE, 1033–1038.

Youcef-Toumi, K., and Asada, H. (1985). “The Design of Arm Linkages with Decoupled and Configuration-Invariant Inertia Tensors: Part I: Open Kinematic Chains with Serial Drive Mechanisms; and Part II: Actuator Relocation and Mass Redistributioa In Donath, M. and Leu, M.” *Robotics and Manufacturing Automation*, 145–152.

Youcef-Toumi, K., and Asada, H. (1986). “The design of open-loop manipulator arms with decoupled and configuration-invariant inertia tensors.” *1986 IEEE International Conference on Robotics and Automation*, 2018–2026.

Youcef-Toumi, K., and Asada, H. (1987). “The Design of Open-Loop Manipulator Arms With Decoupled and Configuration-Invariant Inertia Tensors.” *Journal of Dynamic Systems, Measurement, and Control*, 109(3), 268–275.

Zhu, W., Qu, W., Cao, L., Yang, D., and Ke, Y. (2013). “An off-line programming system for robotic drilling in aerospace manufacturing.” *The International Journal of Advanced Manufacturing Technology*, 68(9–12), 2535–2545.

Appendix A

The closed-loop simulation diagram of the dynamic decoupling model in chapter 2

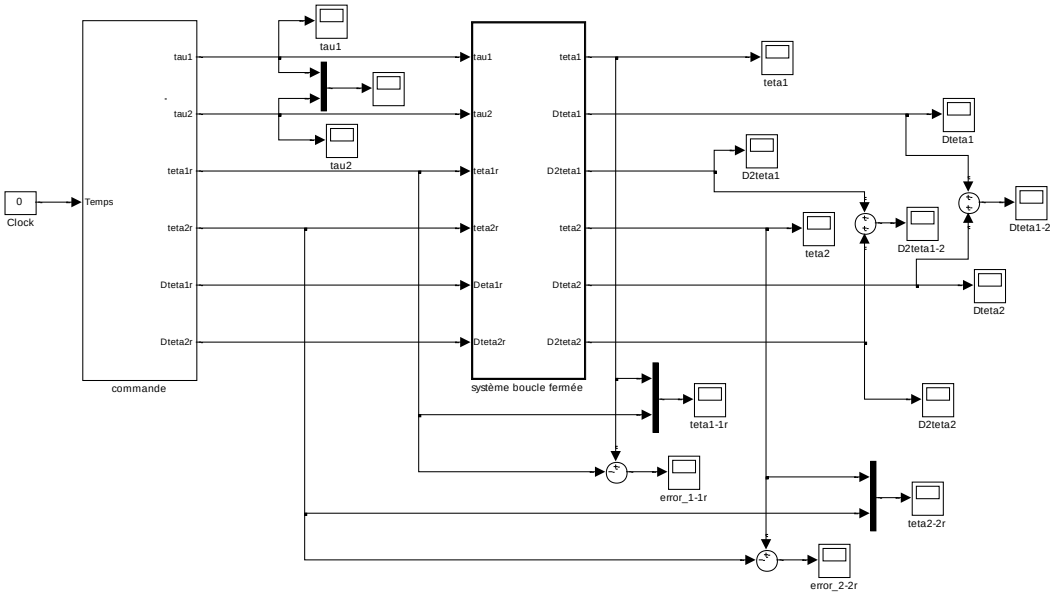

Figure A.1. – The general system of the dynamic decoupling model in chapter 2.

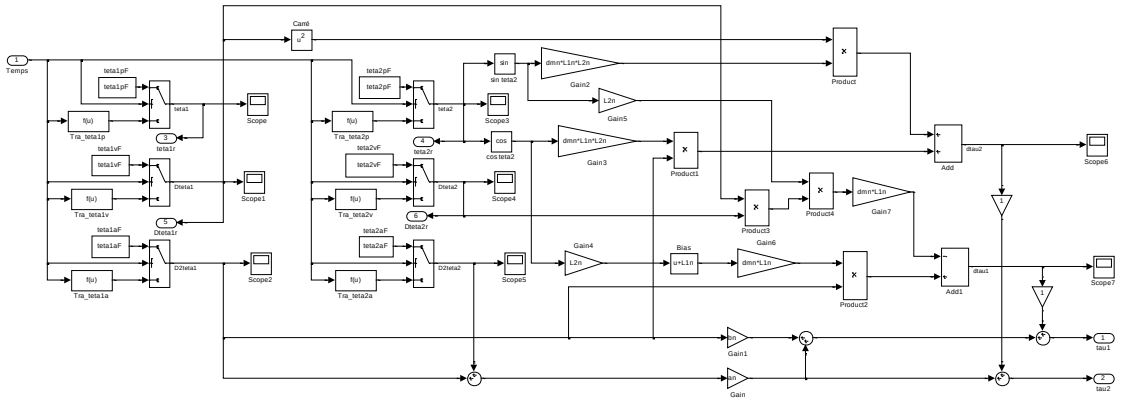

Figure A.2. – The controller diagram of the dynamic decoupling model in chapter 2.

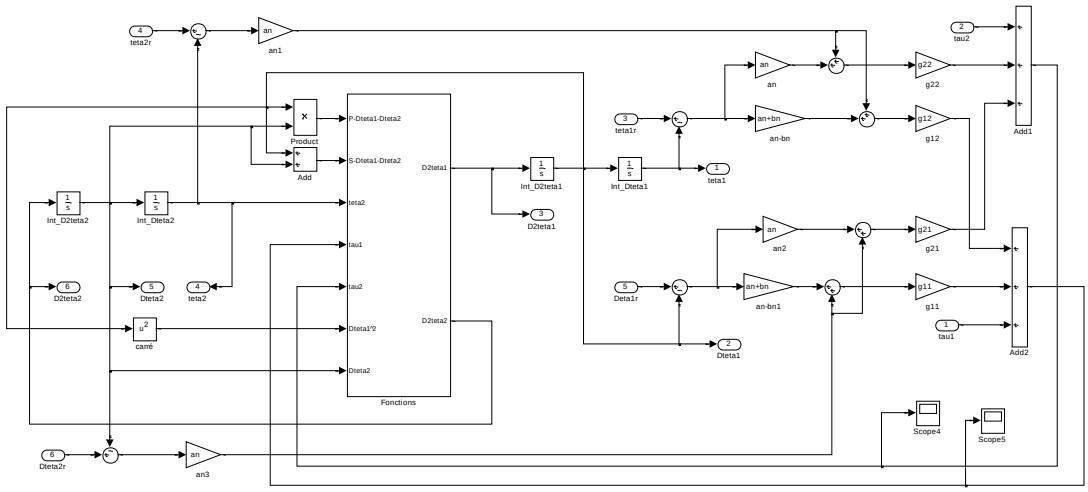

Figure A.3. – The closed-loop diagram of the dynamic decoupling model in chapter 2.

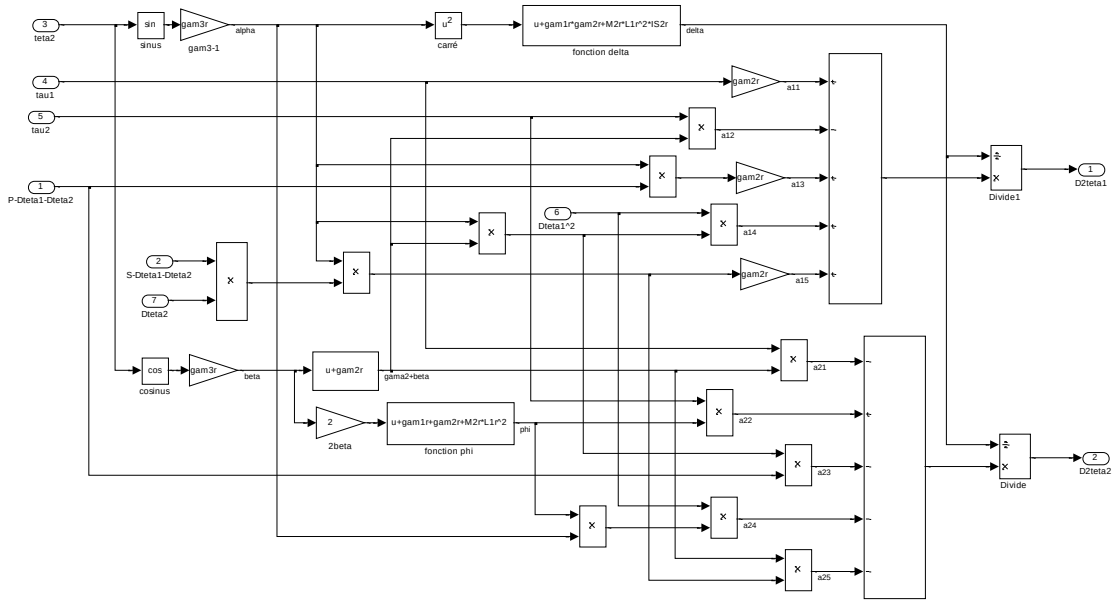

Figure A.4. – The manipulator diagram of the dynamic decoupling model in chapter 2.

Appendix B

The closed-loop simulation diagram of the dynamic decoupling model in chapter 3

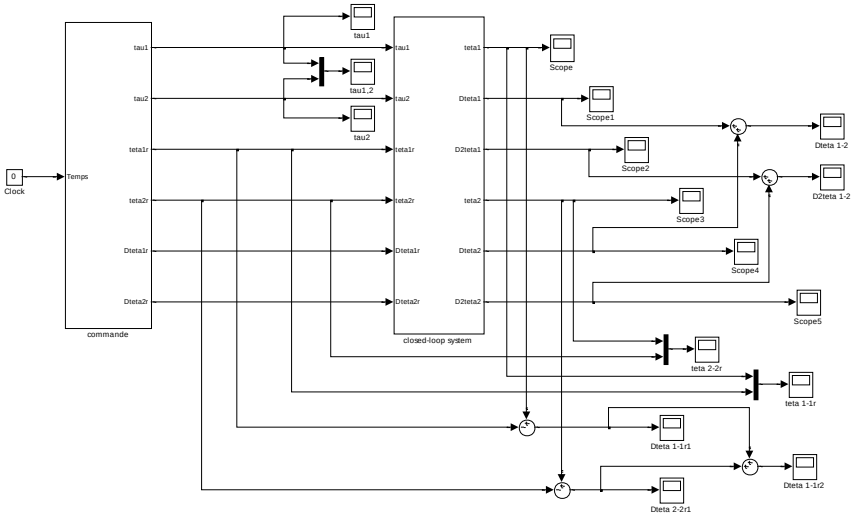

Figure B.1. – The general system of the dynamic decoupling model in chapter 3.

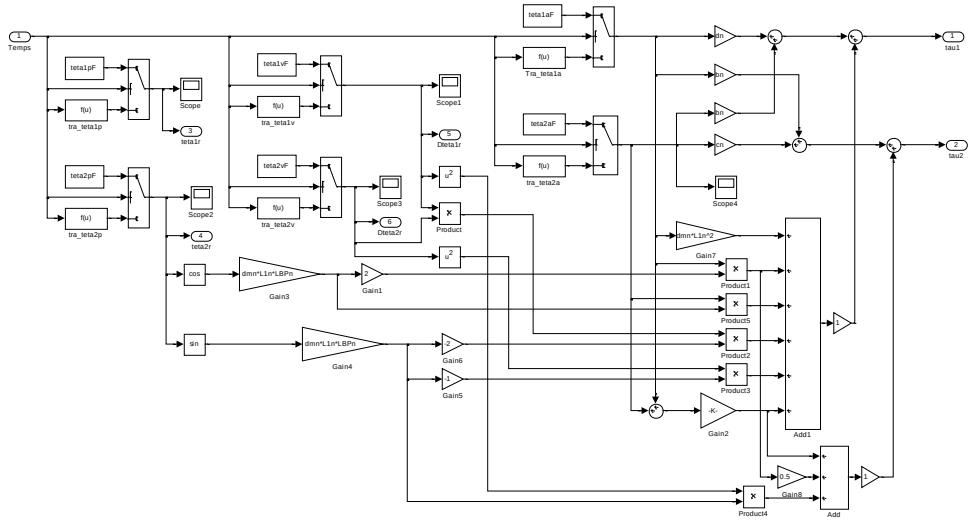

Figure B.2. – The controller diagram of the dynamic decoupling model in chapter 3.

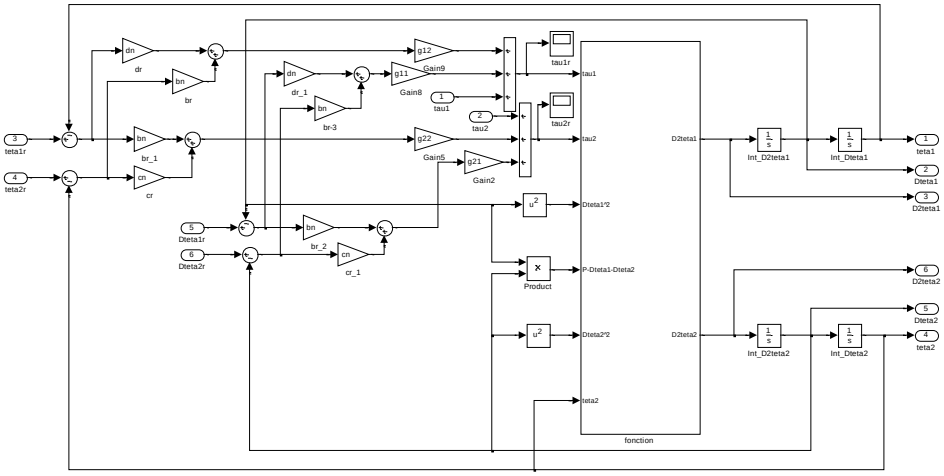

Figure B.3. – The closed-loop diagram of the dynamic decoupling model in chapter 3.

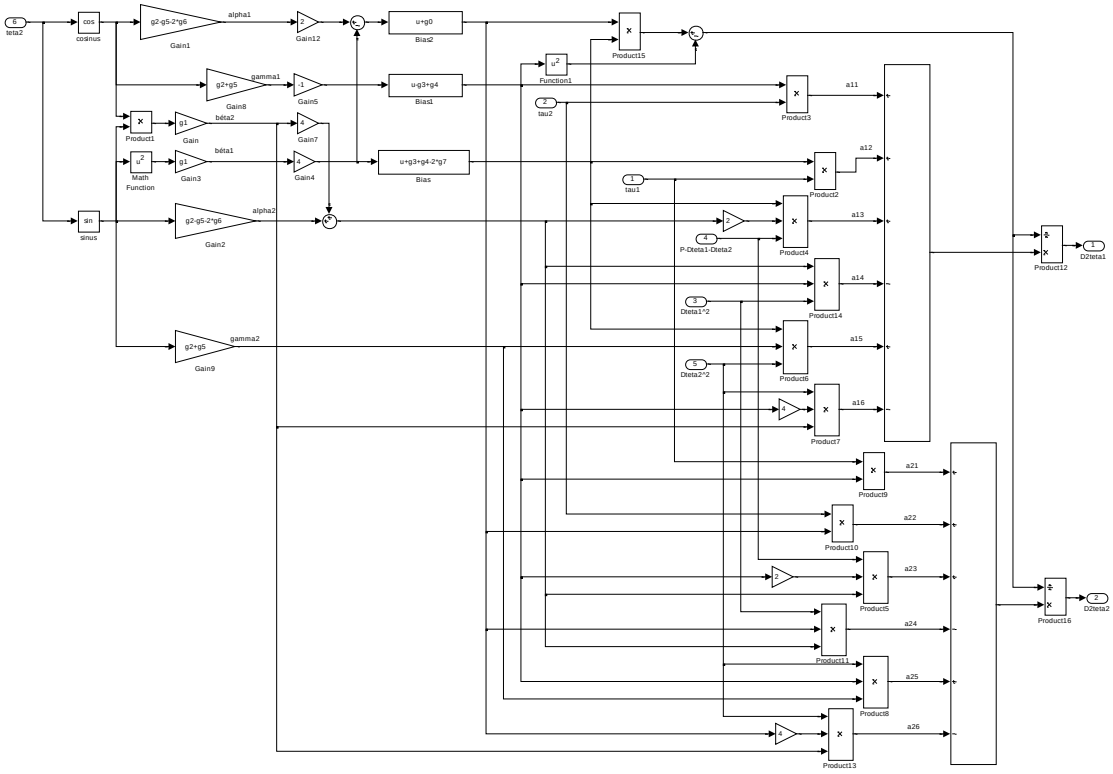

Figure B.4. – The manipulator diagram of the dynamic decoupling model in chapter 3.

Appendix C

The closed-loop simulation diagram of the coupled model

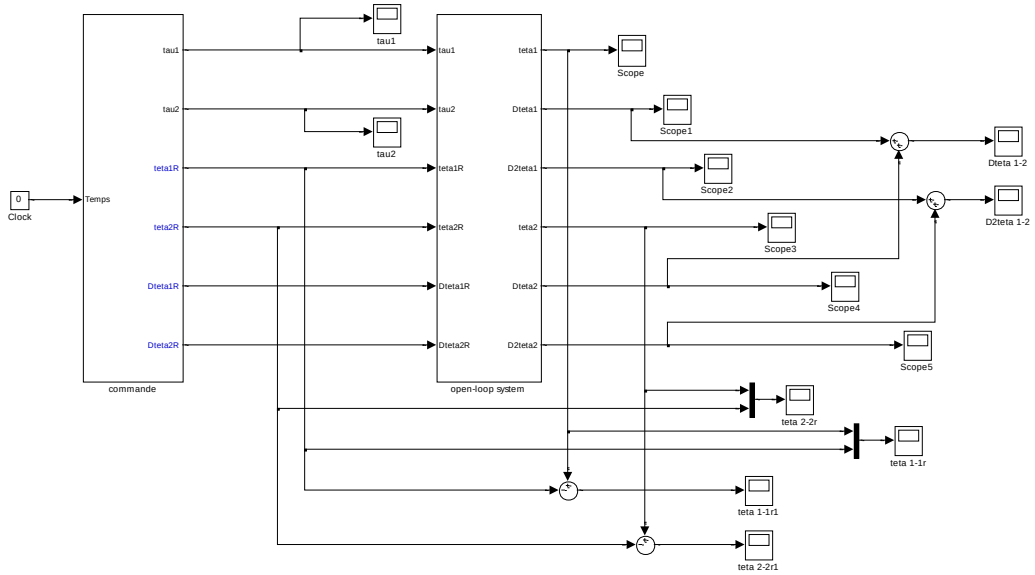

Figure C.1. – The general system of the coupled model.

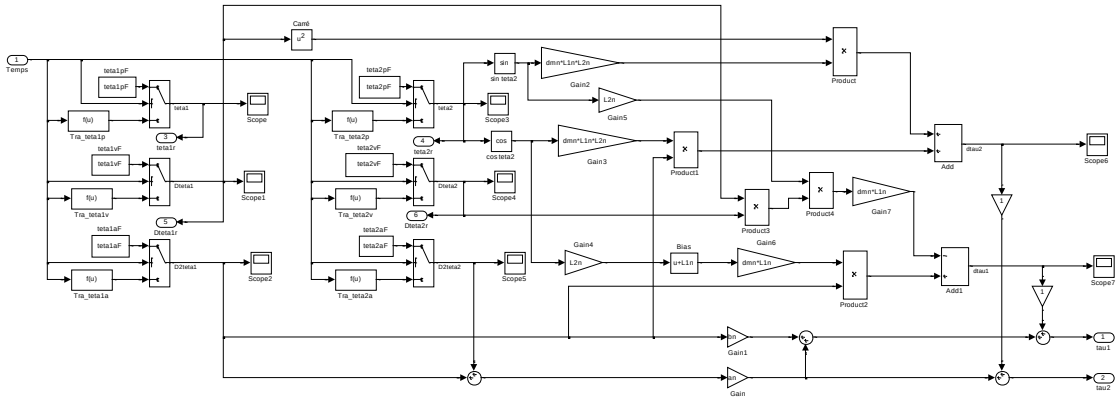

Figure C.2. – The controller diagram of the coupled model.

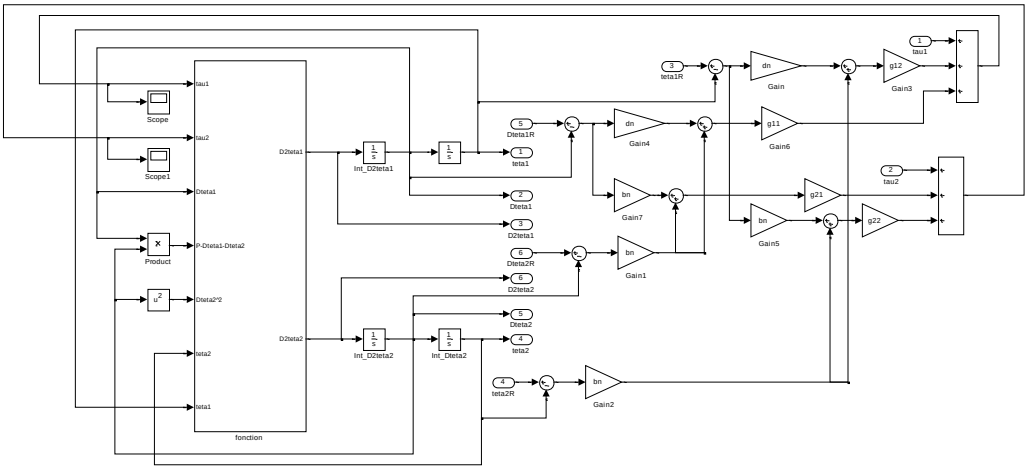

Figure C.3. – The closed-loop diagram of the coupled model.

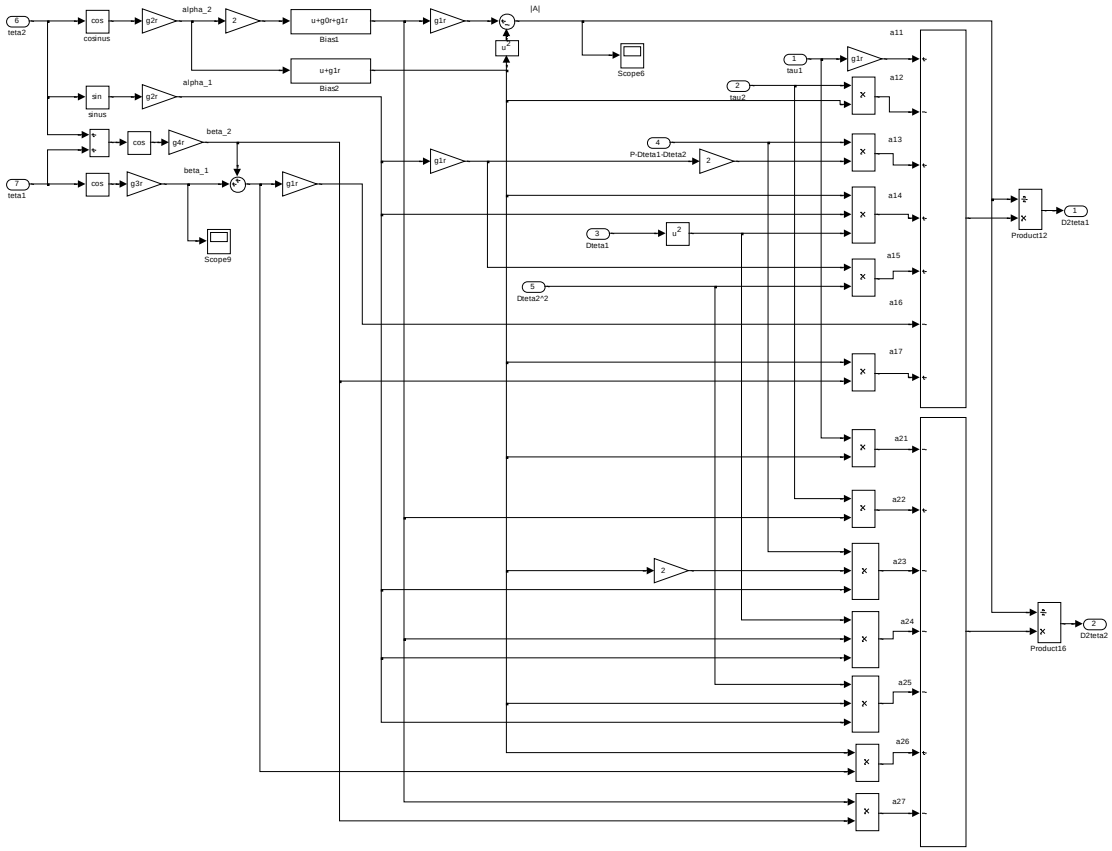

Figure C.4. – The manipulator diagram of the coupled model.

Appendix D

The closed-loop simulation diagram of the decoupled model by feedback linearization

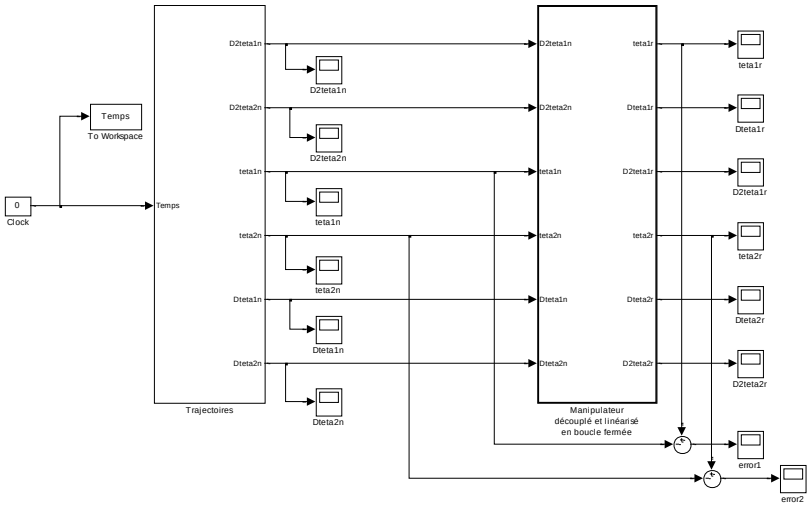

Figure D.1. – The general system of the decoupled model by feedback linearization.

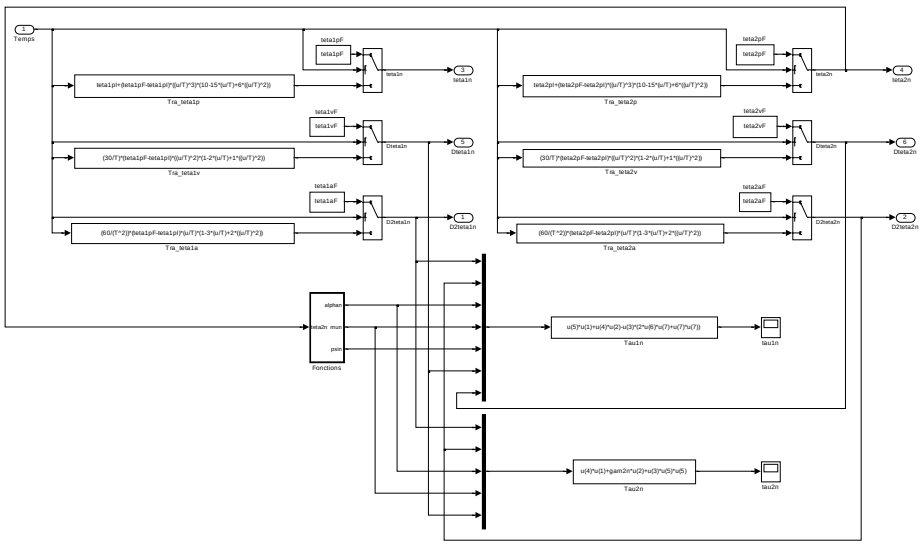

Figure D.2. – The controller diagram of the decoupled model by feedback linearization.

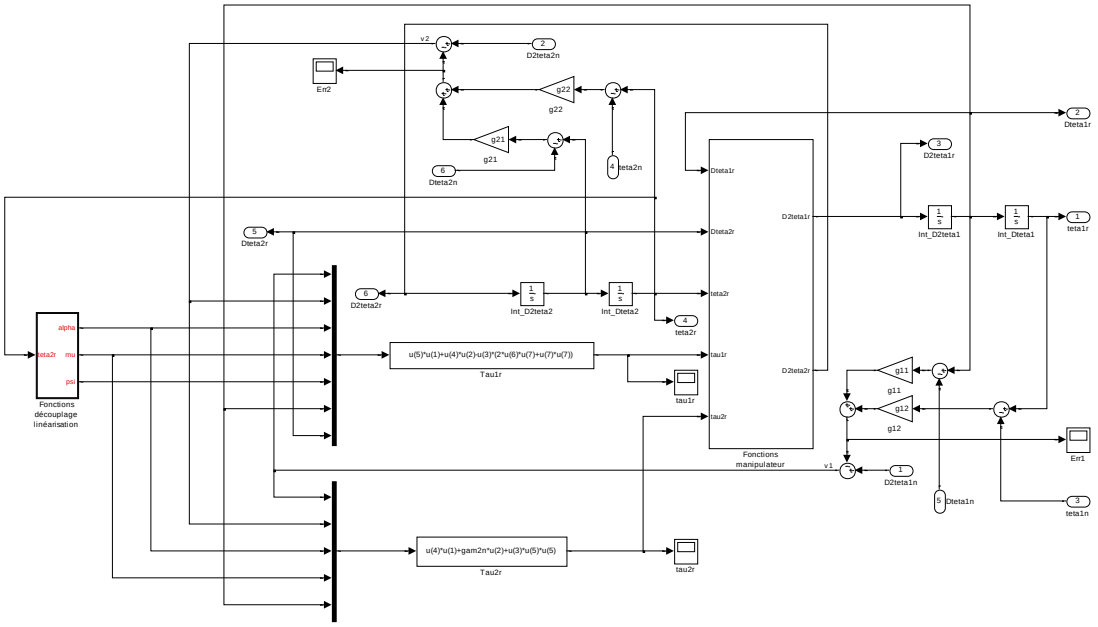

Figure D.3. – The closed-loop diagram of the decoupled model by feedback linearization.

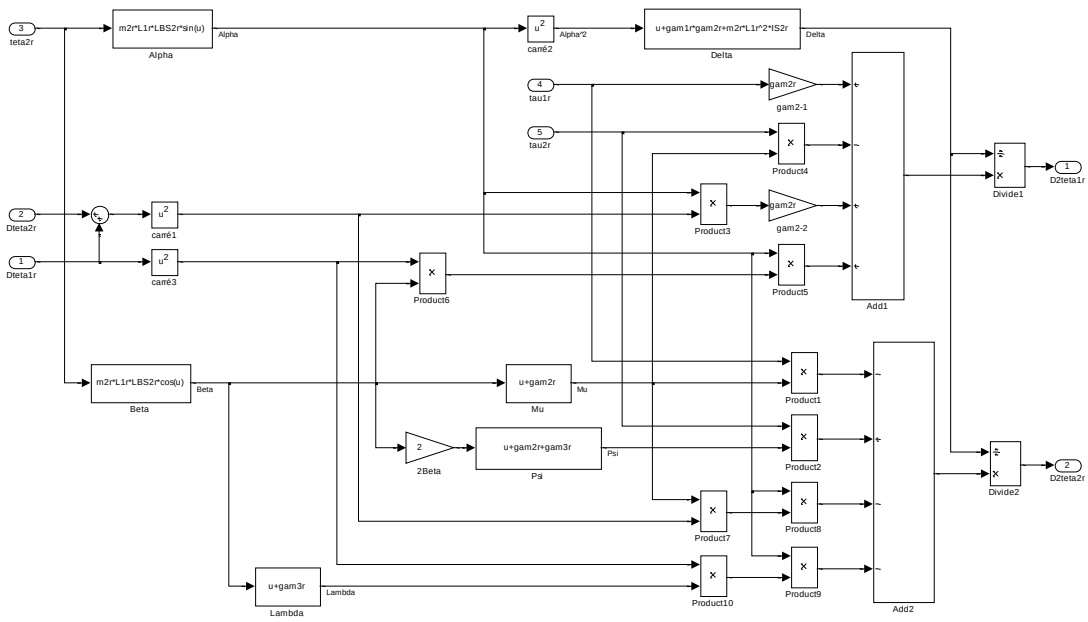

Figure D.4. – The manipulator diagram of the decoupled model by feedback linearization.

Appendix E

List of Publications

Peer-reviewed journals

- V. Arakelian, J. Xu, and J.-P. Le Baron. Mechatronic design of adjustable serial manipulators with decoupled dynamics taking into account the changing payload. *Journal of Engineering Design,* vol. 27, no. 11, pp. 768–784 (2016).

- J. Xu, V. Arakelian and J.-P. Le Baron. The design of planar serial manipulators with decoupled dynamics taking into account the changing payload. *Journal of Robotics and Mechanical Engineering Research,* vol. 1, no. 4, pp. 39-46 (2017).

Conference proceedings

- V. Arakelian, J. L. Xu, and J. P. L. Baron. The design of arm linkages with decoupled dynamics taking into account the changing payload. *Proceedings of the IEEE/RSJ International Conference on Intelligent Robots and Systems (IROS'2015)*, September 28 - October 2, Hamburg, Germany, pp. 3765–3770, (2015).

- V. Arakelian, J. Xu, J.-P. Le Baron and A. Chunikhin. Dynamic decoupling of motions in manipulators based on the properties of the Scott-Russell mechanism. *Proceedings of the 27th International Innovation Conference of Young Scientists and Students (IICYSS-2015),* Moscow, 2-4 December, 2015, pp. 292-295 (2015).

- J. Xu, V. Arakelian, and J.-P. L. Baron. Dynamic decoupling of adjustable serial manipulators taking into account the changing payload. *Proceedings of the 4th IFToMM International Symposium on Robotics and Mechatronics*, 23-25 June, Poitiers, France. In the book "*Robotics and Mechatronics"* Editors: S. Zeghloul, M. A. Laribi, and J.-P. Gazeau, Springer, pp. 313–320 (2016).

- J. Xu, J.-P. Le Baron, and V. Arakelian. Tolerance analysis of planar serial manipulators with decoupled and non-decoupled dynamics. *Proceedings of the 6th European Conference on Mechanism Science*, 20-23 September, 2016, Nantes, France. In the book "*New Trends in Mechanism and Machine Science"* Editors: Ph. Wenger and P. Flores, Springer, pp. 29–37 (2017).

INSA de RENNES
Service des Formations

AVIS DU JURY SUR LA REPRODUCTION DE LA THESE SOUTENUE

Titre de la thèse:
An improved design concept permitting the dynamic decoupling of serial manipulators taking into account the changing payload

Nom Prénom de l'auteur : XU JIALI

Membres du jury :
- Monsieur GUEGUEN Hervé
- Monsieur WENGER Philippe
- Monsieur ABBA Gabriel
- Monsieur LE BARON JEAN-PAUL
- Monsieur ARAKELYAN Vigen
- Monsieur AOUSTIN Yannick

Président du jury : P. Wenger

Date de la soutenance : 21 Avril 2017

Reproduction de la these soutenue

Thèse pouvant être reproduite en l'état
~~Thèse pouvant être reproduite après corrections suggérées~~

Fait à Rennes, le 21 Avril 2017

Signature du président de jury

P. Wenger

Le Directeur,

M'hamed DRISSI

INSTITUT NATIONAL des SCIENCES APPLIQUÉES · RENNES ·

Résumé

Structure simple, faible coût, grand espace de travail et technologie mature, ces avantages font que les manipulateurs sériels sont largement utilisés dans de nombreux domaines industriels. Avec le développement rapide de l'industrie et les diverses applications des manipulateurs sériels, de nouvelles exigences strictes sont souhaitées, telles que la stabilité robuste, la grande précision de positionnement et la cadence élevée.

Un des moyens efficaces pour améliorer les performances mentionnées est la conception de manipulateurs sériels à découplage dynamique. Dans ce cadre, l'objectif de cette thèse est de valider une structure simple permettant de réaliser un découplage dynamique complet des manipulateurs sériels en tenant compte de la charge embarquée.

Le chapitre 1 présente les solutions connues et décrit les inconvénients liés aux différentes techniques permettant une simplification de la dynamique des manipulateurs. L'étude de la bibliographie a permis d'affiner les objectifs à atteindre. Le chapitre 2 traite de la conception de manipulateurs sériels réglables à dynamique linéarisée et découplée. Sans la charge embarquée, la méthode développée réalise le découplage dynamique par rotation inverse des bras et par redistribution optimale des masses. La charge embarquée qui conduit à une perturbation au niveau des équations dynamiques de découplage est compensée par la commande.

Le chapitre 3 envisage un nouveau concept de découplage dynamique qui consiste à relier aux bras initiaux d'un manipulateur sériel, deux bras additionnels pour réaliser un mécanisme Scott-Russell. Les mouvements opposés des bras du mécanisme Scott-Russell associés à une redistribution optimale des masses permettent de supprimer les termes non linéaires des équations dynamiques du manipulateur. Le modèle linéaire et découplé ainsi obtenu permet de tenir compte de la charge embarquée.

Dans le chapitre 4, on considère les propriétés de robustesse (incertitudes paramétriques) de quatre modèles de manipulateurs sériels (un manipulateur couplé, un manipulateur découplé par la commande et les deux manipulateurs découplés qui sont issus des chapitres 2 et 3). Les études qualitatives sont effectuées par simulation en utilisant la même loi de commande optimale et la même trajectoire de référence. Les résultats des simulations permettent de conclure sur la robustesse des manipulateurs décrits aux chapitres 2 et 3 par rapport au manipulateur couplé et au manipulateur découplé par la commande.

La méthodologie de conception et les techniques de commande proposées sont illustrées par des simulations réalisées à l'aide des logiciels ADAMS et MATLAB. Les simulations ont confirmé l'efficacité des approches développées.

Abstract

Simple structure, low cost, large workspace and mature technology, these advantages make the serial manipulators are widely used in many industrial fields. With the rapid development of industry and various applications of serial manipulators, new strict requirements are proposed, such as high stability, high positioning accuracy and high speed operation.

One of the efficient ways to improve the mentioned performances is the design of manipulators with dynamic decoupling. Therefore, the goal in this thesis is to find simple structure permitting to carry out complete dynamic decoupling of serial manipulators taking into account the changing payload.

The review, given in Chapter 1, summarizes the known solutions and discloses the drawbacks of different techniques permitting a simplification of the dynamics of manipulators. It allows an identification of objectives that are of interest and should be studied within the framework of this thesis.

Chapter 2 deals with the design of adjustable serial manipulators with linearized and decoupled dynamics. Without payload, the developed method accomplishes the dynamic decoupling via opposite rotation of links and optimal redistribution of masses. The payload which leads to the perturbation of the dynamic decoupling equations is compensated by the optimal control technique.

Chapter 3 deals with a new dynamic decoupling concept, which involves connecting to a serial manipulator a two-link group forming a Scott-Russell mechanism with the initial links of the manipulator. The opposite motion of links in the Scott-Russell mechanism combined with optimal redistribution of masses allows the cancellation of the coefficients of nonlinear terms in the manipulator's dynamic equations. Then, by using the control, the dynamic decoupling taking into account the changing payload is achieved.

In chapter 4, robustness properties (parametric uncertainties) of four various models of serial manipulators (one coupled manipulator, one decoupled manipulator by feedback linearization and the two decoupled manipulators that modeled in chapters 2 and 3) are considered. The given comparison performed via simulations is achieved with the same optimal control law and the same reference trajectory. Simulation results allow one to derive robustness assessments of manipulators described in chapters 2 and 3.

The suggested design methodology and control techniques are illustrated by simulations carried out using ADAMS and MATLAB software, which have confirmed the efficiency of the developed approaches.

INSA RENNES

N° d'ordre : 17ISAR 09 / D17 - 09

Institut National des Sciences Appliquées de Rennes
20, Avenue des Buttes de Coësmes - CS 14315 - F-35043 Rennes Cedex
Tél : 02 23 23 82 00 – Fax : 02 23 23 83 96